The role of tidal fluctuations in influencing rates of submarine groundwater discharge

by

Catherine Helen Safadi

B.E.Sc., The University of Western Ontario, 2003

A THESIS SUBMITTED IN PARTIAL FULFILLMENT OF
THE REQUIREMENTS FOR THE DEGREE OF
MASTER OF APPLIED SCIENCE

in

The Faculty of Graduate Studies
(Geological Engineering)

THE UNIVERSITY OF BRITISH COLUMBIA
July 2006

Abstract

The following work was undertaken in this study to provide insight about the role of tidal fluctuations in influencing rates of SGD: (1) Improvements were made to the installation method and accuracy of a new tool developed for measuring the transient changes in vertical differential fluid pressures, referred to as the differential pressure system (DPS-II), (2) a field experiment was carried out to obtain measurements of SGD rates by a continuous heat type seepage meter, transient changes in vertical differential fluid pressures heads in shallow sediment by the DPS-II and tidal fluctuations in the near-shore environment, (3) the interpretation of the field data sets were constrained based on calculations using Darcy's Law and a 1D uniform density flow model.

The field experiment was carried out between October 26-28 2005, which was the last of a sequence of nine shorter tests completed to refine field procedures and gain experience using the instruments. Spanish Banks West beach in Vancouver was chosen as the field site because it is close proximity to The University of British Columbia, reasonable rates of SGD were measured during preliminary tests and the location fulfilled many of the logistical demands of testing.

Results of the experiment showed that the highest differential fluid pressure heads (measured between about 0.3 and 0.6 m below the seabed) at two piezometers of the DPS-II and highest SGD rates occurred at low tide. Using

Darcy's Law, SGD rates were calculated based on the differential fluid pressure heads and a hydraulic conductivity value within the constraints of the hydraulic conductivity data set derived from falling head tests completed on core samples from the site. The calculated SGD rates provided a good match with SGD rates by the seepage meter. Results of the 1D hydrogeological modelling suggest that the field based measurements of differential fluid pressure heads and SGD rates can be explained reasonably well by a 1D uniform density dependent flow model.

Table of Contents

List of Tables

List of Figures

Acknowledgements

I owe many thanks to my supervisor Dr. Leslie Smith for giving me the opportunity to work with him on this project. I have especially valued Leslie's many suggestions, patience and of course, humour. From this work I have gained a greater appreciation for the effort involved in creating and implementing a new design as well as an understanding of the driving mechanisms of submarine groundwater discharge (I will not look at a beach the same way!). I am also grateful for the assistance and guidance provided by Dr. Roger Beckie and Dr. Uli Mayer, who were both always available throughout my studies at UBC.

I would like to thank my fellow hydros who have helped with my field work, contributed to my learning by sharing there own experiences and have provided such enjoyable company.

I am grateful to have been a part of such a knowledgeable, supportive and caring group at UBC. I wish you always, all the best.

1. Introduction

1.1 Introduction to Research Topic and Purpose

Submarine groundwater discharge is defined as the total mixture of seawater and fresh groundwater flowing out from the aquifer, into the coastal water, through the underlying sediments (Destouni et al. 2003). Unlike river flow, SGD is a less obvious influx to the ocean, typically occurring as diffuse and temporally variable discharge, in some cases augmented by focused seeps or springs. SGD in the near-shore has been measured and predicted by many researchers (e.g. Kohout 1964; Bokuniewicz 1992; Young 1996; Burnett et al. 2003; Taniguchi et al. 2006) but the exact magnitude of the phenomenon, as well as its impact on the near-shore zone is still not known with certainty. In some cases, the fresh water component of SGD, discharging from local surficial or deeper aquifers, has been shown to represent a potentially important pathway for the transport of anthropogenic substances such as fertilizers and sewage from land to sea (Valiela et al. 1990; Capone and Slater 1990; Corbett et al. 1999; Krupa et al. 2003; Slomp and Van Cappellen 2004; Boehm et al. 2004).

A major question that exists is to what extent SGD is controlled by hydraulic gradients driving groundwater of terrestrial origin into the ocean, and how much is driven by oceanic processes such as tidal forcing, wave action or saltwater fingering (e.g., Li et al. 1999; Rasmussen et al. in press) that could cause a higher quantity of re-circulating seawater to discharge across the seabed. Discharges influenced by terrestrial and marine forces are typically coincident in

time and space but may differ significantly in magnitude. Since such factors as the hydraulic gradient, tidal range, and position of the freshwater-seawater interface change over time; it is possible that the conditions in any one area could shift (e.g., seasonally) between terrestrially governed and marine dominated systems (Burnett 2006). In attempts to distinguish between the mechanisms driving SGD in the near-shore, SGD characteristics such as flux rate and salinity may be monitored in addition to measurements of the SGD driving forces which may include hydraulic gradients and tidal (sea) levels. In this study, transient changes in differential fluid pressure heads in shallow marine sediments, SGD flux rates, and tidal levels were measured at a coastal site at Spanish Banks West beach in Vancouver, British Columbia. This site was chosen because it is in close proximity to The University of British Columbia, reasonable rates of SGD were measured at the site during preliminary tests, and it fulfilled many of the logistical demands for testing. The objectives of this study are to improve the accuracy of a new instrument developed to measure transient changes in vertical differential pressure heads in near-shore shallow marine sediments, and to investigate the role of tidal fluctuations in influencing rates of SGD using the measurements of transient changes in vertical fluid pressure heads, with direct measurements of SGD flux rates, and tidal levels.

1.2 Background and Motivation

Within the last decade there has emerged recognition that at least in some cases, SGD may be both volumetrically and chemically important (Johannes

1980). One of the major objectives of the recent interest in SGD has been to provide both the scientific and coastal zone management communities with the tools and skills necessary to evaluate the influence of SGD in the coastal zone. The three principal approaches used to assess SGD are: (1) direct measurements using manual or automated seepage meters (e.g., Cable 1997a and 1997b; Burnett et al. 2003); (2) geochemical tracer techniques (e.g., Moore 1996; Moore and Wilson 2005); and (3) hydrogeological modelling (e.g., Bokuniewicz 1992; Smith and Zawadski 2003). Many studies have been conducted to evaluate SGD, however up until recently rarely was more than one approach employed in any one study and estimates of measurement uncertainty were almost never provided (Burnett et al. 2001). To improve the confidence in SGD assessments, intercomparison experiments have been performed that directly compare several of the independent measurement approaches (e.g., Burnett et al. 2002). These experiments have shown that careful measurements can accurately estimate SGD, quantify some of the driving mechanisms, and provide insight to the spatial and temporal scales at which these mechanisms operate. In this study I attempt to improve the accuracy and better constrain the errors associated with a new tool, referred to as the differential piezometer system (DPS-II), developed for measuring transient changes in vertical differential fluid pressure heads in the seabed. I also use measurements of the transient changes in vertical differential pressure heads by the DPS-II, in conjunction with SGD rates by an automated seepage meter to investigate the relationship the role of tidal fluctuations in influencing rates of SGD.

1.3 Key Questions

This work focuses on better understanding the mechanisms controlling SGD in the near-shore environment, specifically assessing the role of tidal fluctuations. The key questions are:

(1) What is the relationship observed at the field site between measurements of sea level fluctuations due to semi-diurnal tides, transient changes in vertical differential pressure heads in shallow marine sediment and SGD rates?

(2) What are the roles of transient changes in vertical differential pressure heads in shallow marine sediment and tidal level fluctuations in modulating SGD rates?

(3) What are the best approaches that can be implemented in all aspects of the development of the DPS-II (e.g., design, deployment) to obtain accurate and reliable measurements of transient changes in vertical differential pressure heads by the DPS-II?

(4) What is the uncertainty associated with field measurements of vertical differential pressure heads by the DPS-II?

1.4 Outline of Thesis

The research questions stated above in section 1.3 were addressed, in part, by analyzing field measurements of SGD rates by a continuous heat type seepage meter, transient changes in vertical pressure gradients by the DPS-II and tidal levels. The field measurements were obtained from an experiment completed between October 26 – 28, 2005 which was the last field experiment of a

sequence of nine shorter tests (hours to 1 day) completed to refine field procedures and assess the performance of the seepage meter and DPS-II. The analysis of the data involved calculations using Darcy's Law and a 1D uniform density numerical model to better constrain the interpretation of the field data sets. An error analysis of the DPS-II was also completed to evaluate the error associated with the measurements by the tool and provide recommendations to minimize the error of future DPS-II measurements.

2. Review of Submarine Groundwater Discharge

2.1 Introduction and Significance

In addition to the advective flow of fresh groundwater driven by a hydraulic gradient between the land and sea, there are several oceanic processes that drive the flow of re-circulated seawater across the seabed. The term SGD has been used in different ways over the years, typically to include only freshwater (Zektser et al. 1983) or both freshwater and re-circulating seawater (Church 1996). A clear definition of SGD is important for two key reasons: (1) the ratio of SGD to total water flux into the ocean has a different meaning depending on whether SGD includes re-circulated seawater or not, and (2) SGD values compared to other freshwater discharge estimates to the ocean may lead to misunderstandings if re-circulated seawater is included.

A definition of SGD that is compatible to both terrestrial and oceanic derived flows is important, since either flow could be significant from a biogeochemical perspective. Consistent with recent definitions of SGD (e.g., Kim and Hwang 2002; Burnett et al. 2003; Taniguchi et al. 2004), in this study SGD is defined as all discharge of subsurface fluids across the land-ocean interface without regard to its composition (e.g., salinity), origin, or phenomena driving SGD.

SGD in the near-shore is typically diffuse, patchy and temporally variable and may involve multiple aquifers (Slomp and Van Cappellen 2004; Burnett et al. 2006). The composition of SGD is usually a mixture of waters reflecting different

fluid histories (Figure 2-1). Freshwater is a component of SGD that may discharge from a surficial aquifer driven by a hydraulic gradient between the land and the sea. The oceanic processes that drive the re-circulated seawater component of SGD are not as well understood and it is unclear the amount these processes contribute to SGD. In addition to SGD in the region beyond the low tide line, water will also drain from the seepage face that forms along the shoreline during the tidal cycle. This water includes both freshwater and seawater components (Smith and Zawadzki 2003).

Burnett et al. (2003) summarized some of the more obvious or important components and driving forces of SGD, as shown in Table 2-1. This table is a simplification of the relationships between contributing factors and driving forces. For example, the tidal range likely influences the tidal forcing of re-circulated seawater and would also affect SGD rates by modulating the hydraulic gradient in a coastal setting.

An annual recharge cycle causing a seasonal inflow and outflow of seawater within an unconfined coastal aquifer is a new concept introduced by a team at MIT (Michael et al. 2005). The group had shown earlier in a seepage meter experiment carried out in Waquoit Bay, Massachusetts that the groundwater discharge was largely saline (Michael et al. 2003). A seasonal shift in the freshwater-seawater interface in response to the annual recharge cycle was

proposed to explain the source and timing of the high flux of saline water recorded by the seepage meters.

In addition to the ecological impact of SGD in the coastal zone by groundwater inputs such as nutrients, heavy metals, radionuclides and organic compounds (La Roche et al. 1997), groundwater discharge may also influence seawater intrusion into coastal aquifers. Seawater intrusion is an important process that leads to groundwater salinization to levels exceeding acceptable drinking and irrigation water levels (Van Dam 1999). Due to increasing population growth and the fact that about 70% of the world population occupies coastal regions, such groundwater contamination is clearly a significant issue (SCOR/LOICZ Working Group 112 2000). Seawater intrusion into terrestrial aquifer systems and SGD are closely linked processes that directly affect each other. The freshwater component of discharge to the sea controls seawater intrusion in some conditions. However, the over-pumping of coastal aquifers increases seawater intrusion and may significantly reduce or eliminate SGD, or at least the freshwater component of discharge.

2.2 Measurement Approaches

When SGD assessments are performed, the rate of groundwater discharge can be described in several different ways. One way that is widely used is the specific volume flux across the sea floor, typically expressed as cm/d ($cm^3 \cdot cm^{-2} \cdot d^{-1}$). SGD has also been expressed as the total volume discharge per unit length of

shoreline per unit time (e.g., $L \cdot m^{-1} \cdot d^{-1}$). Such assessments are difficult because more measurements are required but are useful for extrapolating to larger areas (Burnett et al. 2003).

Seepage meters are the only direct method for measuring SGD. The lower bound for reliable measurements using seepage meters is about 2 cm/d (Burnett et al. 2002). The manual seepage meter (Lee, 1977), is essentially a chamber inserted open end down into the sediment (Figure 2-2). A plastic bag covers a small hole drilled into the top of the chamber and is used to collect water that is displaced from the chamber by SGD. The change in the volume of water in the bag over a measured time interval provides the SGD flux measurement. Studies involving seepage meters have reached the following general conclusions: (1) many seepage meters are needed because of the natural spatial and temporal variability of SGD rates (Shaw et al. 1990), (2) the resistance of the tube (Fellows et al. 1980) and bag (Shaw et al. 1989; Belanger et al. 1992) should be minimized to the degree possible to prevent artefacts; (3) use of a cover for the collection bag may reduce the effects of surface water movements due to wave, current or stream flow activity (Libelo et al., 1994), (4) caution should be applied when operating near the seepage meter detection limit (Cable et al. 1997) and, (5) artefacts may exist from pressure gradients developed by unidirectional currents passing over the meter (Shinn et al. 2002).

Manual seepage meters are a simple and inexpensive tool for assessing SGD in a coastal setting but a significant disadvantage of the meters is that they are labour intensive. In order to obtain SGD rates automatically and continuously, various types of automated seepage meters have been developed (Taniguchi and Fukuo 1993; Krupa et al. 1998, Sholkovitz et al. 2003; Paulsen et al. 2001). One example of such an approach is the continuous heat type meter developed by Taniguchi and Iwakawa (2001). The meter uses two thermocouples sensors and a heating wire positioned in a flow tube above an inverted chamber covering a known area of sediment (Figure 2-3). The basis of the method is to measure the temperature gradient of the water flowing between the thermocouple sensors that are located at downstream and upstream positions in the flow tube. Heat is continuously generated at the upstream position. The temperature gradient between the downstream and upstream sensors is dependent on the SGD flux rate. When there is no SGD flux, the temperature gradient in the flow tube is the maximum, and it decreases with increasing SGD. Once the system has been calibrated, measurements of SGD can be made automatically on a near continuous basis. The continuous heat type seepage meter can not measure recharge (i.e. inflow into the seabed). The expected output of the meter if it is deployed in a recharge zone would be measurements outside the range of the calibration curve for the meter (T. Ishitobi personal communication). The continuous heat type meter has successfully measured SGD over several days to months at a typical rate of about one measurement every 10 minutes (Taniguchi 2002; Taniguchi et al. 2004; Taniguchi et al. 2006). Measurement

rates of one measurement every 1 minute have also been recorded using the continuous heat type meter (Taniguchi 2005). In this study, a continuous heat type seepage meter is used to measure SGD rates over a period of about 48 hours at a rate of one measurement every 10 minutes.

The use of geochemical tracers offers a promising approach for regional assessments of SGD. Small scale variability is a serious problem for the use of seepage meters, but small spatial scale variations tend to be smoothed out over time and space in the case of tracer methods. The smooth measurement output is a result of the tendency of the marine water column to integrate the groundwater tracers entering via the aquifers. The use of geochemical tracers requires that all other tracer sources and sinks except groundwater be evaluated and this task can be difficult. Several studies have employed the use of the natural U-decay series nuclides ^{226}Ra and ^{222}Rn to assess SGD (Moore, 1996; Burnett et al. 1996; Corbett et al. 1999; Kim and Hwang 2002; Burnett and Dulaiova 2003). Natural geochemical tracers should be greatly enriched in groundwater relative to coastal waters, be conservative and easy to measure.

Modelling to predict SGD can be categorized into three basic groups: (1) flow equations, i.e. analytical or numerical solutions of Darcy's Law; (2) mass balance approaches that usually consist of water or salt budgets; and (3) hydrograph separation techniques that examine the baseflow from streams and extrapolate the interpreted groundwater flow to the coastal zone. These approaches are

carried out on a variety of spatial scales and levels of complexity but all have certain limitations. Estimates of SGD using Darcy's Law often assume homogeneity of the aquifer when this is not the case. Although numerical solutions are capable of accounting for heterogeneity, it is difficult to obtain representative values of the hydraulic conductivity within an aquifer. Another source of uncertainty may result from the assumption of steady state conditions in some modelling analyses that may not necessarily apply especially considering the effects of tidal and density driven forces in the near-shore zone.

2.3 Local and Global Estimates

Locations of SGD estimates compiled by Taniguchi (2002) show that many studies have been performed on the east coast of the USA, Europe, and Japan (Figure 2-4). No quantitative SGD data was located from South America, Africa, India or China, although indications of SGD were reported for India (Moore, 1997) and Kenya (Kitheka, 1998).

Many studies have observed that SGD decreases exponentially away from the shoreline. The world wide compilation of SGD estimates by Taniguchi (2002) indicated that most SGD rates are below about 10 cm/d. Considering the length of coastal shoreline, this SGD estimate could represent a significant quantity of discharge into the ocean. Various estimates of the role of SGD in the global water balance range over about three orders of magnitude (approximately 0.01 to 10 % of total river flow). Comparing SGD assessments is complicated because of

the differences in spatial scales, assumptions and artefacts associated with each method. As well, one must be cautious about drawing too many conclusions from these SGD results. Most SGD measurements have been performed where it is easily detected and large volumes of SGD are expected. Therefore, the estimates may be more representative of maximum SGD values.

2.4 Relationship between SGD and Tidal Levels

Temporal trends of SGD recorded by seepage meters typically show variations that correspond in timing to the tidal period in that area. In general, the timing of the SGD spikes relative to the tidal level varies depending upon the hydrogeologic setting. For example, Lee (1977) observed that SGD rates were distinctly higher at low tide in a coastal site in Beaufort, North Carolina, whereas, Burnett et al. (2002) showed that the highest SGD rates occurred during the transition from highest to lowest tide during an intercomparison experiment carried out at a site along the northeastern coast of the Gulf of Mexico. Taniguchi et al. (2006) concluded that measurements of SGD in the near-shore at a site near Kyushu Island, Japan, that showed a direct inverse relationship with tidal levels could be explained mainly by terrestrial groundwater, while offshore SGD that showed a lag time of three hours between highest SGD rates and low tide was controlled mostly by oceanic processes that caused the discharge of re-circulated seawater.

Studies have shown longer-term (weeks to months) tidally-modulated cycles in SGD based on continuous measurements of the groundwater tracers radon and methane (Kim and Hwang 2002) and measurements by automated seepage meters (Taniguchi 2002). Taniguchi (2002) continuously recorded SGD rates in Osaka Bay, Japan from May to August 2001 and using a Fast Fourier Transfer (FFT) method was able to identify a semi-diurnal to diurnal variation in SGD as well as a semi-monthly variation in discharge reflecting the neap spring lunar cycle.

It may be possible to explain the SGD spikes corresponding to changes in tidal levels by factors other than tides. It is recognized that benthic chambers deployed on the seabed can cause local pressure perturbations that drive pore water flow (Huettel and Gust, 1992). Tidal currents could also be at a maximum during tidal transition periods suggesting that pressure induced flows may be responsible for these spikes. However, groundwater tracers measured in the overlying water column also show similar variations between SGD and tidal levels (Burnett et al. 2002; Kim and Hwang, 2002). Pressure induced artefacts in seepage meter data would likely not be present in the same manner for tracer assessments.

Superimposed on the tidally driven behaviour of SGD rate, are variations in hydrogeological properties (e.g., water table) that have been shown to have an influence on SGD rates. In a tracer study completed in Korea by Kim and Hwang

(2002), SGD rates were more limited in the dry season when the aquifer was not recharging. These results show that despite it being typical to find a correspondence between tides and SGD rates in the near-shore, the overlapping nature of terrestrial and marine SGD forcing components can also be important.

Components	Driving Forces	Contributing Factors
Meteoric waters (fresh)	Hydraulic gradient	Topography, Transmissivity, Precipitation, Evaporation
Re-circulated seawaters (salt)	Hydraulic gradient, Tidal forcing, Wave set-up	Tidal range, period, frequency, Wind Force, direction
Connate waters (very salty)	Density, Thermal gradient	Geology, Geothermal heating

Table 2.1: Simplified relationships between components, driving forces and contributing factors of SGD (Burnett et al. 2003).

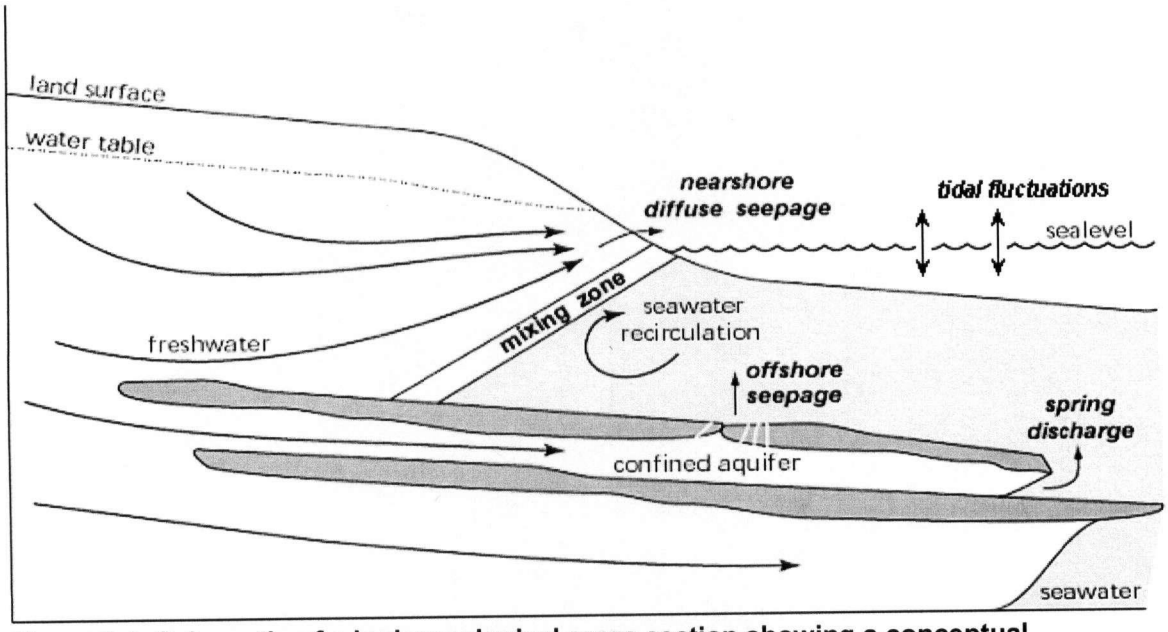

Figure 2-1: Schematic of a hydrogeological cross section showing a conceptual representation of SGD. Modified from Slomp and Van Cappellen 2004.

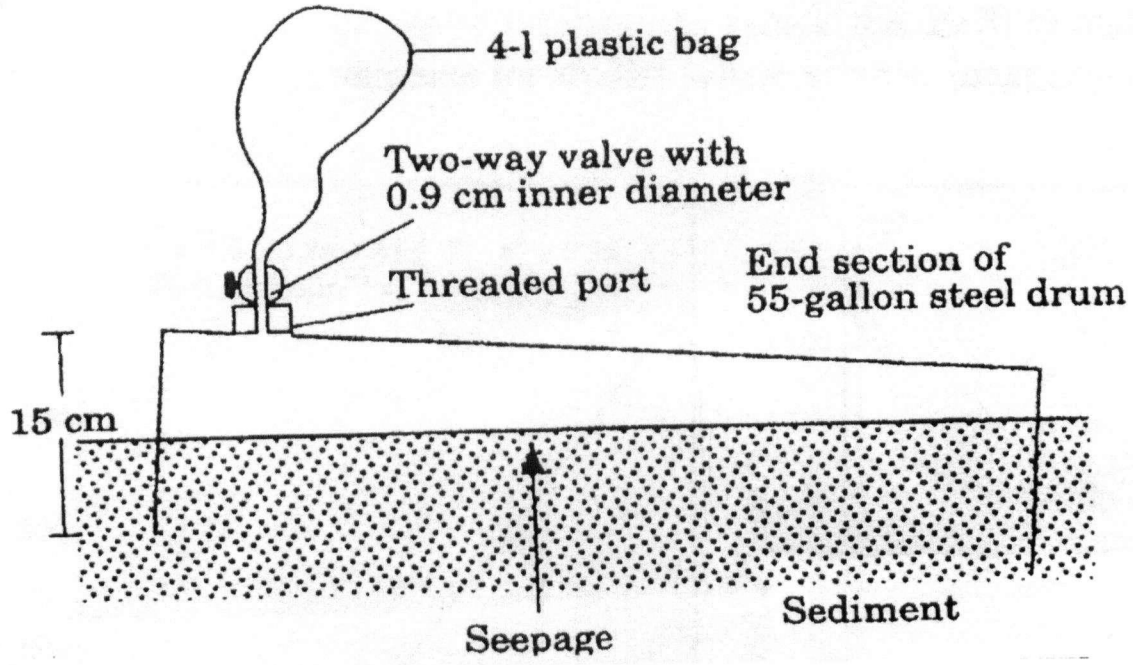

Figure 2-2: Schematic of a manual type seepage meter.

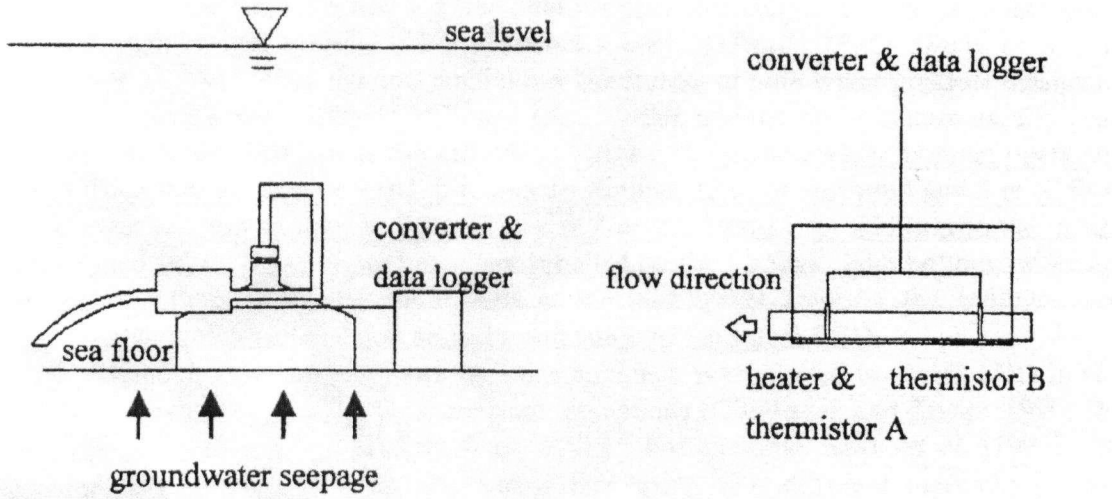

Figure 2-3: Schematic of a continuous heat type seepage meter.

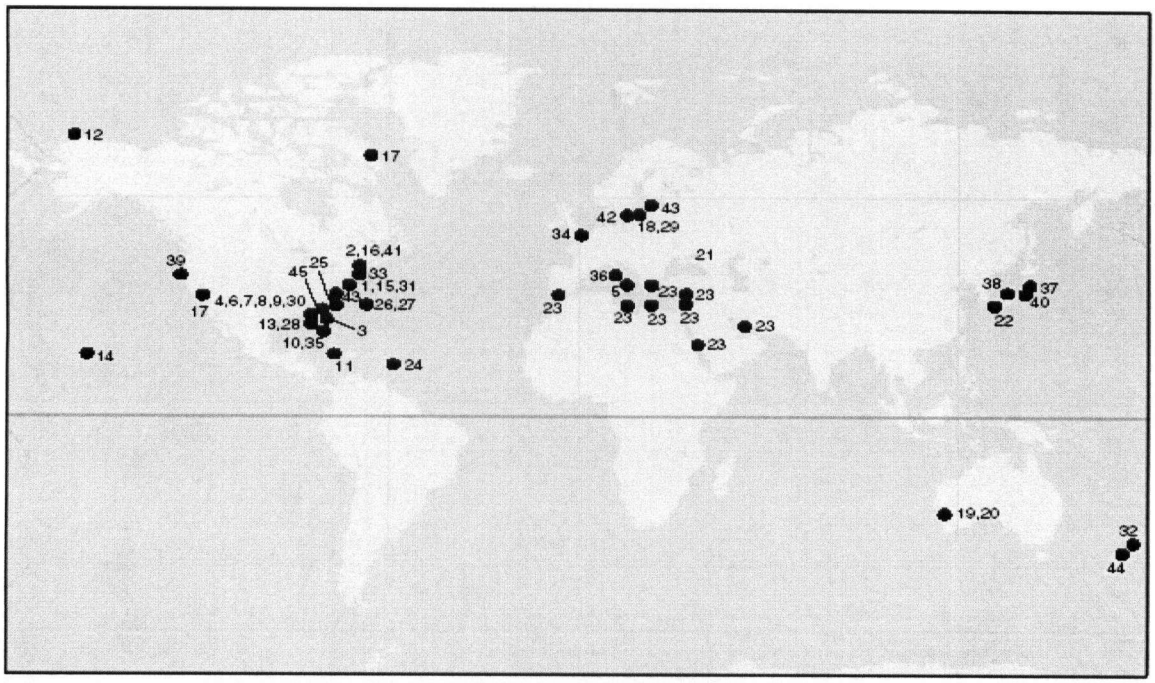

Figure 2-4: Locations of published investigations of SGD by seepage meters, piezometers, or geochemical/geophysical tracers. The numbers refer to Table I in Taniguchi (2002).

3. Instrumentation Development for Measuring Differential Fluid Pressure Heads

3.1 Application of Fluid Pressure Measurements to SGD

Direct in-situ measurements of fluid pressures are one method to detect and quantify SGD. Using measurements or estimates of the aquifer permeability and fluid density, the flux rates of SGD are related to fluid pressure gradients through Darcy's Law written in terms of fluid pressure:

$$q = \frac{k}{\mu}\left(\frac{dP}{dz} + \rho g\right) \qquad \text{(Equation 3.1)}$$

where q is the specific discharge, k is aquifer permeability, μ is fluid viscosity, dP/dz is the pressure gradient, ρ is the fluid density at the calculation point (and time) that SGD is to be determined, and g is the gravitational constant.

Alternatively, for a uniform density flow field, fluid pressure can be converted to hydraulic head using the relationship:

$$h = \frac{P}{\rho g} + z \qquad \text{(Equation 3.2)}$$

where z is the elevation above a datum, and the calculation of SGD can be simplified by using the conventional form of Darcy's Law:

$$q = -K\frac{dh}{dz} \qquad \text{(Equation 3.3)}$$

where dh/dz is the hydraulic gradient and K is the hydraulic conductivity.

In addition to directly assessing SGD rates, data sets of fluid pressures or hydraulic gradients are useful as a calibration constraint in the development of SGD hydrogeological models.

3.2 Fluid Pressure Measurement Approaches

Typically, the hydraulic potential is assessed at several depths in the sediment using multi-level piezometer nests (Freeze and Cherry 1979). It is relatively easy to install piezometers in shallow-water sediments by direct pushing and hammering. Piezometers have been successfully used in conjunction with seepage meters to explain the periodic fluctuations of SGD from measured hydraulic gradients and SGD flux rates (Barwell et al.1981;Taniguchi 1995). However, conventional piezometers may not be suitable for resolving the small hydraulic head gradients at some SGD sites (Smith and Zawadski 2003).

A variety of instruments to measure fluid pressure are used in geotechnical applications (Hanna 1985; Dunnicliff 1988). For measuring fluid pressures in marine sediments, the differential piezometer design is likely the most relevant of the tools used in geotechnical applications and offers an advantage over conventional piezometers. To continuously monitor fluid pressures in the sediment using a conventional piezometer, a pressure transducer may be used to measure the water level above the screen of the piezometer. The accuracy of a pressure transducer is usually expressed as a percentage of the full scale (FS) of the instrument. The FS of the instrument refers to the range of signal input the transducer is intended to measure (i.e., a pressure transducer with a FS of 1 PSI is rated to measure a range of pressures from 0 to 1 PSI). Because of the head of seawater, using a conventional piezometer to measure fluid pressures in the seabed requires the FS of a pressure transducer to be larger and thus increases

the error of the instrument. At some SGD sites, an error associated with a measuring instrument on the order of centimetres may approach the magnitude of the small changes in fluid pressure gradients and/or the small hydraulic gradients that are resolved from the fluid pressure measurements. The differential piezometer design used in this study overcomes the limitations of resolving small changes in fluid pressure gradients from independent measurements of fluid pressures by making a direct differential fluid pressure head measurement between two ports on a piezometer that is driven into the seabed. Since the early 1970s, several designs of differential pressure piezometers have been developed as a means to analyze soil strength (Bennett et al.1979; Davis et al. 1991; Schultheiss 1989; Anderson et al. 1996). The majority of these instruments were used to assess fluid pressures in relatively deep-water sediments requiring specialized installation techniques.

Although less well documented and with fewer piezometers developed than for the deep sea, attempts have also been made to measure fluid pressures in relatively shallow waters using the differential piezometer approach. The lack of literature and limited success using shallow water differential piezometers likely reflects fewer applications in the past for highly accurate shallow marine fluid pressure measurements.

There were three generations of Portable In-situ Pore Pressure Instruments (PISPPIs) developed at the University of Lehigh in Pennsylvania, USA. The

PISPPI-3, shown in Figure 3-1, was designed exclusively for shallow water. The intent of the PISSPI-3 was to determine SGD across the sediment-water interface, for which measurements were needed of both permeability and hydraulic head. The instrument utilizes a differential pressure transducer to monitor the pressure gradient between the sediment water interface and a depth in the sediment determined by the penetration of a probe. Insertion of the probe into the sediment induces a transient excess pressure field around the probe and upon dissipation of this pressure pulse, a small electric pump and a series of valves are activated to conduct a pump or slug test. The instrument also collects a small sample of pore water for subsequent chemical analysis. The probe is hydraulically connected to the pressure transducer through a carrying case left on the seabed and also a datalogger attached to a buoy. The only documentation for the PISSPI-3 is the User's Guide and Technical Manual. The project to develop the instrument was completed in 2001 (B. Carson personal communication).

Figure 3-2 shows the Diver Operated Pore Pressure Instrument (DOPPI) developed by GEOTEK Ltd in the United Kingdom. The only testing of the DOPPI was by GEOTEK Ltd in the Adriatic Sea where many problems were encountered as a result of nearby trawler activity. The instrument is no longer in operational condition (P. Schulthesis personal communication).

A differential pressure sensor instrument was developed for the Geological Survey of Canada to investigate slope failures in the Fraser River Delta. A small consulting company, Adara Consulting in Vancouver, designed the instrument. The differential pressure sensor consisted of two probes and a data acquisition system. The probes were inserted by divers into the seabed to a depth of about 3 to 5 m and each measured the fluid pressure at the seafloor and at a point in the seabed. Several data sets were obtained but information is not readily available about the quality of the measurements. Weather and funding problems prevented the recovery of either of the probes (G. Jolly personal communication; T. Lightfoot personal communication).

Pore pressures and seepage flux rates were measured and compared to tidal levels at a site near Kurobe, Japan (Urakoshi et al. 2003). Pore pressures were measured for 25 days using a newly developed multi-depth pore pressure instrument (Figure 3-3). This device measures pore pressures independently at the slit of two hollow lances that are imbedded into the sediment, using absolute pressure transducers positioned on the seabed. Pore pressure gradients are calculated from the differences in the pore pressure measurements. A disadvantage of this configuration is that errors in the installation depth of the lances will directly influence the interpretation of the data. Obtaining accurate measurements of the installation depth of the lances is a challenging aspect of the design (T. Urakoshi personal communication).

3.3 Description of DPS-I

A new tool, referred to as the differential piezometer system (DPS-I), was developed within the Earth and Ocean Sciences Department at UBC for the measurement and short term monitoring of vertical hydraulic gradients in near-shore, shallow marine sediments (Caulkins, 2003).

The DPS-I consisted of two piezometers and a control box housing the electronics used for data acquisition (2 differential pressure transducers, 4 resistors, 1 datalogger, and 1 power supply). The piezometers were approximately 1 m (3.3 ft) in length, and 4.5 cm (1 ¾ in) outside diameter (OD) and were designed to permit installation by sledge hammering into sandy sediments. Each piezometer was constructed of 0.3 m (1 ft) length steel drill rods and contained two measuring ports with screened diameters of about 6 mm spaced 31 cm apart. By the addition of short lengths of drill rods, this separation distance could be adjusted. The measuring ports of a piezometer were hydraulically connected through plastic tubes filled with deaired water to the pressure sides of a capacitance-type differential pressure transducer (manufactured by Setra, model 230, range +/- 0.5 PSI) mounted inside the control box. Deaired water was used as the hydraulic fluid in the tubes to minimize the potential for air bubbles within the tubes that could affect the accuracy of the measurements. Deaired water was obtained by boiling tap water for 15 minutes, and subsequently cooling and storing the water in 4L glass jars.

Each piezometer was connected to a separate transducer, providing independent measurements of the vertical hydraulic gradient.

In addition to short preliminary tests, the DPS-I was deployed four times over the course of a three week experiment in August 2002. In this experiment, installation of the DPS-I system began just after high tide and took five to six hours for completion. Measurements at the sites began immediately after installation of the system. Data were recorded with a Campbell Scientific CR10X datalogger that measured the voltage output (linearly related to differences in hydraulic head using laboratory calibrations) of the differential pressure transducer. The control box housing the datalogger and transducers did not have a water tight seal and the electronics were not submersible. To prevent submersion of the control box during deployment, it was positioned on a scaffold that was erected to a height above the maximum expected sea level (Figure 3-4).

3.3.1 Field Results using DPS-I

Prior to the first field experiment that implemented the DPS-I to estimate vertical hydraulic gradients in shallow marine sediment (Caulkins, 2003), the performance of the tool was tested by Caulkins (2003) in convenient near-shore locations close to The University of British Columbia in Vancouver, British Columbia (e.g., Spanish Banks, beaches below Burrard Street bridge). Satisfactory hydraulic gradient data were obtained from preliminary tests (2-3 hours in duration) using the DPS-I.

The first field experiment implementing the DPS-I was completed between August 17 to September 7, 2002. The purpose of the experiment was to investigate the influence of tidal levels fluctuations on rates of SGD using measurements of vertical hydraulic gradient, SGD and tidal level. The experiment was conducted in an area adjacent to the Florida State University Marine Laboratory (FSUML) at Turkey Point, Florida, in the northeastern coast of the Gulf of Mexico. This site was chosen to enable data comparisons with an SGD intercomparison study previously completed at the site in August of 2000 by members of the Scientific Committee on Oceanic Research Working Group 112 (Burnett et al. 2002).

During the 2002 experiment the DPS-I was installed at two sites located roughly 25 and 80 m offshore of the low tide line. Two tests were completed at each site, with the tests lasting between two and nine days. The quality of the hydraulic gradient data collected using the DPS-I was too poor to be used for the purposes of the field experiment. The discrepancy between the performance of the DPS-I during preliminary tests and the field experiment was likely in part a result of the different testing duration. As the field experiments were longer than a few hours, the DPS-I may have been affected by significant environmental conditions such as temperature fluctuations, wind and waves that were not present during the brief preliminary tests conducted in Vancouver.

From an analysis of the 2002 field experiment using the DPS-I, completed in this study, as well as considering the sources of errors identified by Caulkins (2003), the main issues identified with the field data collected using the DPS-I during the field experiment were:

1. **The measurement error was the same magnitude as the measurements.** A zero shift of -2 cm for transducer I and –1 cm for transducer II was found between the laboratory calibrations of the transducers undertaken prior to deployment and after completion of the field experiment. The time or reason was not known for the zero shifts and consequently, a regression analysis was performed to account for the shifts. The regression analysis yielded a single calibration curve that was used to interpret the field data and also an error that was associated with each field data point. At a 95% confidence interval, the regression analysis error for the field data for transducer I was +/- 2.1 cm and for transducer II was +/- 1.4 cm. The magnitudes of these errors were significant in comparison to the small hydraulic head differences (averages of 0 to 1 cm using a measuring port separation of 31 cm) measured in the field by the DPS-I. The temperature fluctuations experienced by the electronic components of the DPS-I were suggested as the most likely cause of the zero shifts. The electronic components of the DPS-I (transducers, resistors, datalogger) that were positioned on the scaffold in a closed control box, experienced daily temperature fluctuations over the course of the experiment. A temperature increase from about 25^{O}C at sunrise

to 45°C in the late afternoon was recorded by a temperature probe inside the control box. The performance of transducers and resistors can be affected by temperature changes but the extent of the influence is specific to the electronic device. The potential effects of temperature for the DPS-I were not quantified.

2. **The significant noise in the field data prevented recognition of the true signal.** The significant noise present in the data collected using the DPS-I was considered to be a result of wind and wave disturbances to the exposed portions of the fluid filled tubes. The fluid in these tubes transmits the formation pressures from the measuring ports of the piezometer to the differential pressure transducers housed in the control box. The exposed tubes were shielded using stilling tubes filled with sand and flexible plastic tubing but this may not have been adequate to satisfactorily dampen the winds and wave action at the site.

3. **The small hydraulic gradients at the site were inherently difficult to resolve.** The first two tests at the site used a measuring port separation distance of 31 cm, with the bottom port at a depth of roughly 0.7 m below the seafloor. This separation distance was predetermined prior to deployments and believed to be sufficient to resolve the hydraulic head gradients at the site. The separation distance was constrained by the steel drill rods that were available in 0.3 m (1 ft) lengths. Because small hydraulic head differences were being recorded at the site that were the same magnitude as the accuracy of the DPS-I, the 31 cm port separation distance was increased for

the last two tests to 62 cm. Although larger hydraulic head differences are produced using an increased measuring port separation, the drawbacks are that the assumption of a linear hydraulic gradient between the measuring ports is more uncertain, density variations may exist preventing the application of the conventional form of Darcy's Law and the complete insertion of the piezometer may be more difficult.

4. **Early termination of testing.** Higher than expected water levels as a result of strong waves forced the removal of the control box housing the electronics and consequently early termination of measurements during the last of the four tests. The control box positioned on the scaffold above the high tide level permitted periodic collection of the DPS-I data during testing, however the electronics were also susceptible to water and other environmental damage.

3.4 Description of DPS-II

A key objective of this study was to determine the best approach that would enable accurate field measurements of the small transient changes in vertical differential pressure heads in near-shore shallow marine sediments. To achieve this goal, an attempt was made to improve the accuracy of the DPS-I by recognizing the strengths and weaknesses of the system identified during the FSMUL tests. The instrument used in this study to measure vertical differential fluid pressure heads in shallow marine sediments is a modified version of the DPS-I, referred to hereafter in this study as the DPS-II.

3.4.1 Design Overview

The main components and general installation approach of the DPS-I design were utilized by the DPS-II. However, to improve the performance of the system, particularly with respect to accuracy, the limitations of the system identified in the 2002 field experiment were addressed as follows:

1. An error analysis of the DPS- II system was completed in an attempt to identify, quantify and minimize or eliminate all known factors adversely influencing the performance of the DPS-II.
2. Modifications to the calibration procedure were carried out to improve the accuracy and reliability of the calibration curves.
3. During testing, the electronic components of the DPS-II were housed in a submersible box located on the seabed rather than on a scaffold above the high tide level. The intent of this modification was to stabilize the temperature experienced by the electronics during DPS-II deployments as well as minimize the noise associated with the movement from wind and waves of the fluid filled tubes of the DPS-II.
4. A total of nine trial type tests of the DPS-II, lasting between one and nineteen hours, were completed at near-shore locations close to UBC between May 18 and September 14, 2005. The main goals of the tests were to improve the performance of the DPS-II by identifying problems with the installation method or field data collection and implementing suitable modifications.

The DPS-II consists of two piezometers (Figure 3-5) and a submersible box that houses two differential pressure transducers, four resistors, a datalogger and a power supply (Figure 3-6). The piezometers are roughly 1 m (3.3 ft) in length and 4.5 cm (1 ¾ in) OD and are designed to permit installation by sledge hammering into sandy sediments. The piezometers are constructed of 0.3 m (1 ft) AW steel drill rods with two screened measuring ports of about 6 mm diameter, spaced 31 cm apart. The top port of the piezometer is approximately 30 cm below the seafloor, when the piezometer is inserted into the seabed. The depth to the top port (30 cm) corresponded to the length of a drill rod section that is added above the top port of the piezometer. The 30 cm distance between the seabed and the top port of the piezometer was assumed to be a sufficient depth to allow for pressure perturbations caused by small waves to attenuate and not affect the fluid pressure measurements at the top measuring port (i.e., the top port of the piezometer is assumed to be affected by sea level fluctuations caused by tides but not small passing waves). Formation pressures are transmitted from the top and bottom ports of the piezometer, via fluid-filled, low density polyethylene tubes to a capacitance type differential pressure transducer (manufactured by Setra Systems, model 230, range +/- 0.5 PSI) housed inside a submersible box placed on the seabed (Figure 3-7). Valves located near the positions of the transducers in the submersible box, prevent the deaired water from draining out of the plastic tubes in the field set up of the DPS-II.

Deaired water is used as the hydraulic fluid to minimize the likelihood of air bubbles and thus discontinuities in the fluid filled tubes that can cause erroneous differential fluid pressure head measurements. The effect of air bubbles on measurements by the DPS-II is discussed in detail in the error analysis of the instrument (section 3.5). Deaired water is prepared by reducing the dissolved gas content (i.e. de-airing) of Vancouver tap water using an instrument called the Nold Deaerator, shown in Figure 3-8. The Nold Deaerator consists of a sealed tank, electric motor, impeller and water powered aspirator and operates by mechanical agitation with the application of a vacuum. The agitation/vacuum system is significantly more efficient at removing dissolved gases from water than conventional boiling methods. The dissolved oxygen (DO) level of six litres of water was reduced from air saturation (about 8 ppm) to 1-2 ppm in about 5 minutes using the Nold Deaerator. The deaired water is stored in completely filled 4L glass containers.

The differential fluid pressure values over which the differential pressure transducers of the DPS-II are intended to measure (i.e., range) is specified by the manufacturer specifications as +/- 0.5 PSID. An explanation of the terminology used by the manufacturer specification to express the range of the transducer is required. Differential transducers are designed to simultaneously measure two independent pressure sources; the output is proportional to the pressure difference between the two sources. The +/- part of the expression for the range of the transducer indicates that the greater input pressure can be applied to

either pressure port (i.e., a bidirectional transducer). The value of the highest differential pressure the transducer is designed to measure is 0.5 PSI, which converts to a differential fluid pressure head of 35 cm of water at $4^{O}C$. A standard temperature used to express pressure in terms of centimetres of water is $4^{O}C$. There are insignificant changes in the conversion between pressure in terms of PSI and centimetres of water when the density of water (e.g., fresh vs. seawater) and/or temperature of the water (e.g., $4^{O}C$ vs. room temperature) are considered. From hereafter in this study, fluid pressure head expressed in terms of centimetres of water will omit the reference to $4^{O}C$. The letter D that follows the PSI term refers to differential for the type of pressure transducer.

3.4.2 Data Acquisition System

Data from the differential pressure transducers are recorded with a 16 bit channel datalogger (CR10X manufactured by Campbell Scientific). Four 10 K Ohm resistors (1/4 Watt, +/- 2% tolerance, manufactured by NTE) create a voltage divider that provides a common range over which the transducers can transmit and the datalogger can receive data. A 12 volt rechargeable lead acid battery provides the necessary electrical voltage for the operation of the transducers and datalogger. A differential pressure measurement is obtained by comparing the pressure at the high pressure side relative to the low pressure side of the differential pressure transducer. Therefore, if the high pressure side of the transducer is coupled to the bottom piezometer port, an upward pressure

gradient is indicated when positive differential pressure measurements are recorded.

3.4.3 Differential Fluid Pressure Heads from Transducers

The differential pressure transducers output a linear voltage that is proportional to the applied pressure. The voltage outputs of the transducer recorded in the field are related to differential fluid pressure heads ($d\psi$) using a calibration curve. The outputs of the transducer could have been related to another expression for pressure (e.g., PSI), but the choice of pressure head was a result of using the difference between the heights of columns of water to apply the differential pressures to the transducers to develop the calibration curves. The term calibration, when used in association with transducers, refers to a test during which a known value is applied to the input of the transducer for the purpose of observing the system output. By the application of a range of known values to the input and observation of the system output, a calibration curve for the measurement system is developed. Details of the calibration procedure are found in Appendix A. The general calibration curve is represented by the following form:

$$V = C \times d\Psi + V_0 \qquad \text{(Equation 3.4)}$$

where V is the voltage output of the differential pressure transducer, C is the calibration factor (slope of the best fit line), $d\psi$ is the applied differential pressure head to the transducer, and V_o is the voltage output corresponding to an applied differential pressure head equal to zero.

As a result of the measurement system including two differential pressure transducers (each corresponding to a piezometer) with independent inputs and outputs, a unique calibration curve was developed for each transducer. The calibration curves developed before and after deployments are used to interpret the voltage output recorded by the DPS-II in the field as differential fluid pressure head (Figures 3.9 and 3.10). There is typically no significant difference between the calibrations completed prior to and after deployment. The average of the calibration curves developed for each transducer (differentiated in this study as transducer A and B) before and after the field deployment in this study were $y = 35.4x + 1220$ for transducer A and $y = 35.5x + 1478$ for transducer B. The y-intercepts of the calibration curves for the transducers are different due to the unique conditions for each transducer such as the manufacturing process, material components, previous working conditions and age.

During calibration of the DPS-II, known fluid pressure heads are applied directly to the pressure sides of the differential pressure transducers using columns of waters as opposed to the loading of the transducers in the field configuration, where pressures are applied to the sensing element of the transducer via fluid filled tubes (Figure 3.11). The method for calibration was chosen because of the ease of implementing in the laboratory and relatively high accuracy of the calibration method. However, in the field configuration, the fluid filled tubes exert a constant differential pressure on the pressure sides of the transducer that is not accounted for when the calibration curves are directly used to relate the voltage

output from the transducers to differential pressure head. The constant differential pressure head caused by the fluid filled tubes is a result of the vacuum conditions that are created by the valves preventing the deaired water in the tubes from draining under gravity and is equal in magnitude to the vertical distance between the measuring ports of the piezometer. The constant differential pressure head of -31 cm exerted on the transducers was observed during laboratory tests using the DPS-II. In the laboratory, with the bottom measuring port of the piezometers connected to the high pressure side of the transducer and both measuring ports open to the atmosphere, a constant differential pressure head of -31 cm was recorded as the output when an output of 0 would have been expected considering only the pressures acting on the measuring ports of the piezometer (based on a port separation of 31 cm and a vertical orientation of the piezometer). When the piezometer was placed in a bucket of saturated sand with both measuring ports of the piezometer within the sediment, the differential pressure head output recorded was zero (output of 31 cm expected).

After the DPS-II has been deployed in the field, the voltage outputs of the transducer are converted to differential fluid pressure heads using the calibration curves. To yield only the differential fluid pressure heads contributed by the formation pressures in the field, 31 cm is added to each differential fluid pressure head measurement to correct for the constant differential pressure exerted by the fluid filled tubes.

3.4.4 Deployment

A small inflatable boat was used for the deployment of the DPS-II during this study. The equipment used for deployment was positioned inside the boat and the piezometers were driven into the seabed off the side of the boat while they were attached through the plastic tubes to the differential pressure transducers mounted inside the submersible box (Figures 3-12 and 3-13). The total time required for the complete deployment (not including preparations at the field site) of the DPS-II is on average 0.5 to 1 hour. To ensure the collection of valid data, the following sequence of steps for deployment is completed:

1. *Piezometer Assembly*
2. *Piezometer Insertion*
3. *Bleeding of the Pressure Ports of the Transducer*
4. *Submersion of Data Acquisition Components*
5. *Differential Pressure Head Response*

Piezometer Assembly

Both piezometers are constructed in the laboratory prior to field deployment as shown by Figure 3-5.

Piezometer Insertion

For the purposes of data comparison and reliability, differential pressure heads are recorded between the measuring ports of two piezometers. If required, the DPS-II can be deployed using only one piezometer. Typically the piezometers

are inserted reasonably quickly (5-10 minutes) into fine grained to sandy sediments by sledge hammering. This installation technique may not be practical for some coarse grained sediments because small sized stones may make it difficult to insert a drive point piezometer.

In this study, insertion of the piezometers is at low tide, when the water level is at or near the sediment surface. The hydraulic tubes leading from the measuring ports of the piezometers are connected to the pressure sides of the differential pressure transducers through the submersible box using swagelok fittings. Deaired water is pumped using a peristaltic pump (Masterflex portable sampler manufactured by Cole Palmer) from a 4L glass container through the manifold in the submersible box past the pressure sides of the transducer and through the plastic tubes until the water exits out the measuring ports of the piezometer (Figure 3-14). De-aired water is pumped through the system to prevent the measuring ports from clogging with sediment, while the piezometer is held vertically and hammered into the seabed.

Deployment of the DPS-II at high tide was attempted in a preliminary test using the DPS-II, however several difficulties were encountered because of the higher water levels that were: (1) the distance from shore the DPS-II could be installed was restricted and consequently the piezometers was inserted closer to shore and became uncovered (preventing measurements) during the succeeding low tide, (2) the sediment closer to shoreline at high tide was coarser than a few

meters seaward and hammering the drive point piezometers into the sediment was difficult because of obstruction from small rocks, (3) a longer piezometer (greater than 1 m) would have been more appropriate to permit the top measuring port of the piezometer to be driven to a sufficient depth (top port 30 cm below the seabed) without hammering the piezometer below the water level, (4) longer lengths of tubing between the transducers and pressure measuring ports of the transducer were required during deployment which could cause the DPS-II system to be more prone to noise from the random motions of the tubing, however the test did not last long enough to investigate noise from tubing movement and, (5) submersing the box housing the data acquisition components of the DPS-II on the seabed following the insertion of the piezometers had be done underwater and was cumbersome.

Bleeding of the Pressure Ports of the Transducer

Air bubbles in the plastic fluid filled tubes of the DPS-II that are used to hydraulically transmit the formation pressure to the transducers and/or the pressure cavities (the space that is exposed to fluid and is in contact with the diaphragm of the transducer) of the transducers can cause measurement artefacts. The bleeding of the pressure ports of the transducers allow air bubbles to escape from the fluid filled tubes or pressure cavities of the transducer. After a piezometer has been driven into the sediment, the pressure ports of the transducer hydraulically connected to the installed piezometer are immediately bled. Deaired water is continuously pumped through the system to pressurize the

differential pressure transducers, while the pressure ports of the transducer are bled. The procedure involves backing off the bleed screws until only bubble free liquid flows out. The Setra model 230 transducer installation guide provides information about bleeding the pressure ports of the transducer. After the pressure ports of the transducer have been bled, the two valves on the manifold leading to that transducer are closed and the pumping of deaired water through the lines of that transducer is stopped. The two valves regulating flow to the other transducer are then opened and the insertion of the second piezometer is started. Once both piezometers have been installed, the power source is connected to initiate differential pressure head measurements and the data acquisition components are sealed in the submersible box and submerged.

Submersion of Data Acquisition Components

The box housing the electronic components of the DPS-II is constructed of 1.9 cm (0.75 in) thick PVC plastic. The lid of the box has an o-ring fitted into a groove within the bottom of the lid and is secured to the base of the box, using 24 bolts, to provide a water proof seal for shallow water deployments of the DPS-II. To submerse the box on the seabed the box is strapped in a steel crate, machined to fit the dimensions of the box. The bottom of the steel crate is weighted down using lead shots stored in sealed plastic containers. The steel crate holding the control box is positioned at approximately a meter away from the inserted piezometers to minimize any measurement artefacts caused by the possibility of flow perturbations resulting from the heavy lead weights and/or surface area of

the box and crate. The exposed portion of the two fluid filled tubes leading to each piezometer from a differential pressure transducer in the submersible box is bound together using zip ties to minimize random movements of the hydraulic tubes.

Differential Pressure Response

Differential fluid pressure head data is collected during this stage of the deployment. The beginning portion of the field data sets by the DPS-II (up to 1-1.5 hours) may be omitted to account for disturbances caused by working in the water after installation. Often the deployment of other instruments (e.g., seepage meter) nearby the installed DPS-II is completed after DPS-II measurements have been initiated.

3.5 Error Analysis

An important part of the development of the DPS-II included efforts to minimize the error associated with measurements by the DPS-II and evaluating a reliable estimate of the upper bound of the errors. Dunnicliff (1989) examines the various types of errors that can affect field measurements and provides suggestion of how they may be minimized. The fundamental performance characteristics of transducers and also design related considerations are addressed by Horton (1989). The measurements by the DPS-II are affected by three main types of errors: (1) systematic errors, that refer to an error that is present for every measurement and may be caused by an observation bias, calibration etc., (2)

random errors, which are a result of random fluctuations in the measured value that yield different results each time the measurement is repeated, and (3) conformance errors, caused by the instrument altering the parameter being measured (e.g., drainage paths along the piezometer that reduce measured differential fluid pressure heads below the "true" value).

Sources of errors have been identified in the development of the DPS-II. As shown by Figure 3-15, sources of errors were categorized based on the main stages of DPS-II development that are: (1) choice of instrument, which considers the accuracy of the two Setra model 230 differential pressure transducers that were used in the design of the DPS-II, (2) calibration of the transducers, which is particularly important since the calibration of the earlier version of the DPS-II (DPS-I) was a significant issue pertaining to the poor quality of data obtained using the tool (section 3.3), (3) deployment of the DPS-II, which is one of the most difficult aspect of the error analysis because to identify and/or quantify the errors requires the most experience using the tool, and (4) site conditions, which examines the environmental conditions (e.g., temperature fluctuations, wind and waves) that could adversely affect the DPS-II measurements. The key factors regarding the performance of the DPS-II have been identified within each of the DPS-II stages of development and are discussed in more detail below.

Choice of electronic instruments

The two Setra 230 differential pressure transducers were chosen for use in the design of the DPS-II because they met several constraints relating to the field measurement of differential fluid pressure heads such as a suitable measurement range, relatively high accuracy and reasonable cost. In addition, the Setra 230 differential pressure transducers were a convenient choice as two of these transducers were already available from the design of DPS-I. Two additional Setra 230 differential pressure transducers have since been purchased (one transducer from the DPS-I malfunctioned during laboratory tests in this study and the other is used as an extra) and consequently the transducers used in this experiment were not the ones from the DPS-I.

The accuracy of the differential pressure transducers used by the DPS-II is expressed by the manufacturer specifications as the combined error of non-linearity, non-repeatability, and hysteresis with a value of +/- 0.25 % FS. The FS of the transducers is 1 PSI, which converts to a pressure head of 70 cm of water. The corresponding accuracy for the given FS of the differential pressure transducers is +/- 0.2 mm of water. Non-linearity, non-repeatability and hysterisis are defined as follows: (1) non-linearity is the maximum deviation of the calibration curve from a specified straight line, (2) non-repeatability refers to the ability of the transducer to reproduce output readings when the same measurement value is applied to it consecutively under the same conditions and, (3) hysterisis, is the maximum difference in output at any measurement value,

within a specified range, when the value is approached first with an increasing and then with decreasing measurement values. Since the accuracy and precision of the calibration curve used to interpret the field data is affected by non-linearity and non-repeatability and the field measurements of differential pressure head show that the transducer is loaded by an increasing and decreasing pattern, all three measures of the performance of the transducers are relevant. Manufacturer specifications of pressure transducers are a general guide for the performance characteristics of a given model of differential pressure transducer. For the basis of comparison with the manufacturing specifications, a laboratory test, which assessed the non-linearity, non-repeatability and hysterisis characteristics of the differential pressure transducers used by the DPS-II, was performed at room conditions. The test was carried out by loading the transducers with slow changes in differential pressure head over the full range of the transducer, unloading the transducer and than immediately re-loading the transducer (Figure 3-16). The loading, unloading and reloading curves, (which are fitted to a best fit line) were all linear and in close agreement, reflecting an accuracy in good correspondence or better than the manufacturer specifications of accuracy of +/- 2 mm.

Drift is a common characteristic of transducers and can be a problem for obtaining high accuracy measurements, however the extent of the drift experienced by a transducer is specific to the type and testing conditions of a particular transducer. Defined as the change in output under constant loading

conditions, drift may occur due to several factors such as a change in voltage supply. Drift was characterized by measuring an applied zero differential pressure head to the transducers every 1 s for 24 hrs at room conditions. Figure 3-17 shows the 1 s measurements over the first 8 hours of the experiment. The variation in the output of the transducers is about 0.3 cm. Figure 3-18 shows 1 minute averages of the 1 s measurements over the entire experiment. It should be noted that for each plot the measurement values are rounded to the nearest mm.

Calibration

The errors of the calibration method completed at room conditions are: (1) an error of +/-1 mm that is associated with reading the applied differential pressure head using the rulers attached beside the water columns during calibration of the transducers, (2) the accuracy of the transducers that are specified (and supported by lab tests) as about +/- 2 mm, and (3) variations in the output of the systems between +/-1 to 3 mm for a given applied input caused by slight changes in the shape of the meniscus of the water columns used to apply the differential pressures to the pressure sides of the transducers. To provide consistency between calibrations an effort was made to maintain the same shape of meniscus at each applied pressure using the water columns. Given that the shape of the meniscus can cause variations of +/- 3 mm, by maintaining a consistent meniscus, the calibration curves may have a bias of +/- 3 mm. The

accuracy of the calibration curves developed for each transducer was thus estimated as +/- 3 mm (the largest error associated with the calibration method).

The repeatability of the calibration method is about +/- 1 mm. Calibrations completed within a few days and sometimes weeks (even after they have been deployed in the field and susceptible to stress) are within +/- 1 mm (Table 3-1).

Deployment

An air bubble of sufficient size in the vertical segment of the fluid filled tubes of the DPS-II can cause erroneous measurements. A few small pin sized bubbles about the diameter of 1 mm or less in the tubing of the DPS-II did not appear to be significant during testing in the laboratory, although numerous bubbles of this size could form a larger air bubble. At each air/water meniscus, surface tensions cause the air bubbles to be at a slightly higher pressure than the water and these air/water menisci oppose the transmission of the formation pressure causing a pressure different than the formation pressure to be sensed by the transducer. As well, the contraction or movement of air bubbles in the system can cause fluid motion that can produce false changes in formation pressure head measurements. Errors on the order of at least centimetres were recorded during laboratory tests when air bubbles were visible within the system. The primary methods used to reduce the likelihood of air bubbles in the fluid filled tubes are: (1) the use of deaired tap water as the fluid in the hydraulic tubes, (2) colouring the deaired water with a dye to easily observe air bubbles in the visible portions

of the fluid filled plastic tubes of the DPS-II (i.e., the tubing not enclosed by the piezometers), and (3) bleeding of the pressure ports of the transducers during deployment of the DPS-II to eliminate air in the hydraulic tubing and pressure cavities of the transducers. No air bubbles were observed in the visible portions of the fluid filled plastic tubes either after installation of the DPS-II or completion of the field deployment.

During the insertion of the piezometers in the seabed, deaired water is constantly pumped out the measuring ports of the piezometer to prevent sediment from clogging the ports. Although clogged ports, itself, may not interfere with the measurement of differential fluid pressure, if the sediment clogging the ports is of a significantly lower hydraulic conductivity than the surrounding sediment at the installation depth, false measurements of differential pressure may be recorded. There is no method to determine if clogged ports are a source of error during field tests. Increasing the rate of flow discharging from the ports during installation of the piezometers may minimize the potential for clogged ports. A higher flow rate, however, increases the likelihood of creating temporary drainage paths along the sides of the piezometers that would reduce the measured differential fluid pressures to below the "true" value. Water that is pumped out of the piezometer ports at a higher rate than can be easily transmitted through the formation sediment will likely flow along the side of the piezometer. The discharge of water at the surface of the seabed from along the piezometer has been observed during installation of the piezometers in the

preliminary field deployments and during the deployment in this study (Figure 3-19). It is assumed that if preferential flow paths are created during installation they will be eliminated over a short period of time due to the relatively permeable marine sediment and dynamic action of the waves that will likely cause the sediment to collapse against the piezometers.

An aspect of the installation method that has not been satisfactorily addressed is whether the act of inserting the piezometers causes a significant increase in fluid pressures in the sediment and if so the length of time required for dissipation of the fluid pressure spike. Because of the relatively slow rate of installation, small diameter of the piezometer and the permeable marine sediment, installing the piezometers likely does not cause a significant insertion pressure. No measurements of fluid pressures in the seabed have been made to monitor fluid pressures during piezometer insertion. It may be difficult to use the differential fluid pressure measurements by the DPS-II, even if a long data set was obtained (e.g. 7 days), to observe if there is a decline in fluid pressure in the seabed over time after the installation of the piezometers, because the measurements are differential.

Site Conditions

A deployment configuration has been chosen that would minimize the extent of environmental sources of errors. The box housing the electronic components of the DPS-II was submerged on the seabed, thus providing fairly stable temperature conditions for the electronics. Because both the zero output and

sensitivity of the differential pressure transducers can change with temperature, a stable temperature environment ensures the most stable measurements. It should be stressed the resistors used in the configuration of the electronics of the DPS-II are also susceptible to changes in performance given a change in temperature. Because the calibration curves for the measurements by the DPS-II are developed at room conditions but the tool is used at temperatures away from room temperature in most cases, the calibration curves need to be corrected, if temperature has a significant effect on the output of the transducers.

The operating temperature range of the differential pressure transducers is from –18 to 80^{O}C, which indicates the limits within which the transducer will not be damaged. The compensated temperature range, -1 to 65^{O}C, is the range in which the pressure transducer will meet the specifications for zero and sensitivity (slope of calibration curve) shift as given in the data sheets. The thermal effects of the transducers have been compensated by the manufacturer to reduce the thermal zero and sensitivity shift to a maximum of + 2 % FS (+1.4 cm of water) given a change in operating temperature between 0 - 50^{O}C from room temperature. To restate in another way, the thermal specification indicate that the maximum shift that could be expected is + 1.4 cm (although the shift could be less) and could occur for a temperature change of 1^{O}C or 50^{O}C from room temperature, depending on the transducer. Because of variations such as material properties and manufacturing processes, the performance of a group of the Setra 230 differential pressure transducers will scatter about the stated

thermal specifications. The manufacturer of the differential pressure transducers does not characterize the thermal effects of individual transducers because of the time and labour involved in the calibration process of numerous transducers. A shift in the zero and/or sensitivity of the transducer output because of a temperature change is not permanent (i.e., the output of the transducer may shift at different temperatures but should output the same value at a given temperature if all other conditions are constant).

The temperature inside the submersed box housing the data acquisition components of the DPS-II during the field test in this study was recorded using the internal temperature of the datalogger. The temperature inside the submersed box stabilized at about 11 ^{O}C after about 8 hours from the start of the test (Figure 3-20). The period between 22 to 32 hours during field test, showed lower temperatures that corresponded to the time the submersible box housing the electronics was uncovered by a low tide.

The performance of the transducers and resistors of the DPS-II at conditions away from room temperature was investigated by comparing the calibration curves of the transducers developed: (1) at room temperature (23^{O}C), (2) in a cold room set to a temperature between 11 to 13^{O}C, and (3) in a cold room set to 5 ^{O}C. The calibration tests were completed over three days, with a test at a given temperature carried out on each day. Before the calibrations in each cold room were started, the transducers, resistors and datalogger were placed in the cold

room for 4 hours to permit the temperature of the electronics to reach the testing temperature. The reason for not placing the instrument in the room for 8 hours (the time required for the instruments to reach a stable temperature in the field experiment in this study) was because the key objective at the time of the tests was not to simulate the exact conditions during the field deployment but to gain insight about the effect of temperature on the output of the transducers. Also the cold rooms were located in a room accessible to all individuals in the building, requiring constant supervision of the electronics, and consequently the amount of time chosen to leave the electronics in the room was also a practical consideration. Four hours was sufficient time to permit the transducer to reach the approximate temperature of the cold rooms. For the experiments, the electronics were housed in the submersible box that is used for the field deployments but the box remained uncovered. After the 4 hours had elapsed, the internal temperature of the datalogger was measuring a temperature 2-3^{O}C higher than the expected ambient temperatures in both the 11-13^{O}C and 5 ^{O}C cold rooms. The slightly higher temperatures measured by the CR10X may have been because the expected temperatures of the cold rooms were not exact. No independent measurement was obtained of the temperature in either of the cold rooms. Also there is an error associated with the internal temperature measurement by the CR10X of about +/- 0.5 ^{O}C (Campbell Scientific personal communication). The transducers were loaded, unloaded and reloaded over the entire range of the transducer for the calibrations tests at room temperature and in the 11-13 ^{O}C cold room. The purpose of the loading, unloading and reloading

was to complete several calibrations and thus improve the reliability of the calibrations curves at the specified temperature. Other than it is slightly more time efficient, as a result of not having to refill the water columns after each calibration, no additional benefit or information was gained by the approach of loading, unloading and reloading the transducer as opposed to loading the transducer three times.

The calibration test in the 5^{O}C cold room was completed by twice loading the transducers. The different calibration method used in the 5^{O}C cold room was a result of the significant variations (e.g., +/- 5 mm) in the output of the transducers that were observed when loading each of the transducers. Instead of unloading and reloading the transducers to produce additional calibration curves for comparison at that temperature, as in the calibration test in the 11-13^{O}C cold room, the entire calibration process was begun again. Deaired water was pumped through the system and the pressure ports of the transducers rebled before the transducer was again loaded. The purpose for beginning the calibration process from the start for the second calibration was to ensure the noise in the output was not from air bubbles present in the pressure cavities of the transducer. Because both of the loading curves for each transducer were affected by variations in the output of the transducer, the noise was likely caused by vibrations of the water in the water columns of the calibration stand, caused by continuously operating fans in the room that prevented the applied pressure from remaining constant. Typically during a calibration test, the outputs of the

applied pressures to the transducer are recorded from real time data. Because of the noise in the output (+/- 5 mm) during the calibrations in the 5^{O}C room, it was more difficult to read an exact output for the applied pressures (usually output variations are +/- 1 mm or less). Consequently, the average observed output value over about a minute was used to develop the calibration curves. Although there was noise in the output for both the transducers in the 5^{O}C cold room, the variations in output were higher and not as consistent for transducer B making it more difficult to assess an average output value for a given applied differential pressure. As a result, a calibration curve could not be developed for transducer B. Transducer B was closer than transducer A to the closest two fans in the cold room (about 30 cm away), which may account for the more significant noise. An effort to shield the water columns of the calibration stand from the wind produced by the fans, did not reduce the noise in the output of Transducer B.

Table 3-2 shows the calibration curves developed at each of the testing temperatures. The discrepancies between the calibration curves at room conditions and in the 11-13^{O}C cold room showed a shift of +1 mm in output for transducer A and no measurable change for transducer B. The discrepancy between the calibration at room temperature and in the 5^{O}C cold room for transducer A was +3 mm. No change could be noted at transducer B because a calibration curve was not developed as discussed earlier. Although there may be a bias associated with the accuracy of the calibration curves of about +/- 3 mm, the accuracy of the transducers is +/- 2 mm or better. Also in general the

repeatability of calibration curves is within +/- 1 mm as shown by Table 3-1. The discrepancy of +3 mm is larger than would be typically expected for calibrations completed within days apart. The accuracy of measurements that is required to measure the changes in differential pressure at some coastal sites, require all sources of error at this order of magnitude be identified. A potential cause for the calibration shift is because of errors reading the output of the transducer due to the significant variations in output of the transducer. Given that both calibration curves developed for the transducer in the 5^{O}C cold room showed the same magnitude of shift, errors in the reading of the output are a less likely source for the shift. Another potential explanation for the shift in output is the decrease in temperature.

The calibration tests completed at room temperature, and in the 11-13^{O}C and 5^{O}C cold rooms aided with better constraining the magnitude of the shift that may be caused by temperature changes. The tests showed that the potential maximum shift of +1.4 cm from thermal effects that is specified by the manufacturer's specifications for the transducers does not occur for a decrease in temperature of almost 15^{O}C from room temperature and that the zero shift may be closer to +3 mm (at least for transducer A). However, the + 3 mm shift experienced between the calibration tests completed at room temperature and 5^{O}C tests has not been clearly identified as a result of temperature change. It should be noted that the effects of temperature on the output of the DPS-II could change as the transducers and resistors age.

In addition to stabilizing the temperature of the electronics, submersing the electronic components of the DPS-II on the seabed aids with minimizing the motion of the fluid filled tubes of the DPS-II from wind and wave effects. The random fluctuations in the output of the DPS-II caused by wind and waves were also reduced by averaging the 1s measurements of differential pressure head by the DPS-II over a minute. Figures 3-21 and 3-22 shows the variation in output of the DPS-II at 1 second measurements for 10 minute periods of testing taken at the highest high tide (2.3 m of water above the seabed) and the lowest low tide (75 cm of water above the seabed). The variation in the 1 s measurements of the DPS-II was about +/- 0.4 cm at both piezometer A and piezometer B at the highest water level and increased by a factor of two to +/- 0.8 cm at piezometer A and by an order of magnitude to +/- 2 cm at piezometer B during the lowest low tide. Because of the time of day the lowest low tide occurred (10 pm), it was difficult to observe the condition of the DPS-II. The observations of the DPS-II at the lowest low tide were taken over a 30 minute period at the time of predicted low tide, from on shore (about 20 m away from the instruments) because the darkness, rough waves and high water levels at the site prevented entering the water. From observations of the DPS-II during the low tide, a portion of the plastic fluid filled tubes of the DPS-II, likely the section of tubing that comes out from the top of the piezometers, could be seen to be periodically uncovered by passing waves. The uncovered tubes would have been susceptible to movement from the wind in addition to the waves and may explain the larger variations in

output at low tide than at high tide. The greater variation in the output at low tide at piezometer B than at piezometer A may have been a result of the greater length of exposed tubes at piezometer B (about 30-50 cm longer), that are used to hydraulically connect the measuring ports of the piezometer to the transducers in the submersible box (Figure 3-7). The piezometers are prepared in the lab prior to deployment and excess tubing is left leading from the measuring ports of the piezometers to permit the tubes to be connected to the transducers in the field prior to insertion of the piezometers. Typically, the excess tubing from the piezometer is shortened in the field before a connection is made to the transducers. More effort could be made in the field to ensure a closer agreement between the lengths of exposed tubing for each piezometer, which may provide more consistency between the measurements at each piezometer. The exposed portions of the lengths of tubes at each piezometer were not measured in this study but were about 1-1.5 m. The length of tubing was more than sufficient (could have used 0.5 m less tubing at each piezometer) to position the submersible box with the transducers, on the seabed away from the piezometers.

3.5.1 Error Estimate

The error associated with the differential pressure head measurements by the DPS-II was estimated as +/- 3 mm. The error estimate was calculated based on the largest error that was estimated for the calibration method. The error estimate of the differential fluid pressure head measurements is likely an underestimate, given the uncertainty associated with several aspects of the DPS-II design during

field deployments. The largest sources of uncertainties with the field deployment is the possibility of a temporary calibration shift due to temperature fluctuations during deployment, the potential for clogged ports (for which there is currently no method to detect) and the formation of drainage paths along the sides of the piezometers and/or a transient excess pressure during insertion. Given the 1D modelling that showed a fairly good agreement with the measurements by the DPS-II (section 5.2), and also considering the temperature tests which showed little shift due to temperature changes and relatively high permeability of the sediment combined with wave action at the site (making conditions less likely for drainage paths and/or insertion pressures to be maintained) the error estimate of +/- 3 mm, likely only slightly underestimates the error of the DPS-II measurements. More experience using the tool in the field would increase the confidence associated with the estimate of error. Several recommendations have been proposed in section 6.2, to better constrain the error estimate.

If a uniform density flow field is assumed, the differential pressure head measurements by the DPS-II can be used to calculate the magnitude and direction of hydraulic head gradients in the shallow marine sediment. The difference in hydraulic head between the measuring ports of a piezometer of the DPS-II can be calculated based on the measured differential fluid pressure heads by the DPS-II and the distance between the measuring ports of the piezometer using the following relationship:

$$dh = d\psi + dz \qquad \text{(Equation 3.5)}$$

The first term on the right side of Equation 3.5 represents the measurements of differential pressure head by the DPS-II. The error associated with the calculated difference in hydraulic head values is equivalent to the error of the differential fluid pressure head measurements (+/- 3 mm).

Hydraulic gradients based on the differences in hydraulic head can be calculated according to the following equation:

$$\nabla h = \frac{dh}{dz} \qquad \text{(Equation 3.6)}$$

An error of 0.01 is estimated for the calculated hydraulic gradients values, derived using the rule of error propagation (Taylor 1997) that is expressed for the general relationship defined as z = y/x and written as:

$$\Delta z = |z| \cdot \sqrt{\left(\frac{\Delta x}{x}\right)^2 + \left(\frac{\Delta y}{y}\right)^2} \qquad \text{(Equation 3.7)}$$

where Δz is the absolute error associated with quotient (i.e. hydraulic gradient), Δx is the absolute error of the dividend (i.e. distance between the measuring ports of the piezometer) and Δy is the absolute term of the divisor (i.e. difference in hydraulic head).

Date of Calibration Test	Transducer B	Transducer C
August 15, 2005	y = 35.7x + 1470	y = 35.0x + 1658
August 23, 2005	y = 35.5x + 1469	y = 34.8x + 1660
September 1, 2005	y = 35.6x + 1472	y = 34.8x + 1664
September 14, 2005	y = 35.5x + 1471	y = 35.0x + 1667

Table 3-1: Calibration curves completed several days to weeks apart typical show variation less than +/- 1-2 mm. Transducer C was used in the DPS-II prior to the transducer being replaced by Transducer A.

Date of Test	Calibration Temperature (^{O}C)	Calibration Curve	Transducer A	Transducer B
5/9/05	23	I	y = 35.6x + 1224	y = 35.5x +1478
		II	y = 35.5x + 1228	y = 35.4x + 1479
		III	y = 35.5x + 1227	y = 35.3x+ 1477
		Average		
5/10/05	14-15	I	y = 35.7x + 1229	y = 35.4x + 1479
		II	y = 35.8x + 1229	y = 35.5x + 1478
		III	y = 35.8x + 1232	y = 35.5x + 1479
		Average		
5/11/05	7-8	I	y = 35.7x + 1238	N/A
		II	y = 35.6x + 1236	N/A
		Average	y = 35.6x + 1237	

Table 3-2: Calibration curves developed at different temperatures to investigate the effect of temperature on the electronic components of the DPS-II. Calibration curves were not developed for transducer B at 7- 8^{O}C because of significant noise in the output of the transducer.

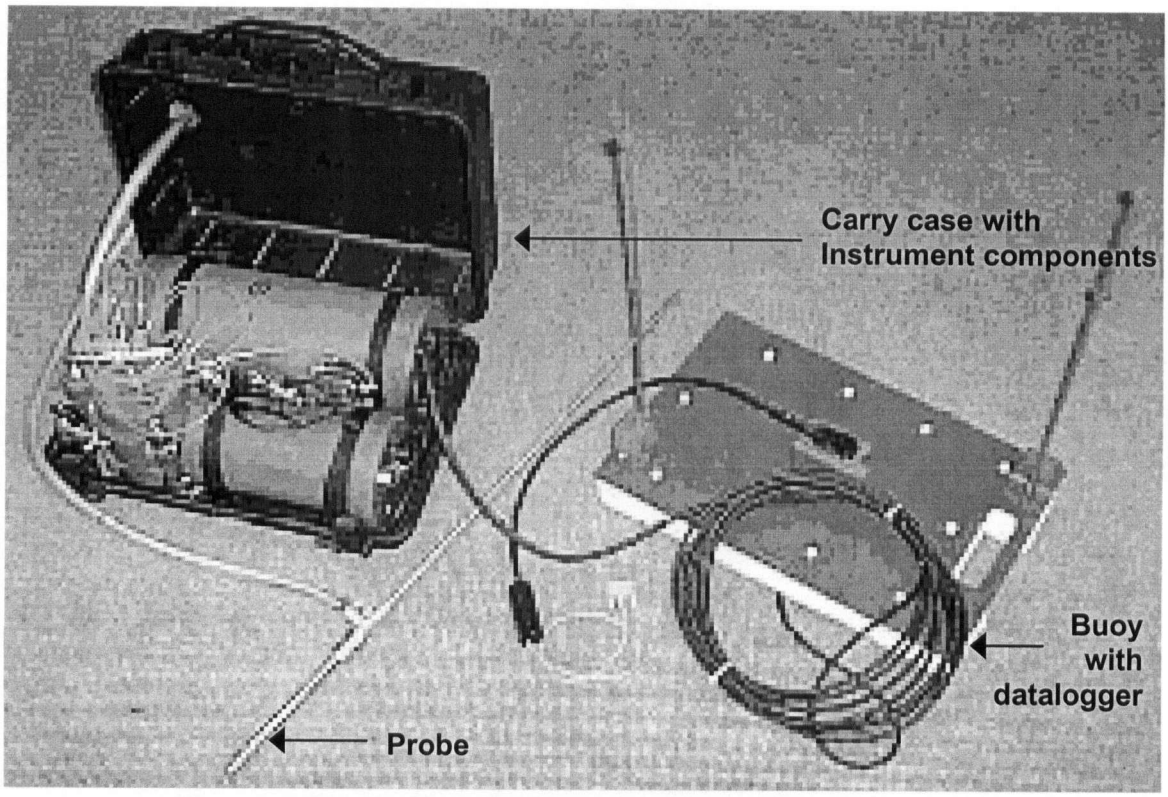

Figure 3-1: The PISSPI-3 developed at the University of Lehigh (photo provided by B.Carson).

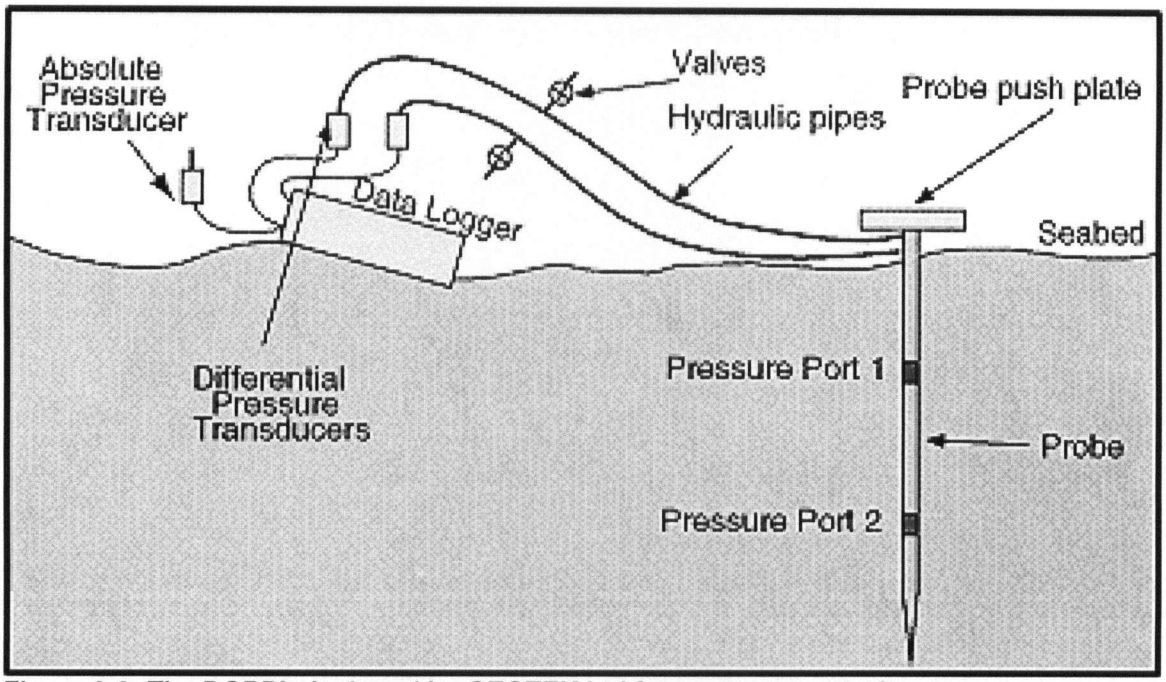

Figure 3-2: The DOPPI, designed by GEOTEK Ltd for measurement of pore water pressure in shallow marine sediment. (schematic provided by GEOTEK Ltd.).

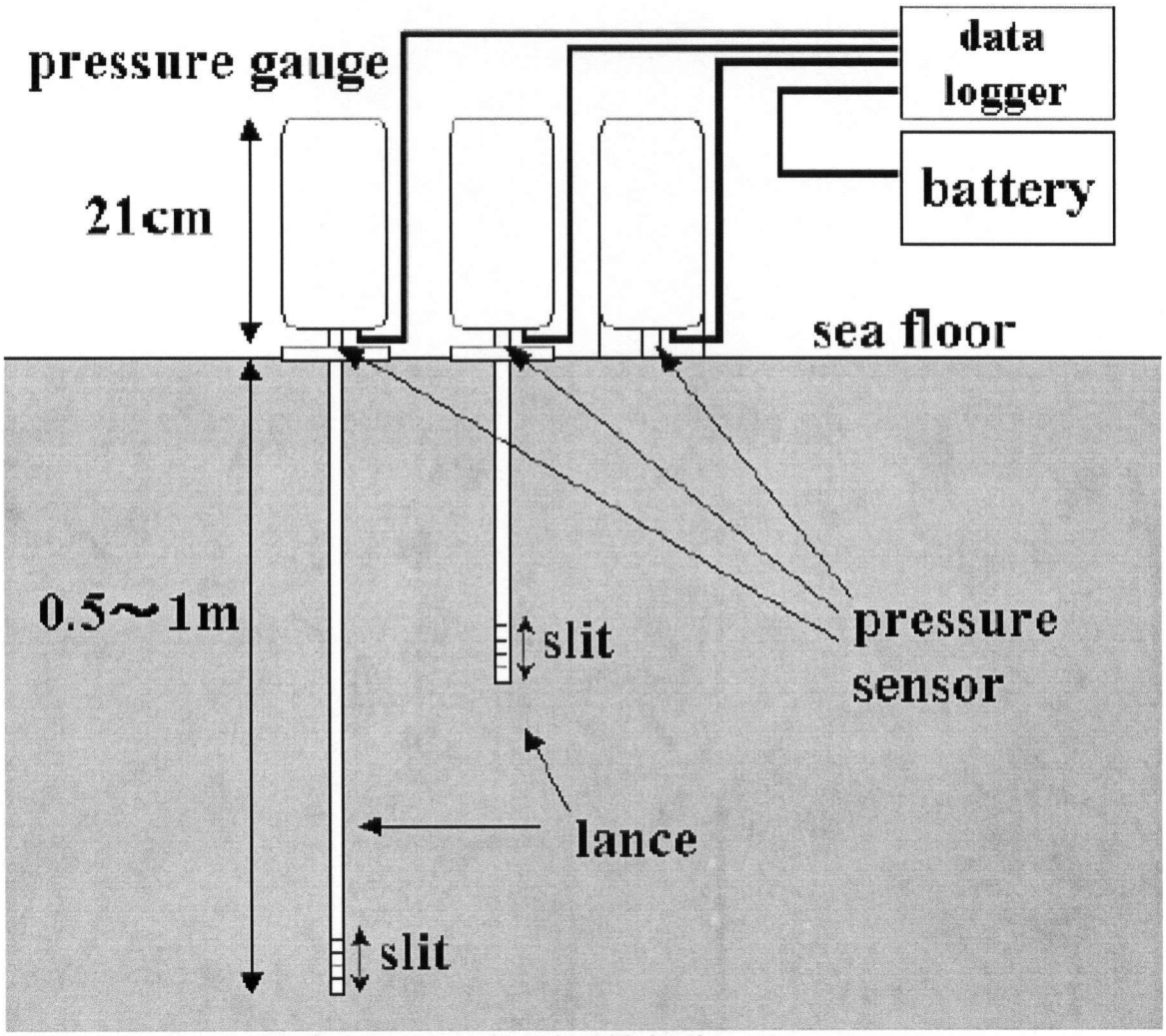

Figure 3-3: Schematic of a newly developed multi-depth pore pressure measurement device by Urakoshi et al. (2005).

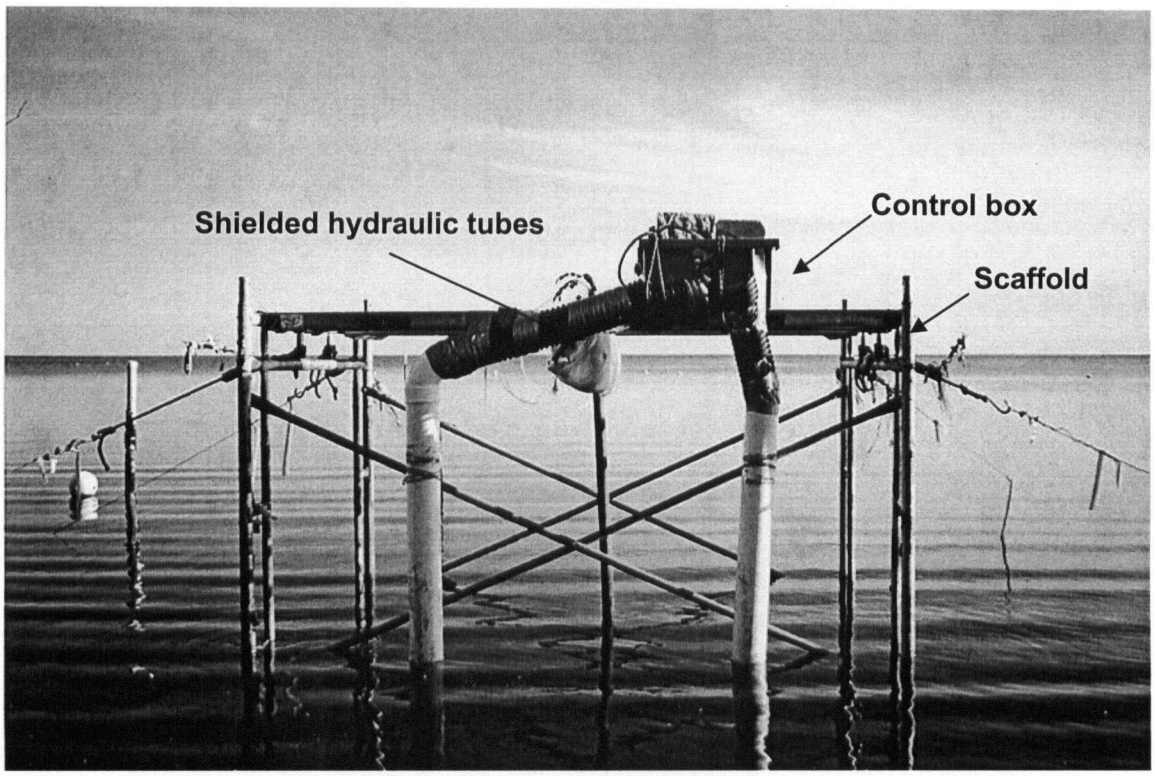

Figure 3-4: The DPS-I deployed at high tide near the FSMUL in 2002 (photo by J.Caulkins).

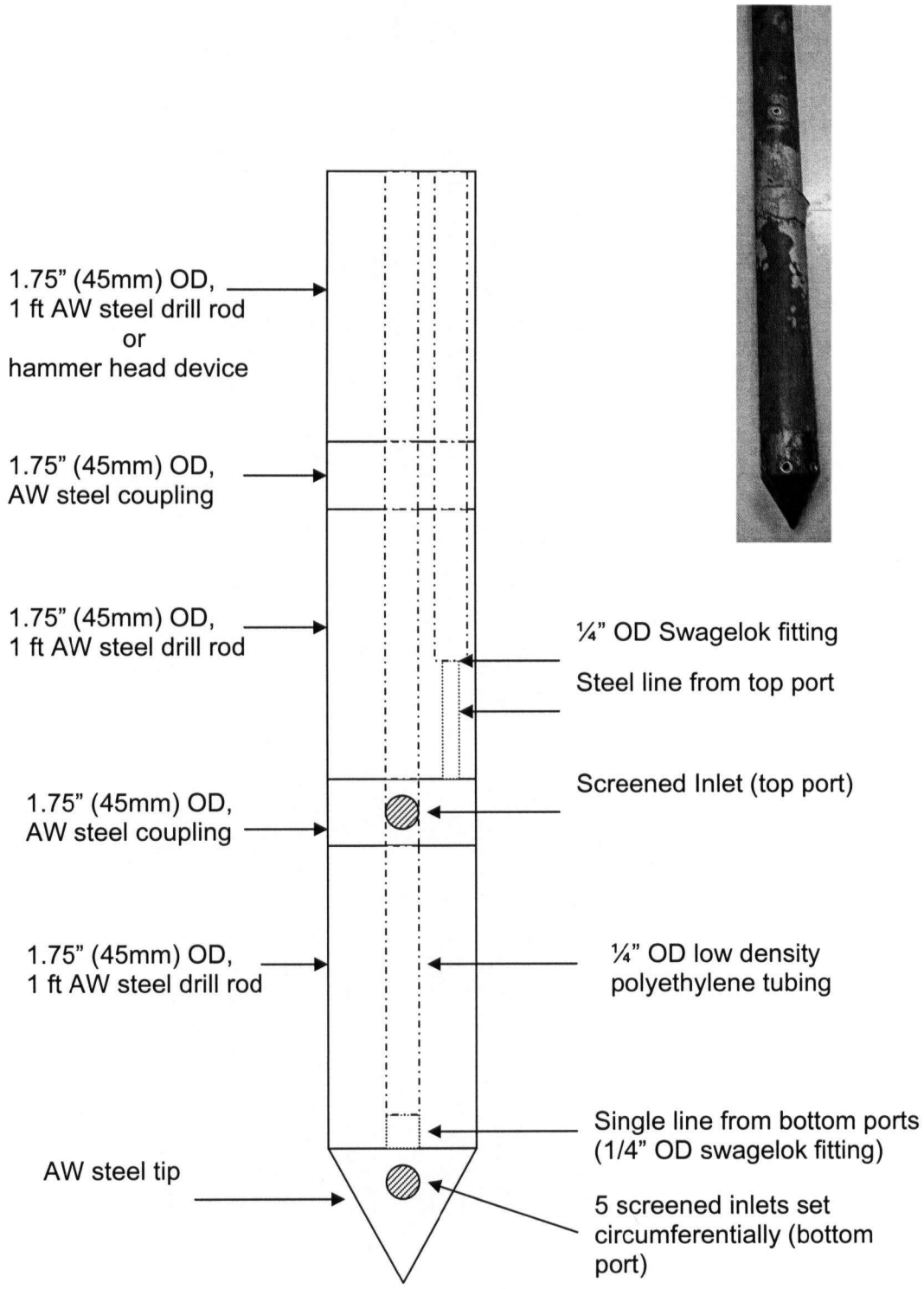

Figure 3-5: Schematic of a DPS-II piezometer.

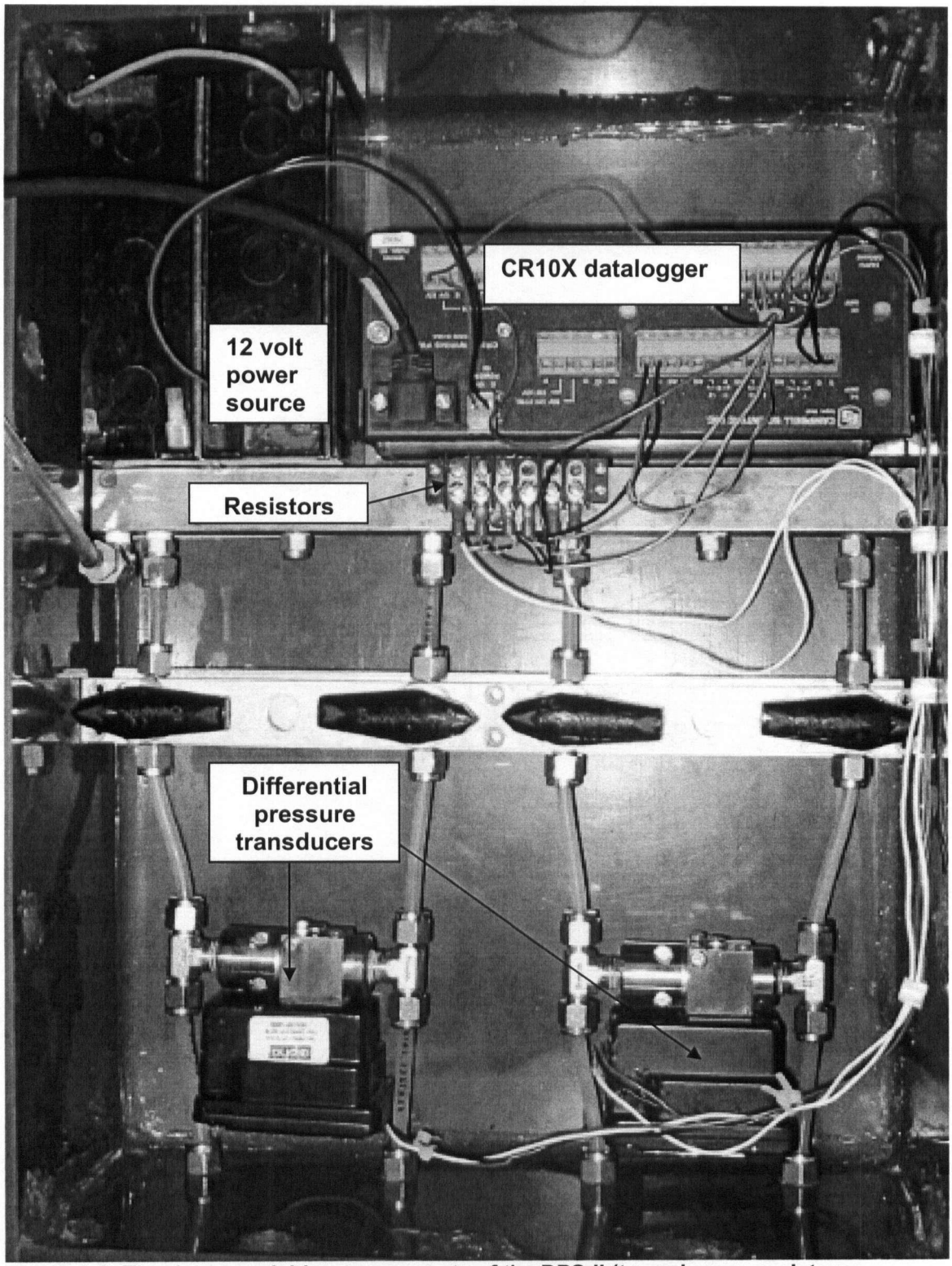

Figure 3-6: The data acquisition components of the DPS-II (transducers, resistors, datalogger and power source) housed inside a submersible (i.e. water proof) box for deployments.

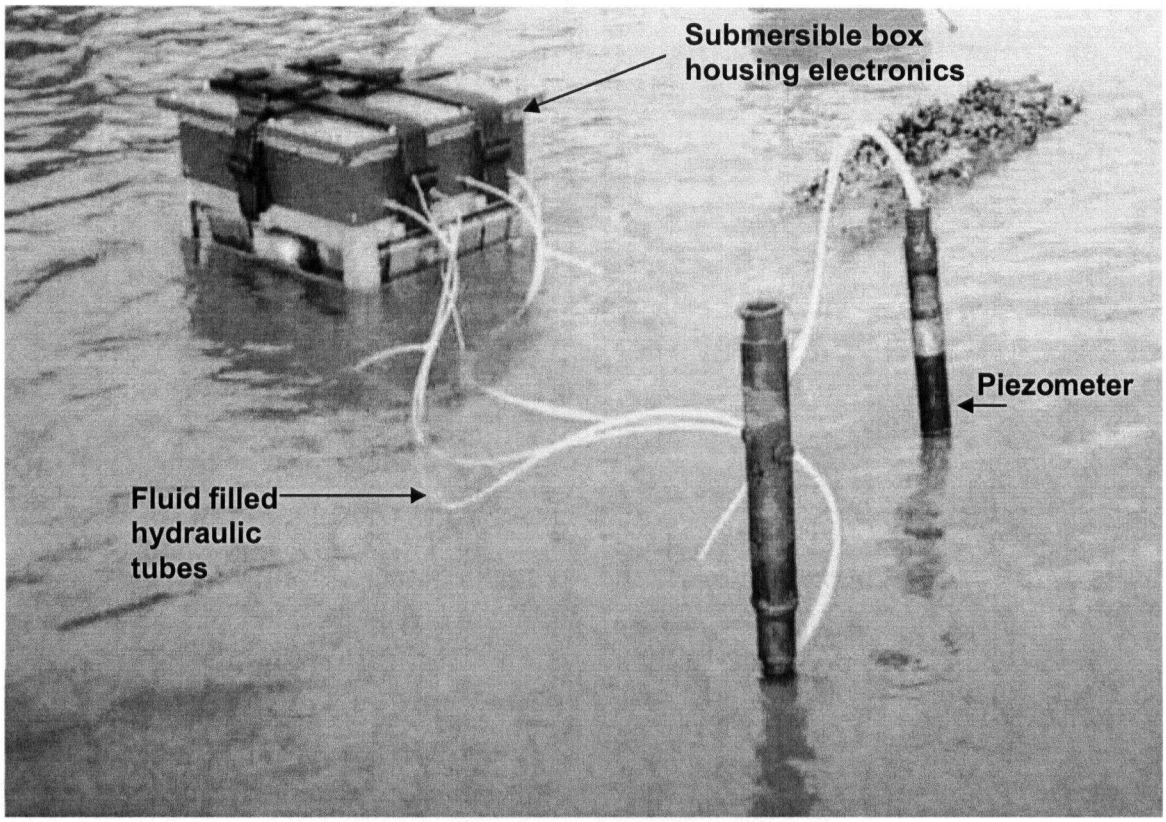

Figure 3-7: The DPS-II after completion of installation at low tide at Spanish Banks West beach, Vancouver.

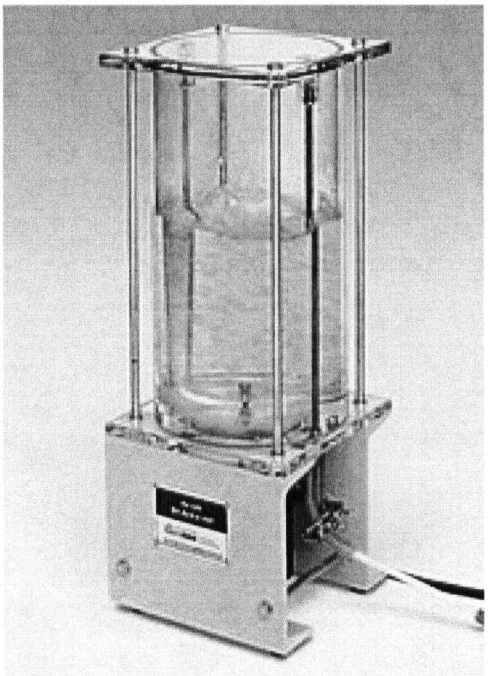

Figure 3-8: The instrument, Nold Deaerator, used to prepare deaired water for the installation of the DPS-II.

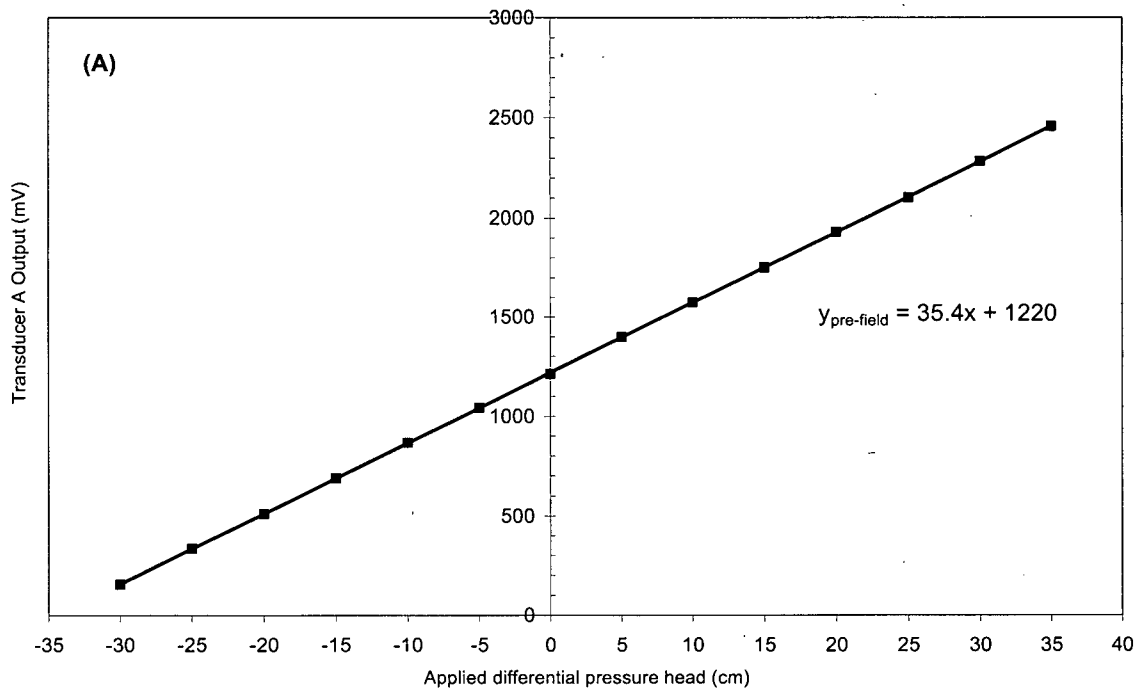

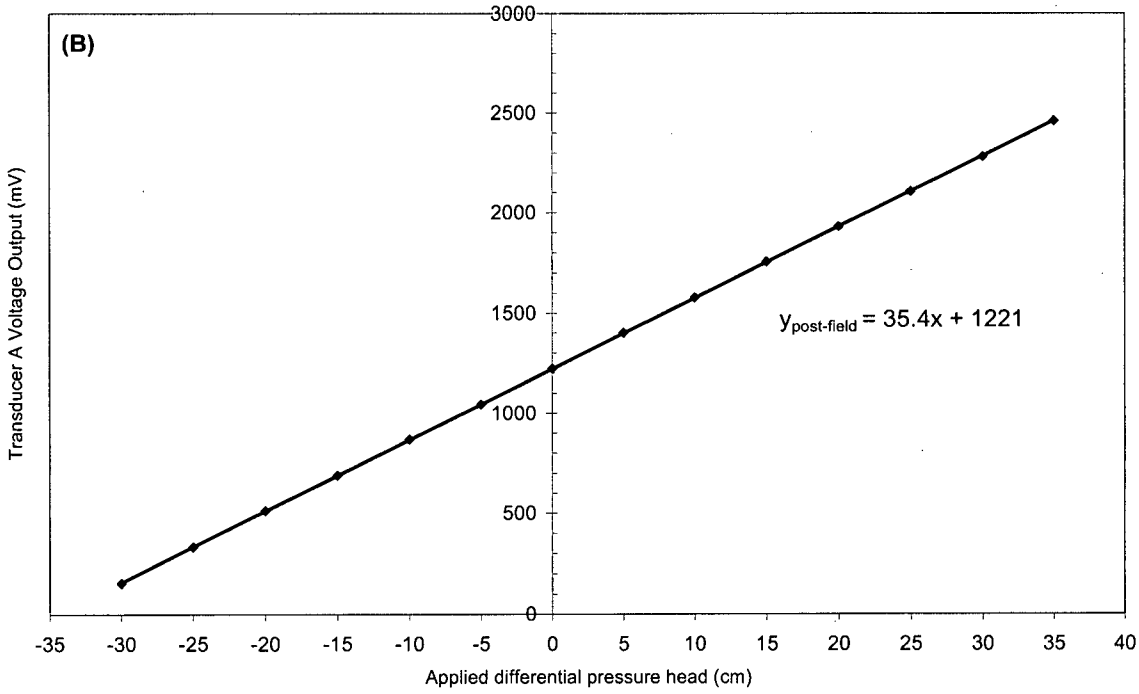

Figure 3-9: Calibration curves developed for transducer A of the DPS-II in this study. (A) Pre-field deployment calibration curve developed October 21, 2005. (B) Post-field deployment calibration curve developed October 31, 2005.

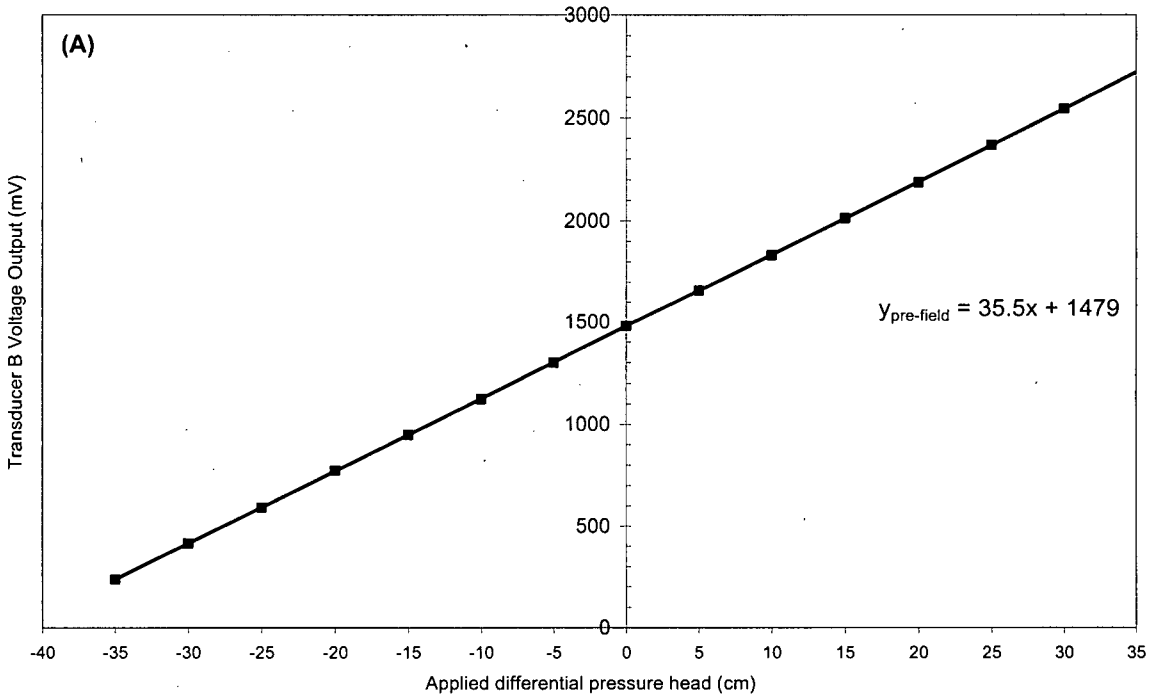

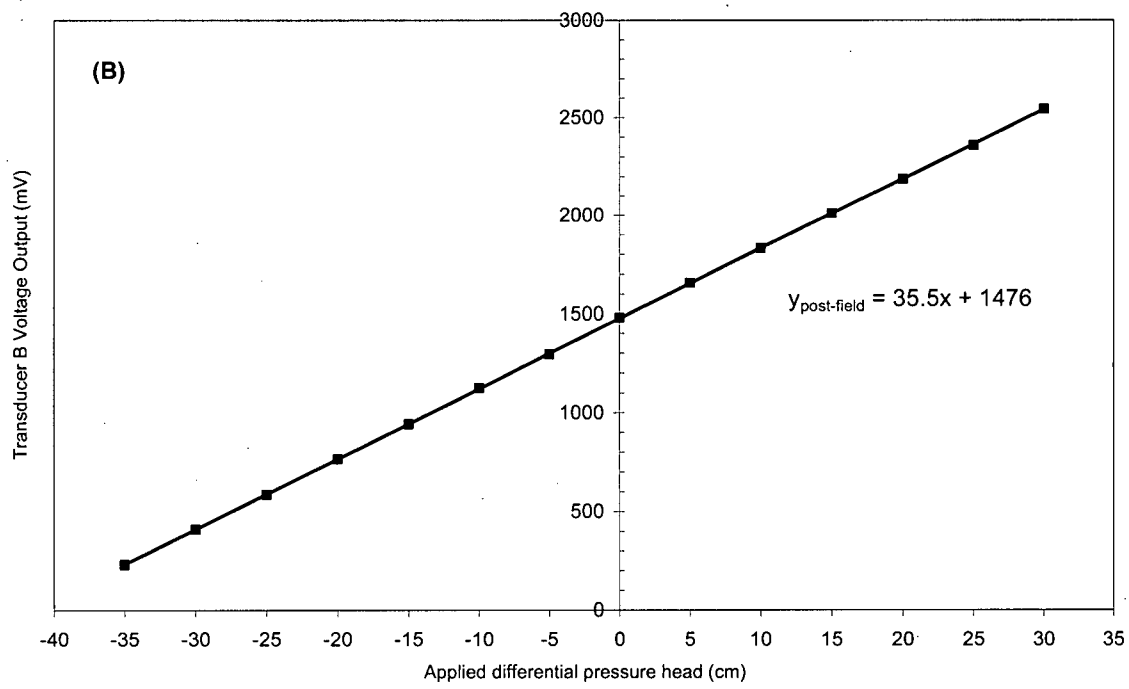

Figure 3-10: Calibration curves developed for transducer B of the DPS-II in this study. (A) Pre-field deployment calibration curve developed October 21, 2005. (B) Post-field deployment calibration curve developed October 31, 2005.

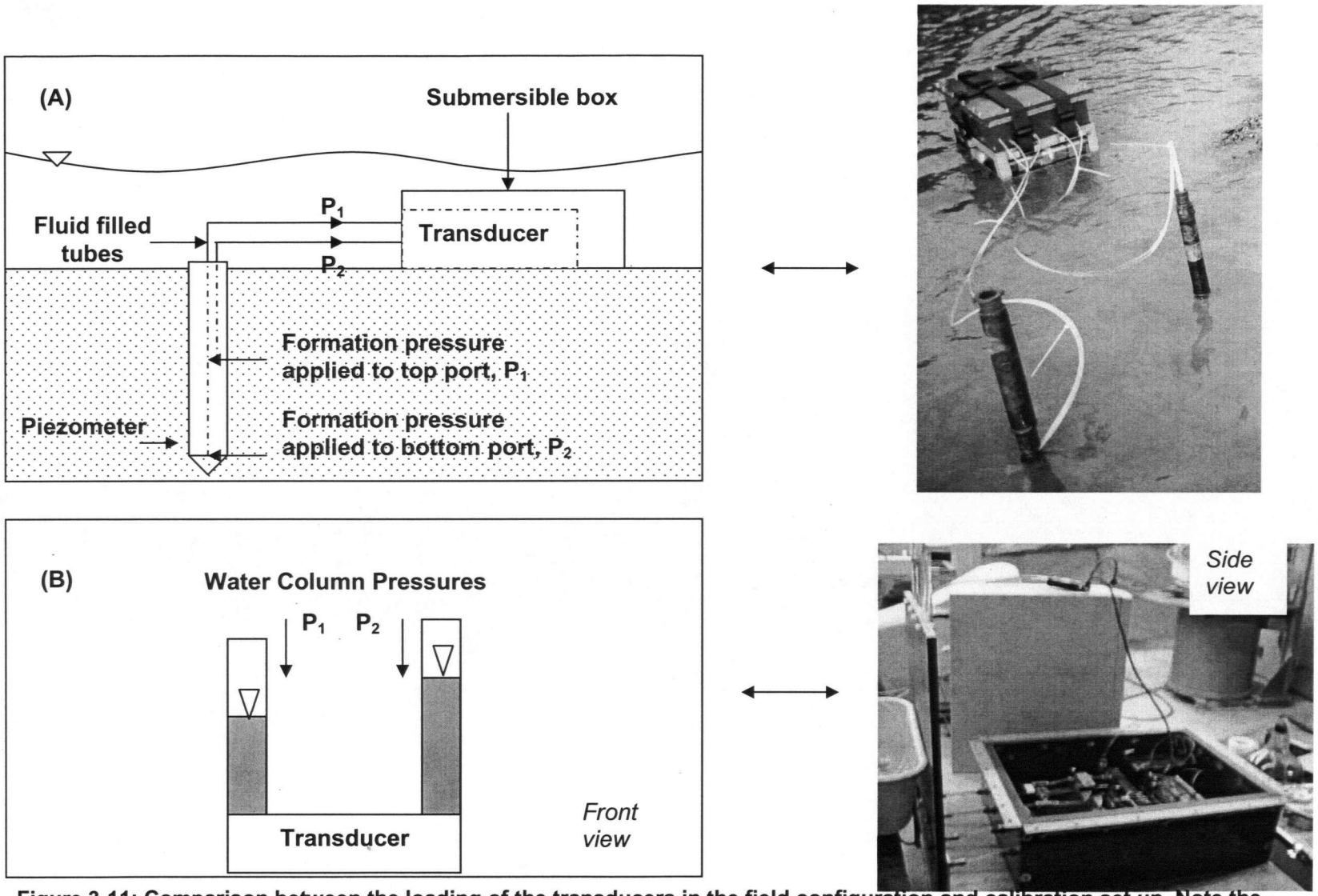

Figure 3-11: Comparison between the loading of the transducers in the field configuration and calibration set up. Note the orientation/position of transducer in the submersible box does not change in the configurations.

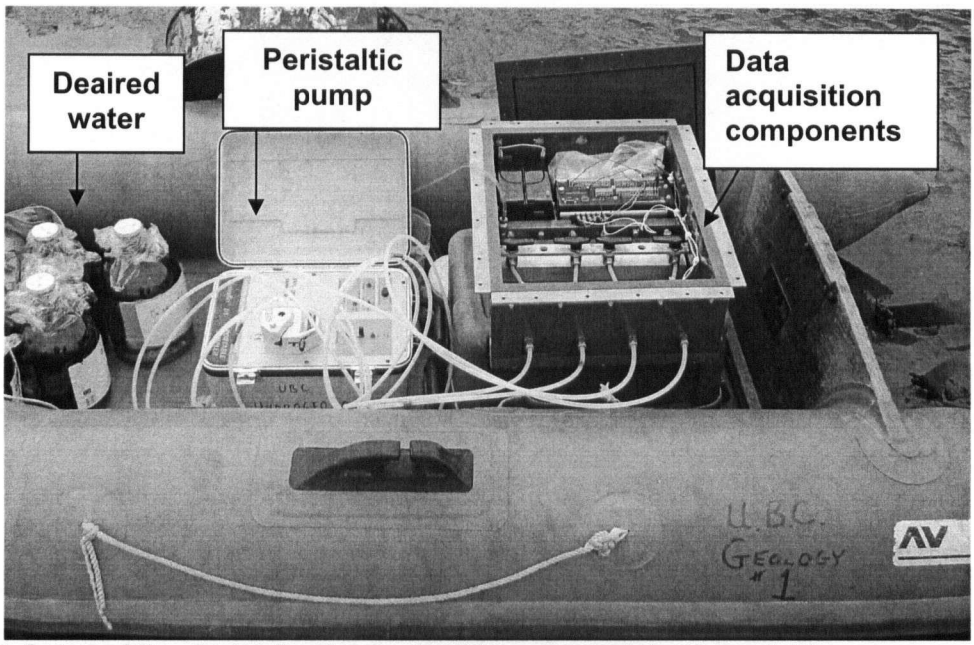

Fig. 3-12: Setup of the deaired water, peristaltic pump and data acquisition components in a small inflatable boat in preparation for insertion of the DPS-II piezometers into the seabed.

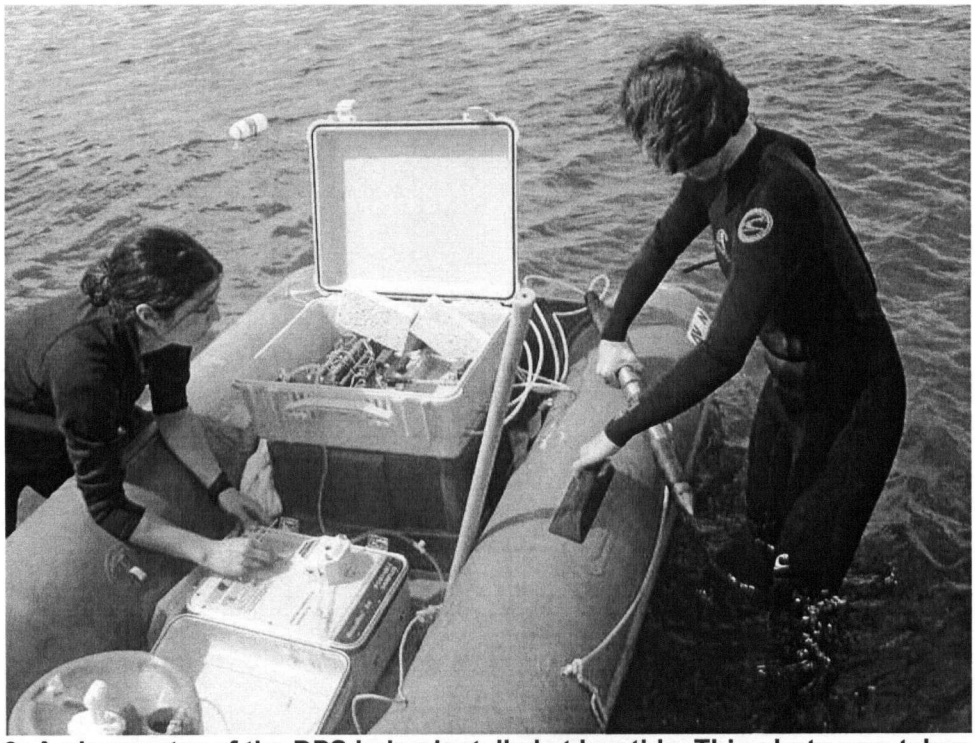

Fig. 3-13: A piezometer of the DPS being installed at low tide. This photo was taken during an earlier trial deployment of the DPS-II in May 2005.

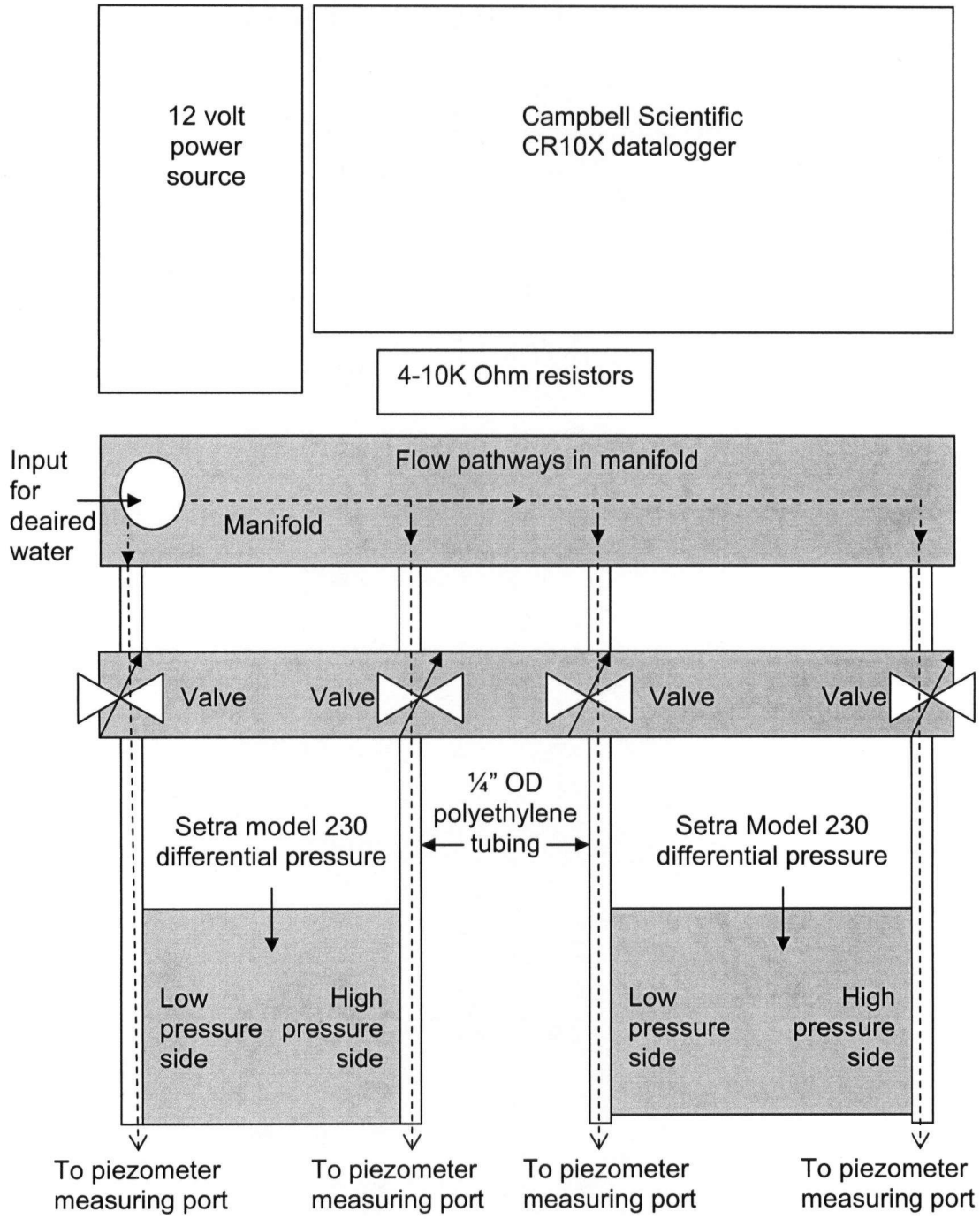

Figure 3-14: Schematic of set up inside the submersible box. During insertion of the piezometers of the DPS-II, deaired water is pumped through the manifold past the sides of the transducer and out the ports of the piezometer via low density polyethylene tubing. When a piezometer is inserted, only the pair of valves on the manifold that regulate flow to that piezometer are open.

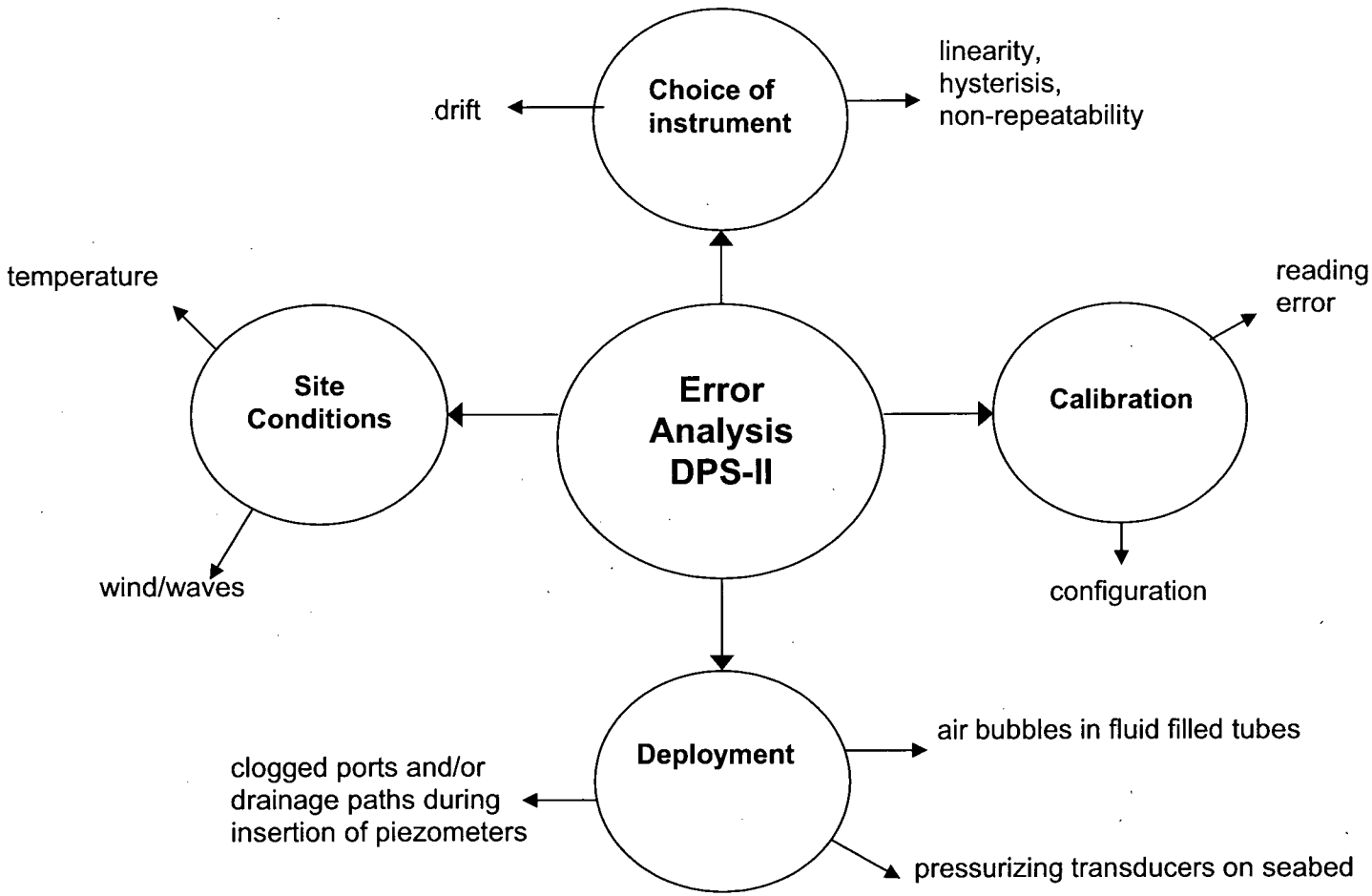

Figure 3-15: The sources of error identified within the main stages of the DPS-II development.

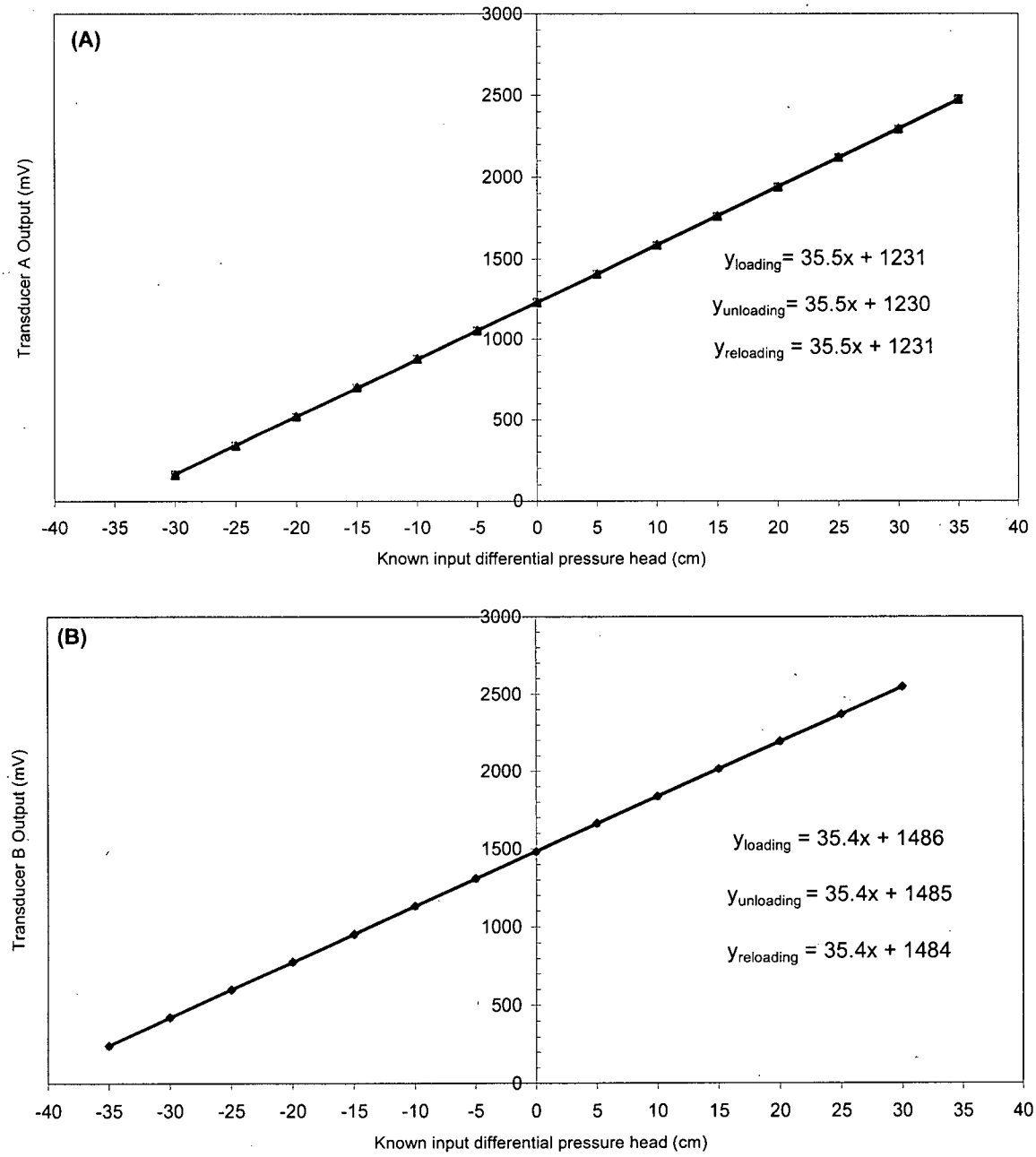

Figure 3-16: Calibration of the DPS-II differential pressure transducers to assess non-linearity, non-repeatability, and hysterisis. (A) Calibration of transducer A. (B) Calibration of transducer B.

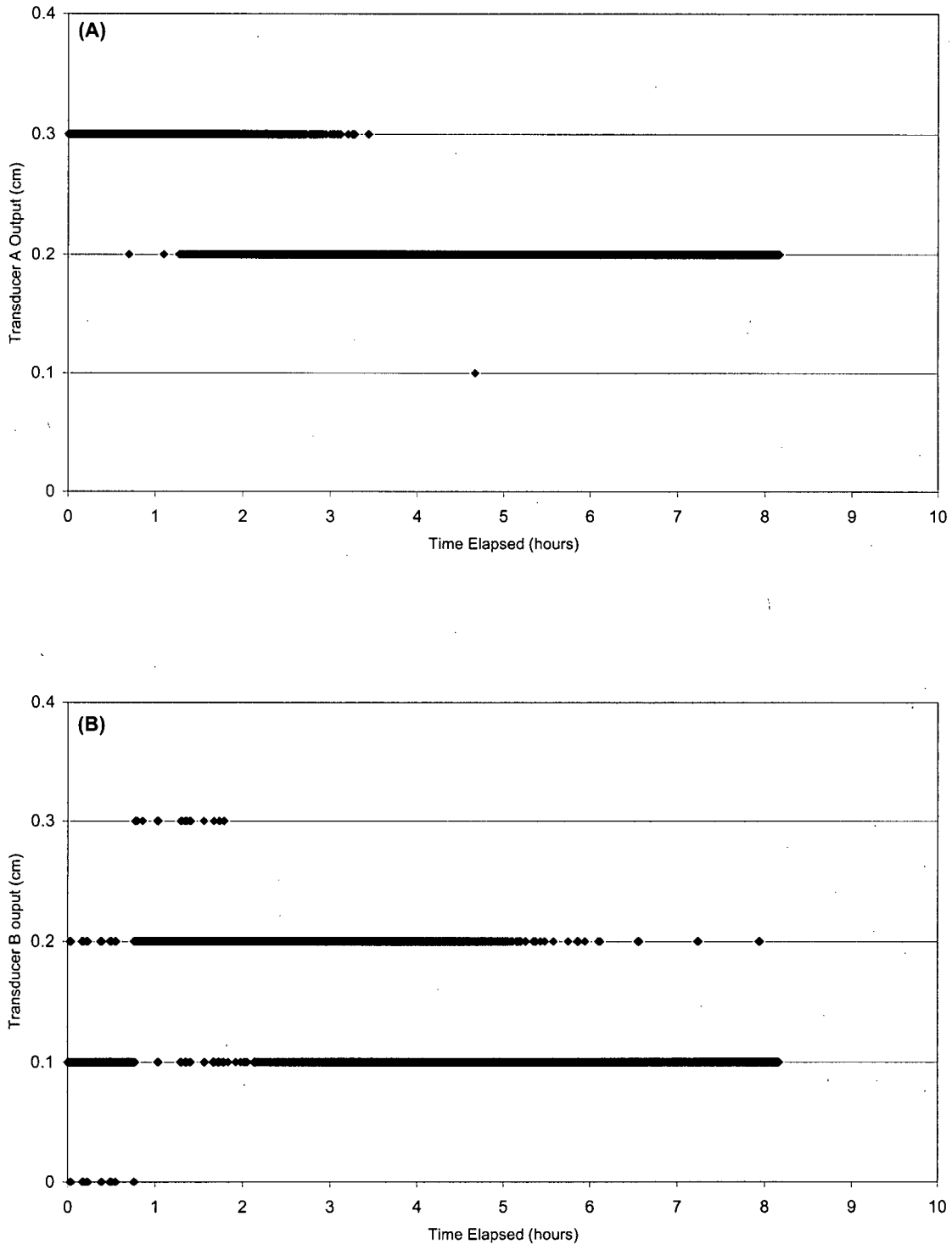

Figure 3-17: 1s measurements that show the variation in output when a constant zero differential pressure is applied to the transducers. (A) Transducer A. (B) Transducer B.

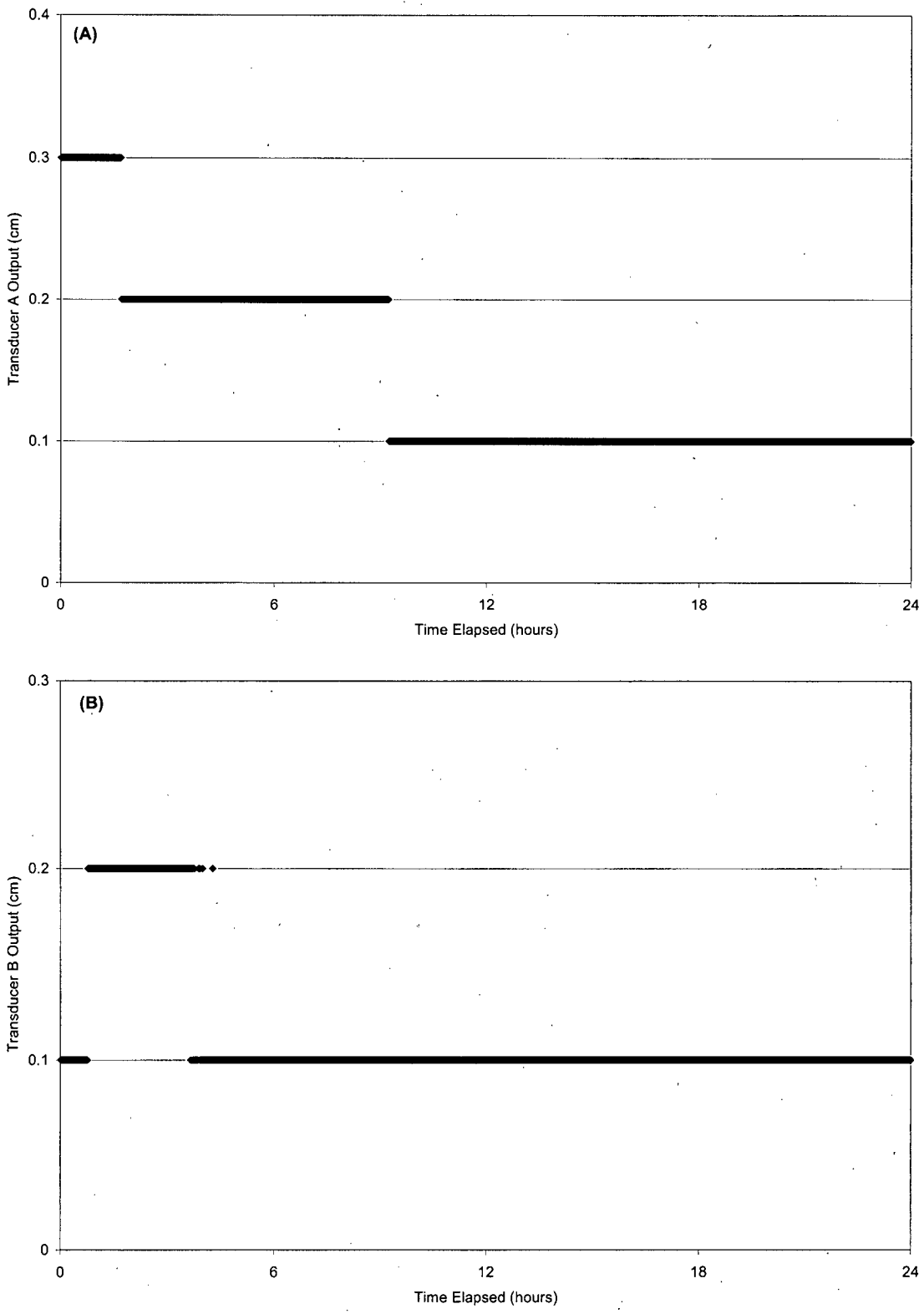

Figure 3-18: One minute averages of 1 s measurements that show the variation in output when a constant zero differential pressure is applied to the transducers. (A) Transducer A. (B) Transducer B.

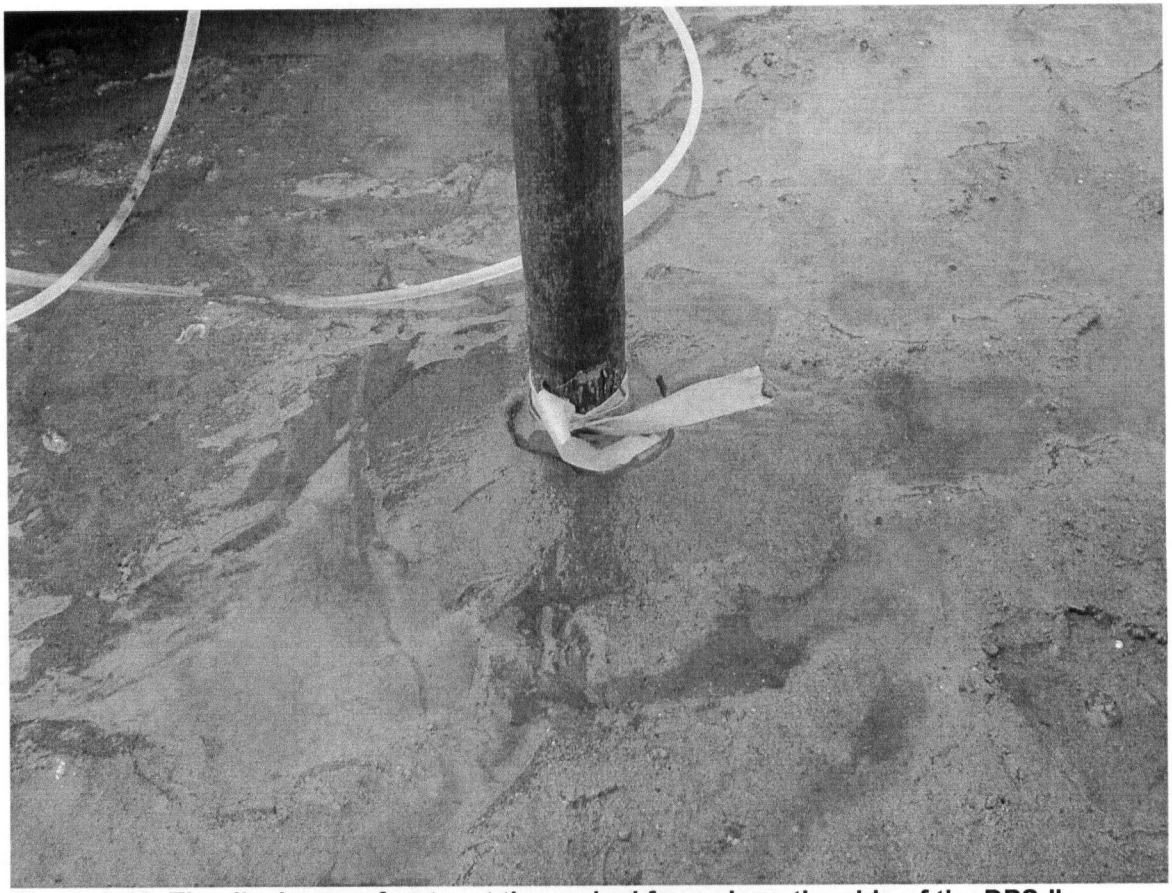

Figure 3-19: The discharge of water at the seabed from along the side of the DPS-II piezometers was observed during the insertion of the piezometers.

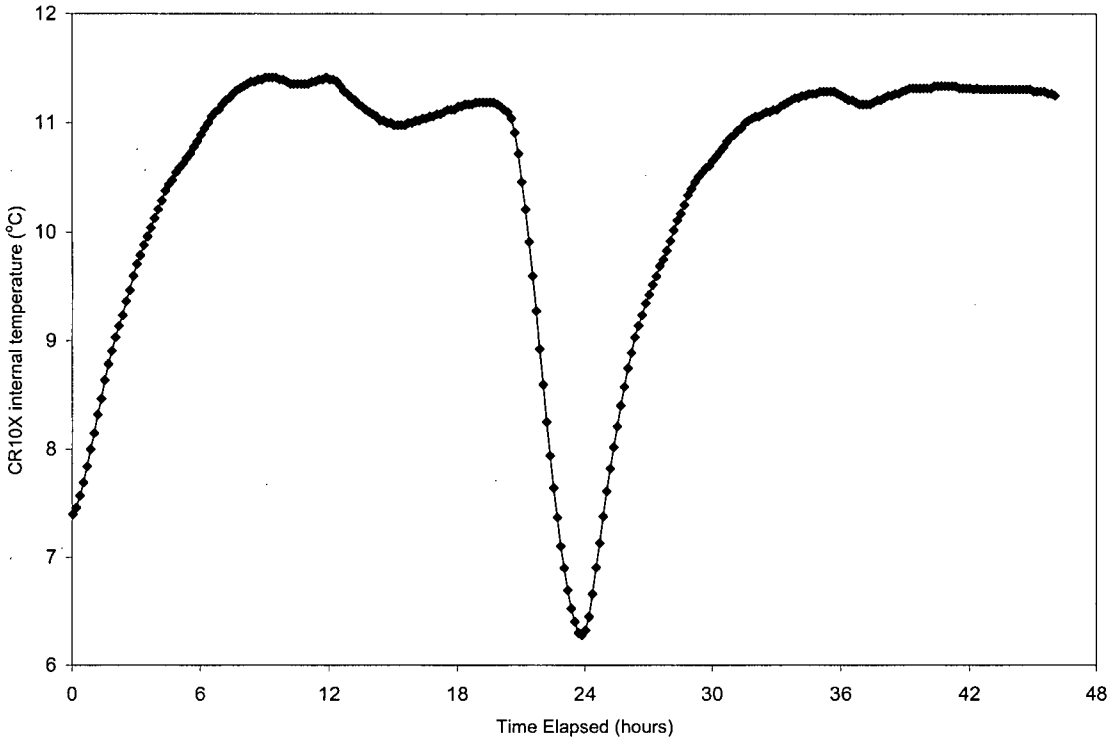

Figure 3-20: Temperature measured inside the submersible box, housing the electronic components of the DPS-II, by the internal temperature of the CR10X. The decrease in temperature after about 20 hours from the start of the experiment corresponds to the timing of the low tide that uncovered the box.

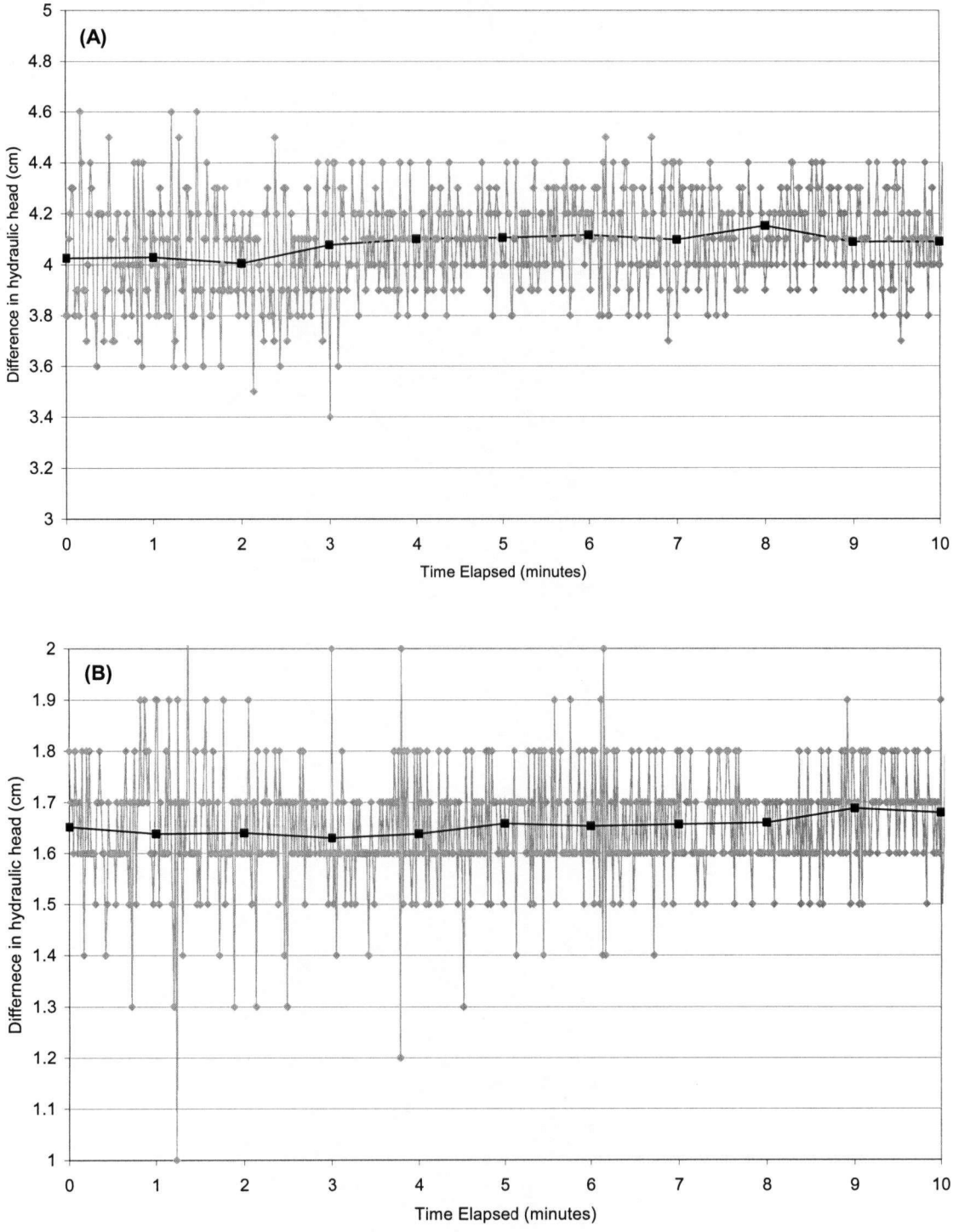

Figure 3-21: Variation in the output of the transducers at 1 second measurements is compared to 1 minute averages of the data, for a 10 minute interval occurring at the highest high tide (2.3 m) over the experiment. (A) Transducer A. (B) Transducer B.

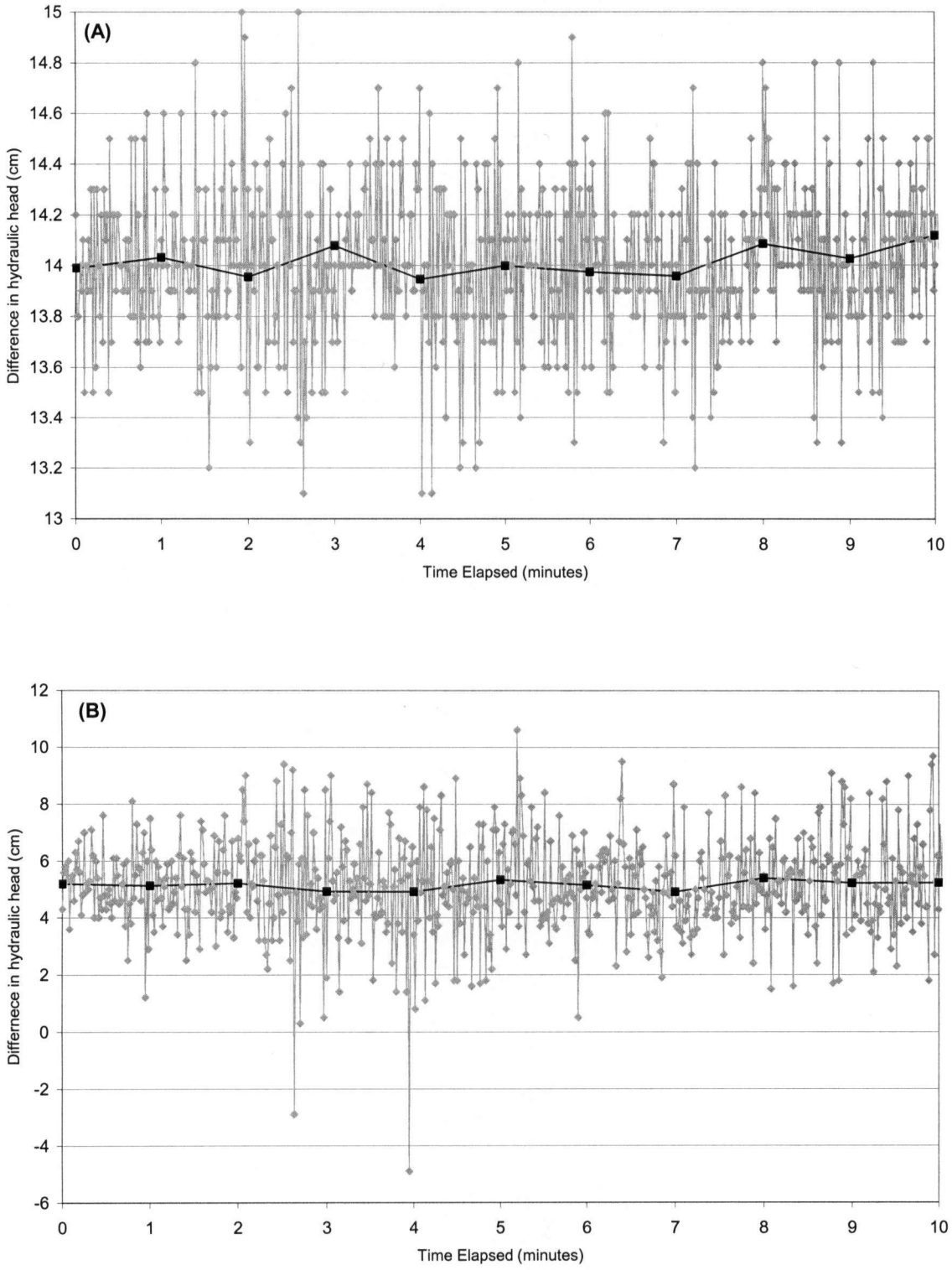

Figure 3-22: Variation in output of the transducers at 1 second measurements is compared to 1 minute averages of the data, for a 10 minute measurement interval occurring at the lowest low tide (0.76 m) over the experiment. (A) Transducer A. (B) Transducer B.

4. Field Experiment

4.1 Field Site

The field data was collected from an area at Spanish Banks West beach, within English Bay, located in the most western part of Vancouver, British Columbia (Figure 4-1). The Spanish Banks West beach is bordered to the south by steep slopes and cliffs that are approximately 60 m above sea level. The base of the slopes is roughly 100 m back from the experiment area. The cliffs are composed primarily of a deposit known as Quadra Sands. In general, the stratigraphy of the cliffs is comprised of a layer of medium to coarse sized sands, overlying a layer of relatively finer grained sand, silts, and organic materials inter-layered with sand (Piteau Associates 2002). Jericho and Kitsilano beaches are located to the east of the site. The foreshore of these beaches is characterized by mostly Quadra medium-grained sands and well exposed bedrock in some areas (P. Mustard personal communication). There are no borehole data at the Spanish Banks West beach that define the local stratigraphy of the near-shore. Clague (personal communication), roughly estimates that bedrock may be within a few tens of metres of sea level at the site. English Bay is a tidal salt-water body and extensive sand flats are present at the Spanish Banks West beach.

4.2 Experimental Method

From October 26 - 28, 2005 a field experiment was carried out at the Spanish Banks West site to measure: (1) the transient changes in vertical differential fluid pressure heads in shallow marine sediment by the DPS-II, (2) SGD rates by a

continuous heat-type seepage meter, (3) tidal levels by a water level sensor and, (4) the EC of pore waters and hydraulic conductivity of marine sediment from pore water and sediment samples collected in the immediate area of testing.

Figure 4.2 shows the tidal level measured over the course of the experiment. The period of time represented by the plot is from October 26th at 9:30 am to October 28th at 7:30 am. The period of time chosen for the experiment was constrained by several factors relating to the tidal level at the site that were: (1) during deployment the water level had to be sufficiently low to make working conditions suitable, (2) the instruments should remain fully submerged over the course of the experiment, (3) at least one tidal cycle should occur over the course of the experiment (several tidal cycles would provide more data to compare the relationship between differential fluid pressure heads, SGD rates and tidal levels) and, (4) a sufficiently low water level to enable removal of the instruments after the experiment was completed. Tidal predictions were obtained from The National Tides, Currents and Water Levels website (Vancouver station # 7735) provided by Fisheries and Oceans Canada. The period chosen for the experiment met all the requirements except that the instruments were uncovered for about 5 hours by the low tide approximately 20 hours after the start of the experiment. The uncovering of the instruments for the 5 hours during testing was acceptable compared to the limitations of other periods considered for deployment at the site.

The DPS-II, seepage meter and water level sensor were deployed approximately 20 m seaward of the high tide line in a configuration that would best permit comparison between the SGD rates measured by the seepage meter and the differential fluid pressure heads measured by the DPS-II (Figure 4-3). The piezometers of the DPS-II were spaced approximately 0.5 m on either side of the seepage drum to minimize effects from spatial heterogeneities in hydraulic conductivity between the measurements by the DPS-II and the seepage meter. Because SGD has been observed to decrease exponentially from shore in some studies (e.g., Bokuniewicz 1980; Shaw and Prepas 1990), the piezometers were also aligned parallel to each other. The piezometers and seepage meter were positioned away from the boxes housing the data acquisition components of the instruments to minimize any measurement artefacts caused by potential flow perturbations from the surface area or weight of the submerged boxes. To differentiate between the measurements from the piezometers, the piezometers are referred to as A and B (piezometer A is connected to transducer A and piezometer B to transducer B). Piezometer A is positioned east of piezometer B at the site as shown in Figure 4-3.

On the morning of October 26th, at the predicted low-low tide time for the day, the equipment used for the installation of the field instruments was set up in a small inflatable boat positioned in the near-shore at the site (Figure 4-4). Preparation for installing the instruments, which in addition to setting up the gear in the boat also involved preparing the electronics of the seepage meter, took approximately

1 hour. Insertion of the piezometers of the DPS-II was begun roughly 15 minutes after the set up for installation was completed.

4.2.1 DPS-II

The water level was a few centimetres above the sediment-water interface when the piezometers of the DPS-II were hammered into the seabed. Insertion of each piezometer took approximately 5-10 minutes. Differential fluid pressure heads were measured at the bottom measuring port of the piezometer relative to the top measuring port, thus a positive differential fluid pressure head indicated a vertical pressure gradient in the direction toward the seabed. Differential fluid pressure head was measured simultaneously at both piezometers of the DPS-II, at a rate of one measurement every 1 second.

4.2.2 Continuous Heat Type Automated Seepage Meter

Approximately 1 hr after installation of the DPS-II, water levels at the site were sufficiently high to deploy the seepage meter (i.e., water was deep enough to fully submerge the seepage drum and flow tube of seepage sensor unit). A continuous heat-type automated seepage meters was installed directly between the piezometers of the DPS-II (Figures 4-5 and 4-6). Air bubbles were purged from the seepage drum and flow tube of the seepage sensor unit during deployment of the seepage meter. An attempt was made to position the flow tube of the seepage sensor unit parallel to the direction of the waves. Wave motions can effect SGD measurements made by the seepage meter by interfering with

discharge from the flow tube of the seepage sensor unit. Two small rocks were placed on the drum to provide stability from waves. Measurements of SGD were made every 10 minutes and provided an estimate of SGD at that instant in time.

4.2.3 Levelogger and Barologger

Tidal levels were recorded every 5 minutes by a pressure transducer (F15/M5 LT levelogger, Solinst), that was attached to piezometer B, about 5 cm above the sediment-water interface. Barometric pressures used for the tidal level measurements, were recorded every 5 minutes by a pressure transducer (F5/M1.5 Barologger, Solinst) located onshore.

4.2.4 Pore Water Sampler

Pore water samples (30 ml) were collected daily over the course of the experiment during the morning low tide with a disposable syringe connected to a 0.6 cm diameter, 90 cm long stainless steel Push Point sampler (MHE product), shown in Figure 4-7. The electrical conductivity (EC) of the samples was measured in the laboratory.

A pore water sample was collected each day, adjacent to the top measuring ports of both piezometers. It was not possible to obtain pore water samples adjacent to the bottom measuring ports of the piezometers. This condition may reflect finer sediment at this depth that clogs the port of the sampler. The sediment cores collected from adjacent to the piezometers (section 4.2.5) did not

support the assumption of finer sediment with depth. However, a complete recovery of the core samples collected using the coring instrument that was driven to a depth of 60 cm below the seabed was not achieved (cores represented about a 40 cm length from within the 60 cm depth). Thus the samples may not have been comprised of the sediment present at the bottom port (60 cm below the seabed). As a result, the lack of observation of finer sediment at the bottom portion of the cores does not exclude the possibility of a finer layer at depth. After sampling pore waters from the top measuring port of the piezometers, two seawater samples were also collected from the surface water.

On the last day of the experiment, in addition to collecting a porewater sample adjacent to the top port of each piezometer, a pore water sample was also taken at about 10 cm below the seabed from directly beside each of the piezometers. These extra pore water samples were collected for comparison with the samples at the top ports of the piezometers, to provide insight about whether the EC of the pore water changed significantly closer to the seabed.

4.2.5 Core Sampler

Three core samples (3.5 cm diameter and 40 cm length) were collected at the end of the experiment by a core sampler that utilizes a core catcher technique (Figure 4-8). The core sampler consists of a removable transparent plastic core tube that fits into a 0.9 m (35 1/2 in) length core barrel and a core catcher that is

attached to the bottom end of the core barrel. During core collection, the fingers of the core catcher allow the sediment to pass up into the core tube, but spring back into place to prevent the core material from falling out during core handling.

The core sampler was hammered into the sediment surface to a depth of approximately 0.6 m (bottom piezometer port) but a full recovery of the core sample was not possible due to such factors as the saturation of the sediment and grain size which influence how well the core catcher can retain the sample during retrieval. The location of the core samples are shown in Figure 4-3. Two samples (referred to as A-in and A-out) were obtained from either side of piezometer A, parallel to the shoreline. A core sample (referred to as B-in) was also taken from adjacent to piezometer B, between the seepage drum and the piezometer. A second attempt for a core at piezometer B was unsuccessful. The core samples were transported to the laboratory to examine the sediment profile and estimate the hydraulic conductivity of the sediment using the falling head test.

4.3 Results

Figure 4.9 compares the measurements by the DPS-II of differential fluid pressure head at both piezometer A and B with the measurements of tidal level at the site. The plot shows 1 minute averages of the differential fluid pressure head measurements for the entire duration of the experiment. There is a gap in the field measurements because the piezometers of the DPS-II were uncovered

for five hours by the low tide occurring between 20 –25 hours after the beginning of the experiment.

The differential fluid pressure head measurements at both piezometers A and B showed temporal variations that corresponded to the semi-diurnal tides at the site, with the highest differential fluid pressure heads occurring at low tide. The magnitude of the differential fluid pressures measured at piezometer A, however, were on average 13 % higher than at piezometer B. The differential fluid pressure heads at piezometer A ranged from 34.4 cm to 46.7 cm with an arithmetic mean of 39.9 cm. The differential fluid pressure head at piezometer B was between 32.6 cm and 37.3 cm with an arithmetic mean of 34.6 cm.

For the first high/low tidal cycle between 0 and 18 hours of the experiment, the tidal level changed by 1.37 m and the corresponding change in differential fluid pressure head at piezometer A was 6.8 cm and at piezometer B was 2.7 cm. The tidal level changed by 1.56 m for the second tidal cycle between 24 and 37 hours into the experiment, and the corresponding change in differential fluid pressure head at piezometer A was 10.3 cm and at piezometer B was 3.7 cm.

Figure 4-10 compares the SGD measurements recorded every 10 minutes by the seepage meter with the measurements of tidal level at the site. As was the case for the DPS-II field data, there is also a gap in the SGD measurements that corresponds to the complete exposure of the meter during the low tide. Because

the exact depth of water that resulted in the seepage meter starting to become uncovered is not known with certainty, the SGD measurements immediately before and after the gap in the field data (i.e., the low tide completely exposing the seepage meter) may be affected by measurement artefacts. The high SGD rates immediately preceding the gap in the SGD field data may reflect measurement artefacts rather than true discharge rates. The seepage drum and flow tube of the seepage meter must be completely filled with water to permit valid SGD measurements. As a result the high values of SGD measured at around 20 hrs after the beginning of the experiment may not be accurate.

The reason for the fluctuations in SGD rates over short measurement intervals is not certain but may be the result of several causes that are: (1) environmental factors (e.g., wind, waves), (2) poor electrical connections, (3) instrument noise and/or, (4) the natural variability in SGD over time. In some cases, SGD data sets obtained using a continuous heat type seepage meter have also shown abrupt changes in discharge rates (e.g., Taniguchi 2006). The deployment of two seepage meters was preferred for this experiment, to increase the reliability of SGD measurements, but was not viable because of problems with a second seepage meter that was constructed. Figure 4-11 shows the plots of the SGD measurements averaged over time intervals of 20, 30 and 40 minutes.

The SGD rates showed temporal variations that corresponded to the semidiurnal tides at the site, with the highest SGD rates occurring at low tide. SGD rates

averaged every 30 minutes over the duration of the experiment have been used for a comparison with tidal level fluctuations because the SGD pattern is clearer than the plot of the 10 minute SGD measurements. The SGD rates at the site varied from 5 cm/d to 103 cm/d, with an arithmetic mean of 38 cm/d. Over the first high/low tidal cycle of the experiment, the change in SGD rates was about 42 cm/d. The SGD rate changed by about 35 cm/d over the high/low second tidal cycle.

The averages of the EC measurements of the seawater samples collected at low tides during the experiment, showed an increase from 15 mS/cm to 31 mS/cm (Figure 4-12a. These results may suggest the EC of the seawater at the experiment site is affected by circulation patterns in English Bay that transports fresh water from the Fraser River as it moves around from Point Grey. Daily changes in the EC of the water column could be important if the EC of the pore waters in the shallow seabed are affected because of mixing processes operating close to seabed. However, a higher frequency of sampling is needed to validate and more accurately represent the daily fluctuations of EC for the water column.

Table 4-1 shows the estimates of the EC measurements for the pore water samples collected during the low tides over the experiment, at 10 cm below the seabed and adjacent the top measuring port of piezometer A and B. Figure 4-12b illustrates the averages of these EC measurements at each depth below the

seabed. The EC pattern at the site suggests: slightly brackish water (average EC 8 mS/cm) at a depth of 10 cm below the seabed that overlies a component of fresh water (average EC of 0.3 mS/cm) at 30 cm below the seabed during low tide conditions. Improving the characterization of the EC profile by additional EC measurements at smaller vertical intervals within the seabed was unsuccessful because of difficulties collecting pore water samples with the water sampler.

Figure 4-13 shows the three core samples collected from adjacent to the piezometers. With the exception of the core sample identified as A-in, each of the core samples was divided into two equal sections for the purpose of identifying any discrepancies in hydraulic conductivity with depth. The core sample, A-in, was divided by separating coarser sediment occurring in the top portion of the sample (about top ¼ of core) from a finer sediment that was similar to that comprising the other core samples.

Figure 4-14 shows the estimate for hydraulic conductivity found for both the top section (closer to the seabed) and bottom sections using the falling head test. The hydraulic conductivity test was completed twice for each sample, once using tap water and also using seawater as the hydraulic fluid. Other than discrepancies, which were likely a result of the accuracy of the permeameter test, no differences were observed between estimates of hydraulic conductivity using tap water and seawater. The estimates of hydraulic conductivity (including estimates from the top and bottom sections of the core) at piezometer A ranged

from 1 x 10^{-5} to 1 x 10^{-4} m/s, with a geometric mean of 4 x 10^{-5} m/s. The values of hydraulic conductivity at piezometer B ranged from 9 x 10^{-7} to 1 x 10^{-5} m/s with a geometric mean of 4 x 10^{-6} m/s. The geometric mean of all the samples was 2 x 10^{-5} m/s. It should be recognized that the values are from disturbed samples that may have experienced possible compaction during sampling and disruption of macropore structures when the cores were prepared for the permeameter tests.

The average of the hydraulic conductivity measurements at piezometer A were an order of magnitude higher than at piezometer B. The higher average hydraulic conductivity does not agree with the higher differential fluid pressure heads measured at piezometer A, if the conventional form of Darcy's Law is to be applied to calculate SGD rates from the DPS-II field data. Because the differential fluid pressure heads measured by the DPS-II are over a depth of roughly 0.3 to 0.6 m below the seabed (the depths corresponding to the measuring ports of the piezometer), the estimates of the hydraulic conductivity of the bottom core sections may be a more appropriate choice for comparison with the differential fluid pressure heads measured at the piezometers. The average of the hydraulic conductivity estimates for the bottom sections at piezometer A, were still higher but by a factor of 3.5, compared to the average hydraulic conductivity of the bottom core sections at piezometer B.

Analytical and model based methods have been used to provide a basis for comparison with field measurements and also to better constrain the interpretation of the field data sets. A prediction of SGD rates based on Darcy's law at the Spanish Banks site has been developed using the transient changes in vertical pressure gradients in the seabed measured by the DPS-II, the hydraulic conductivity estimates from falling head tests completed on core samples and the EC of water samples collected from near the piezometers and the water column. Data available to develop a hydrogeologic model of SGD rates and shallow vertical pressure gradients in the seabed at the site consisted primarily of the hydraulic conductivity data set and a rough estimation of the depth to bedrock.

Location of pore water sample	Sample date: October 26	Sample date: October 27	Sample Date October 28
10 cm below seabed	N/A	N/A	6 and 9
Adjacent top port of piezometer A (30 cm below seabed)	0.23	0.47	0.27
Adjacent top port of piezometer B (30 cm below seabed)	0.20	0.27	0.33

Table 4-1: Values of EC measurements (mS/cm) from pore water samples collected at low tides over the experiment. Two pore water samples from 10 cm below the seabed (each adjacent to a piezometer) were collected only on the last day of the experiment.

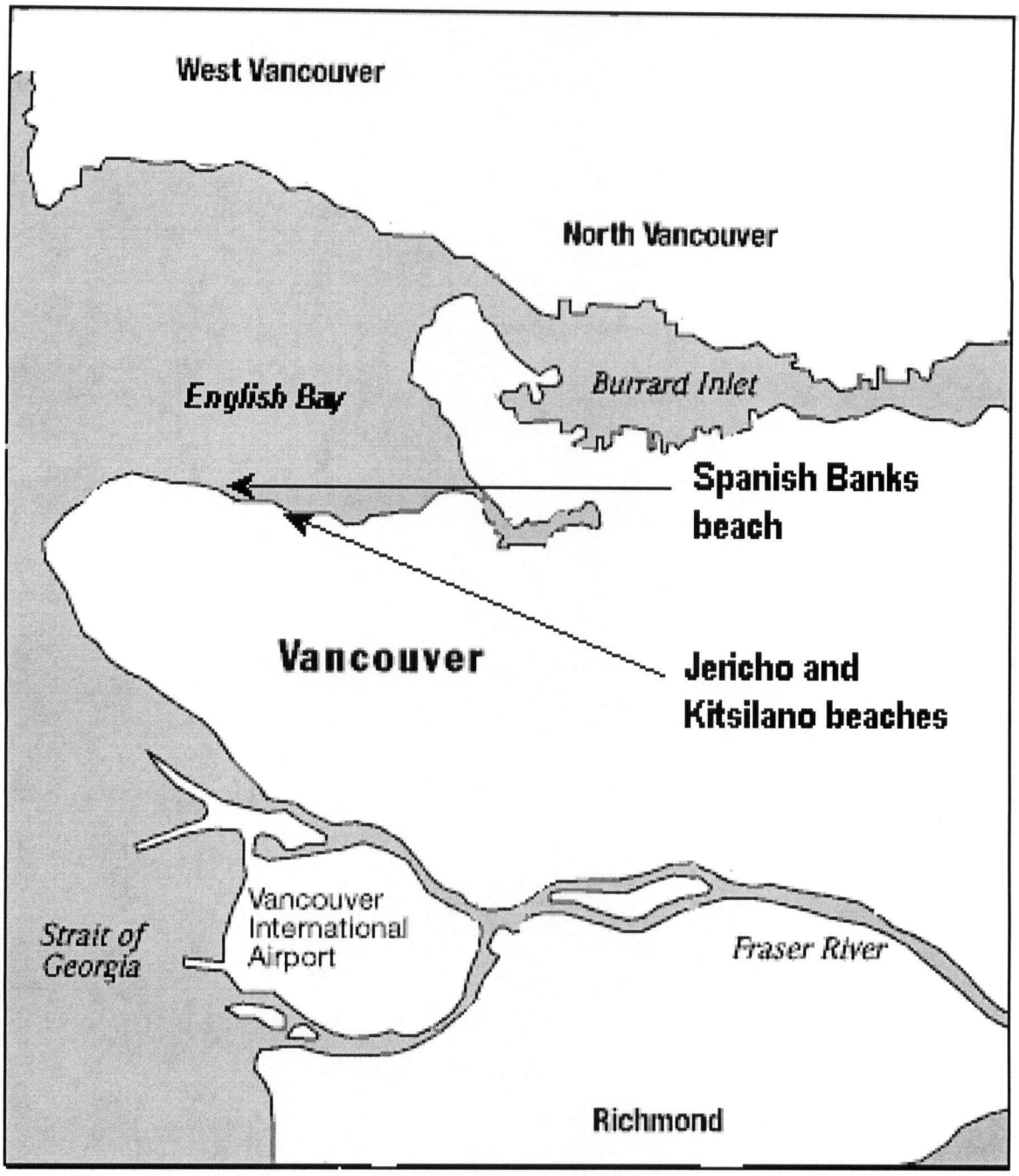

Figure 4-1: Map of Vancouver, BC with location of field site, Spanish Banks beach.

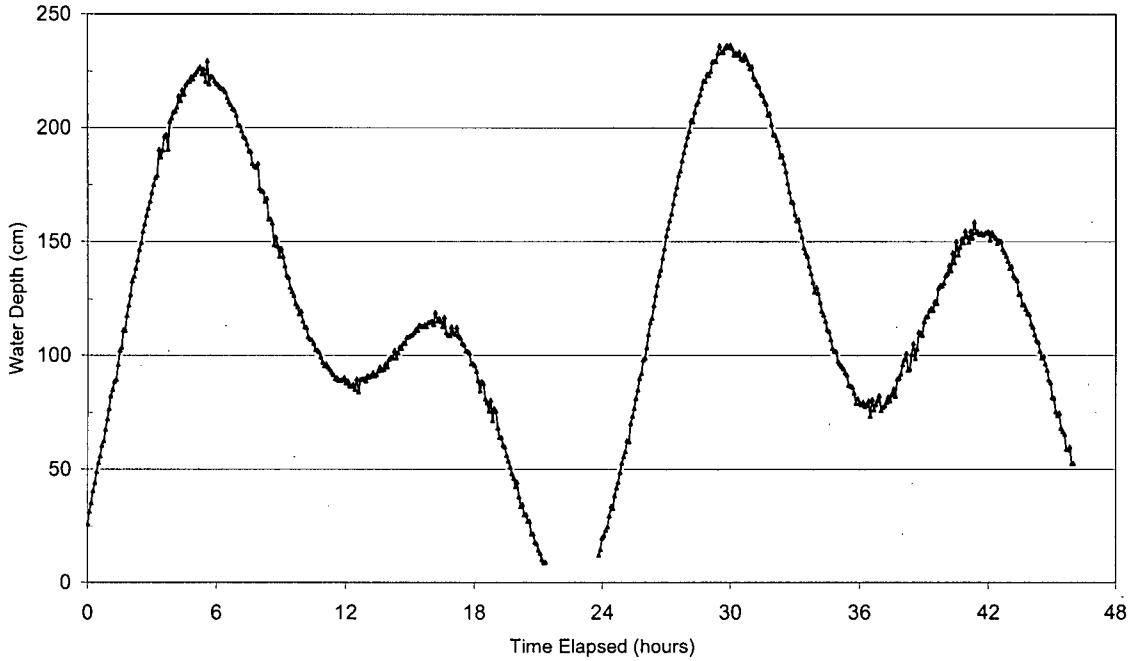

Figure 4-2: Tidal level measurements over the period of the field experiment at the site. The tide line receded to several 100s of meters away from where the field instruments were deployed during the low tide that occurred about 20 hours after the beginning of the experiment.

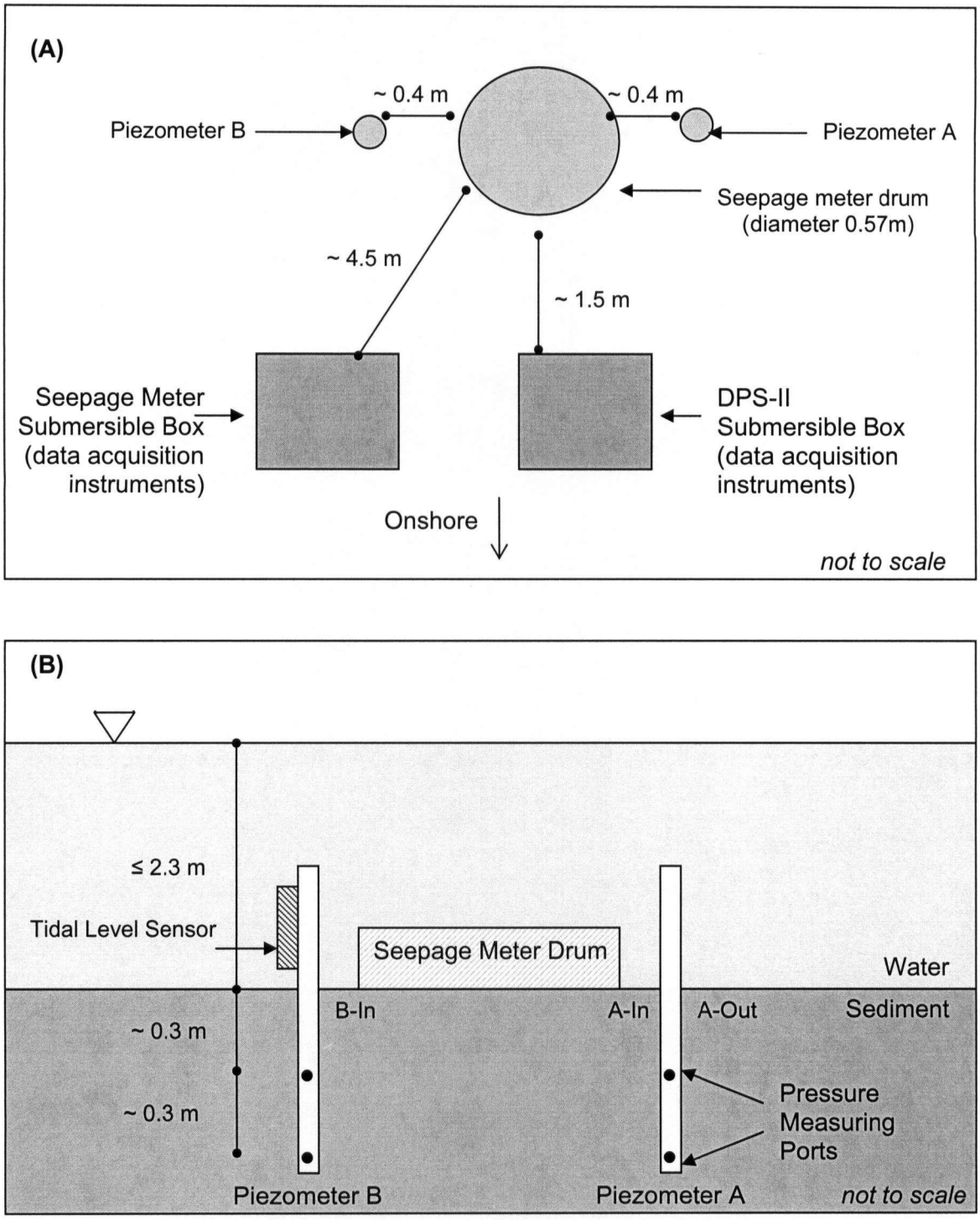

Figure 4-3: Schematic of installation configuration. (A) Top view. (B) View in the direction offshore. The A-In, B-In, and B-Out labels refer to the position of core samples relative to the piezometers collected at the end of the field experiment.

Figure 4-4: The boat containing the equipment to install the piezometers of the DPS-II and the seepage meter is positioned about a meter in land of the location where the DPS-II and seepage meter were installed in this study.

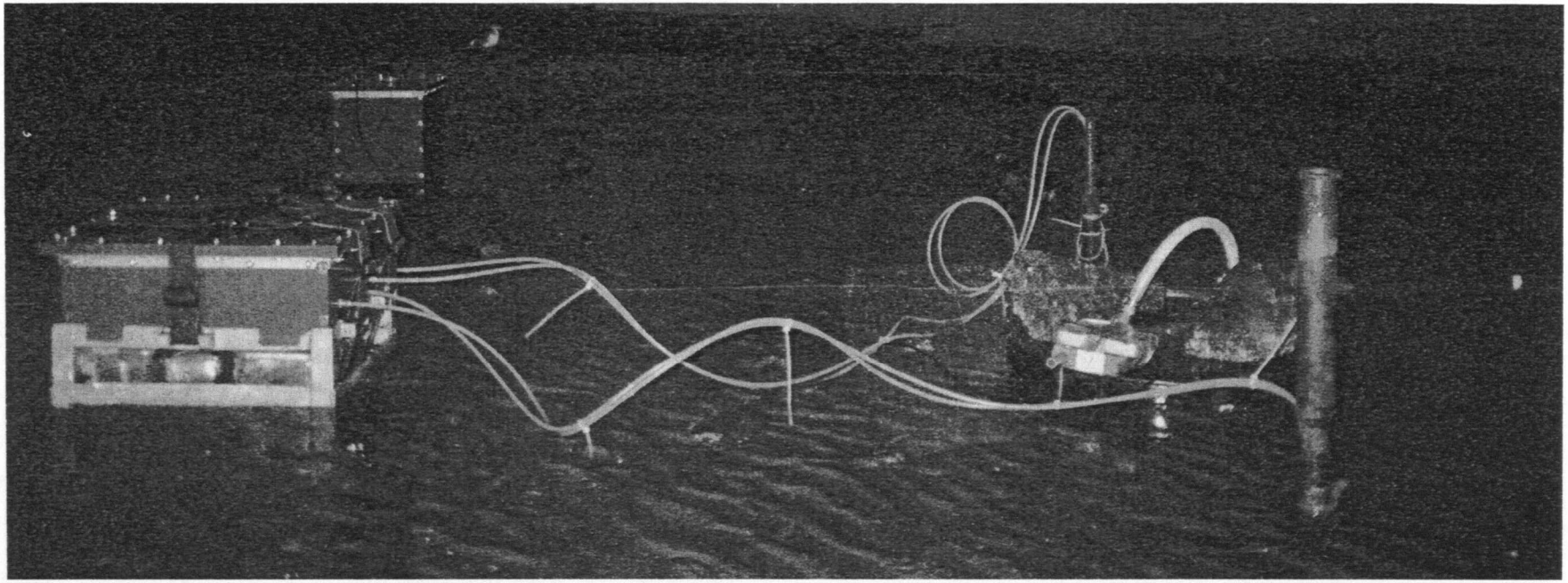

Figure 4-5: A continuous heat type seepage meter was deployed between the piezometers of the DPS-II during the experiment at the Spanish Banks West site (photo taken looking west of the site).

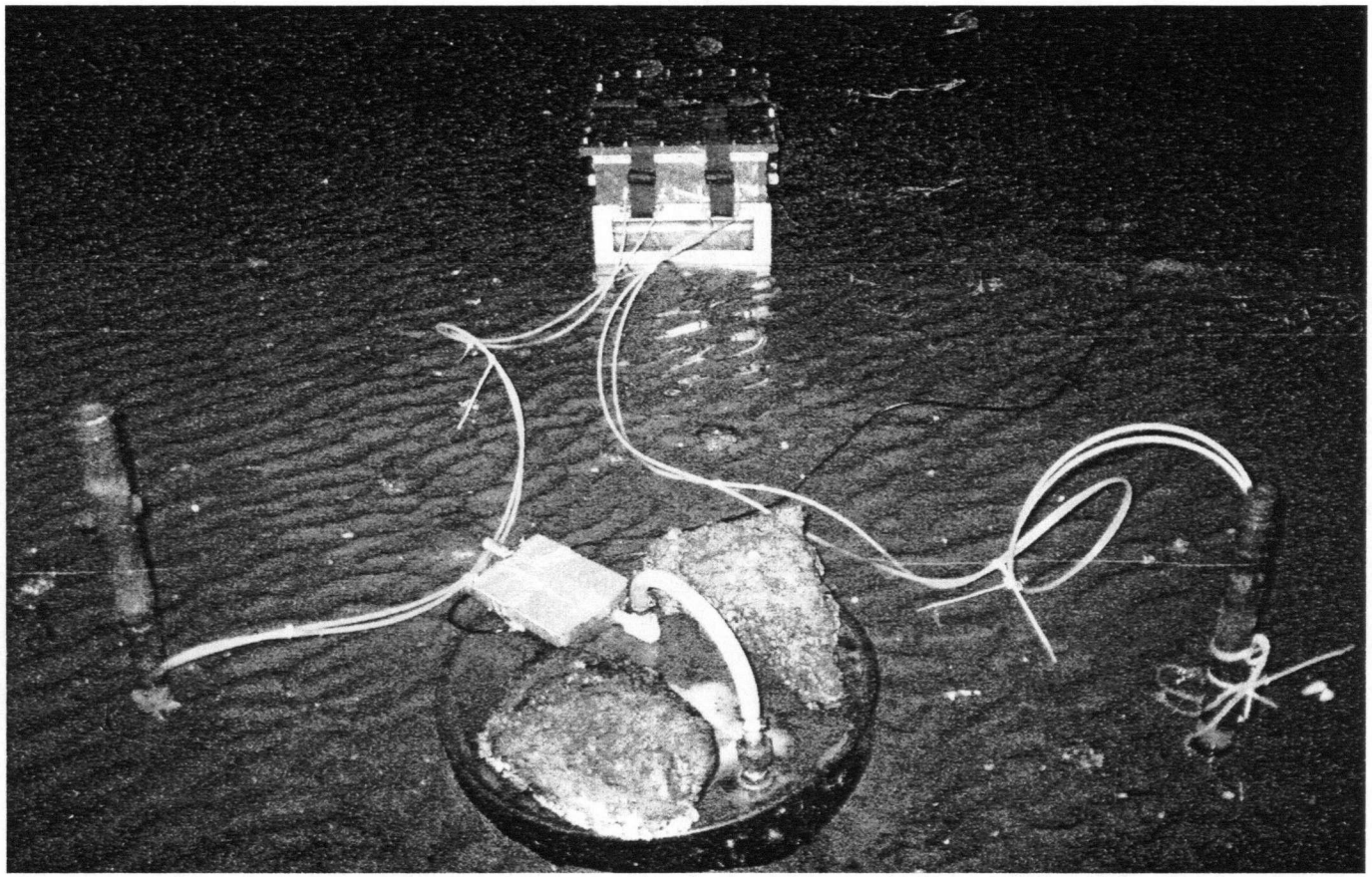

Figure 4-6: The seepage meter and piezometers were uncovered by the low tide on the second day of testing for about 5 hours (photo taken in the direction of shore).

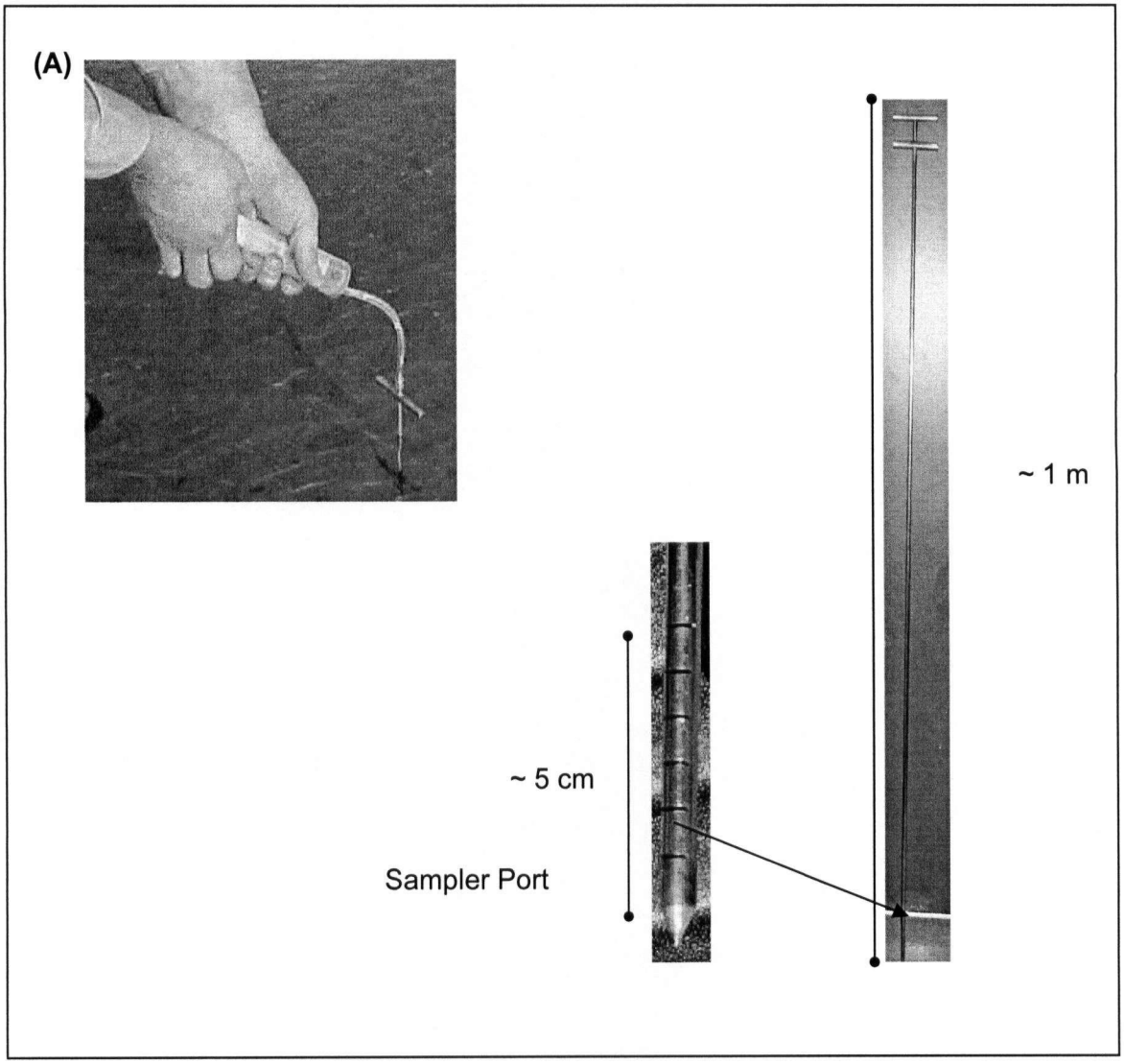

Figure 4-7: Water sampler used to collect pore water samples from within the seabed. The water level was typically 30 to 60 cm above the seabed during pore water sampling. (A) An example of a pore water sample being retrieved using the water sampler.

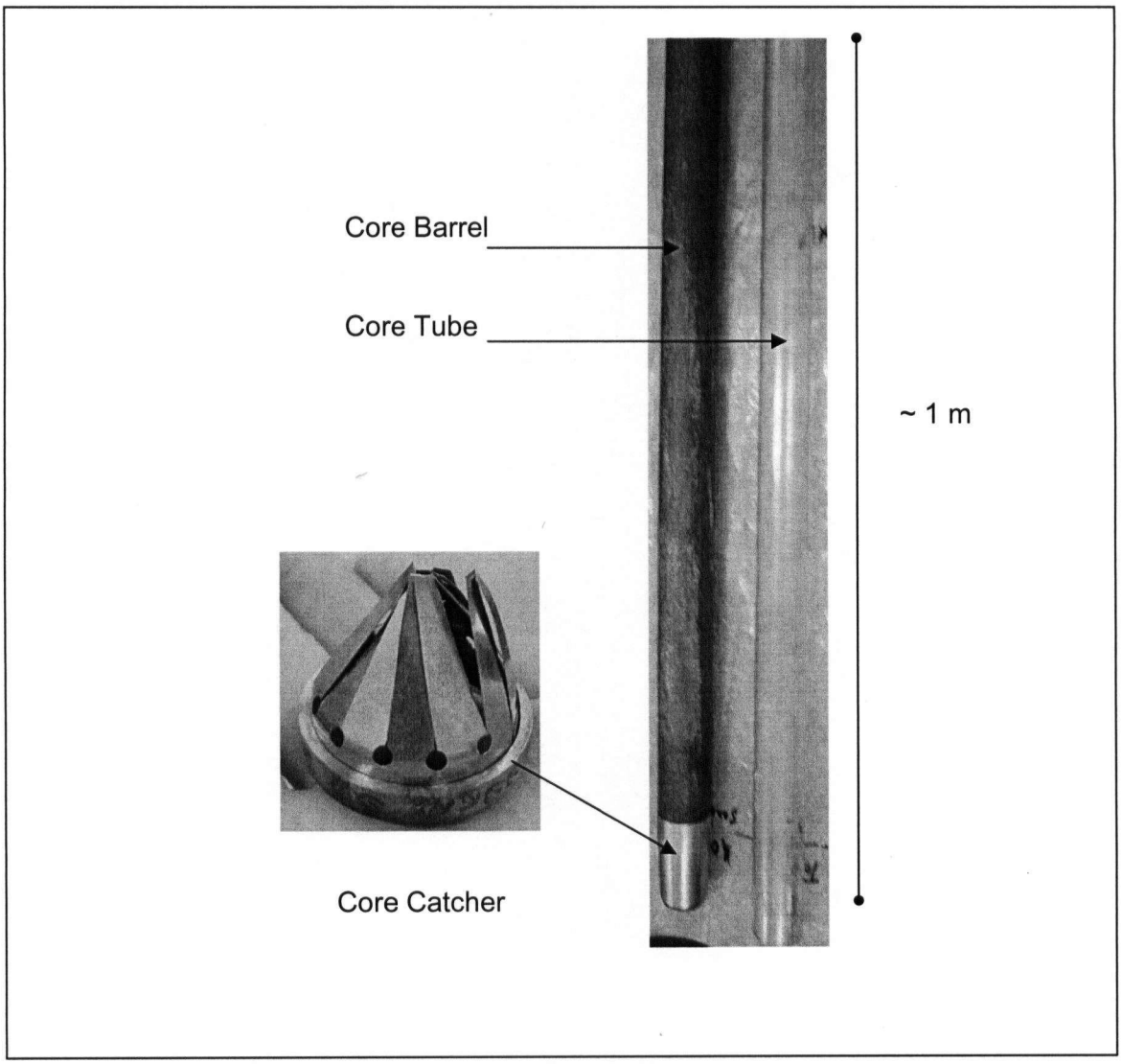

Figure 4-8: Core sampler used to collect sediment samples from adjacent to the piezometers of the DPS-II.

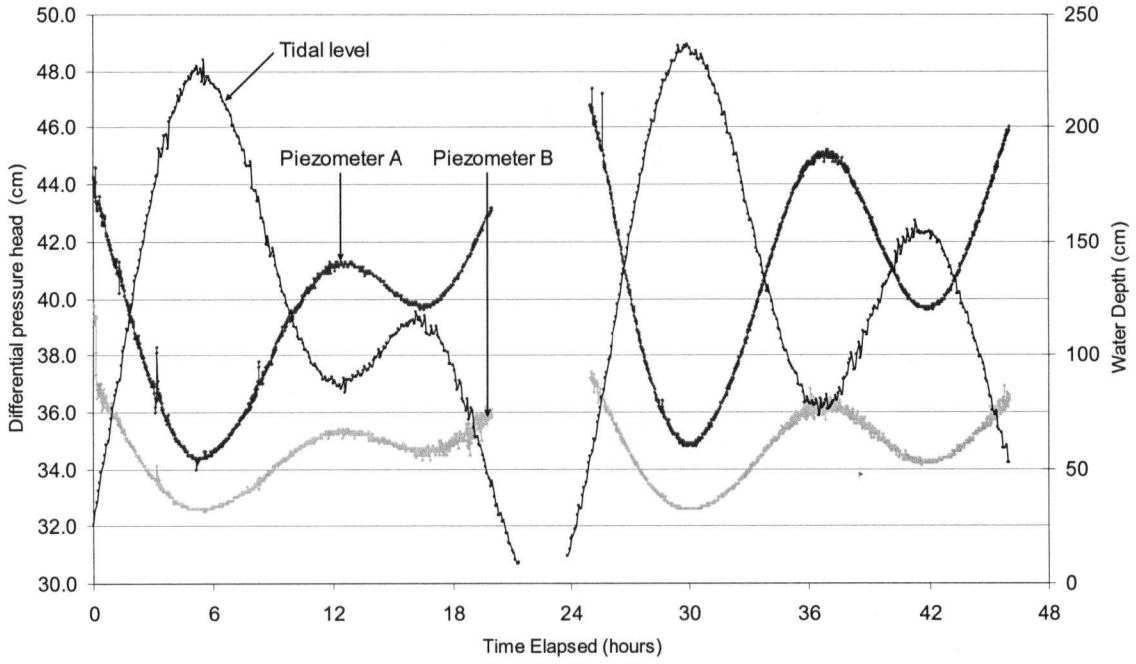

Figure 4-9: Comparison between 1 minute averages of the differential pressure head measurements by the DPS-II and 5 minute measurements of tidal levels collected in the near-shore at the Spanish Banks site. There is a gap in the field data because of the low tide occurring between 20-25 hours after the beginning of the experiment, which uncovered the instruments.

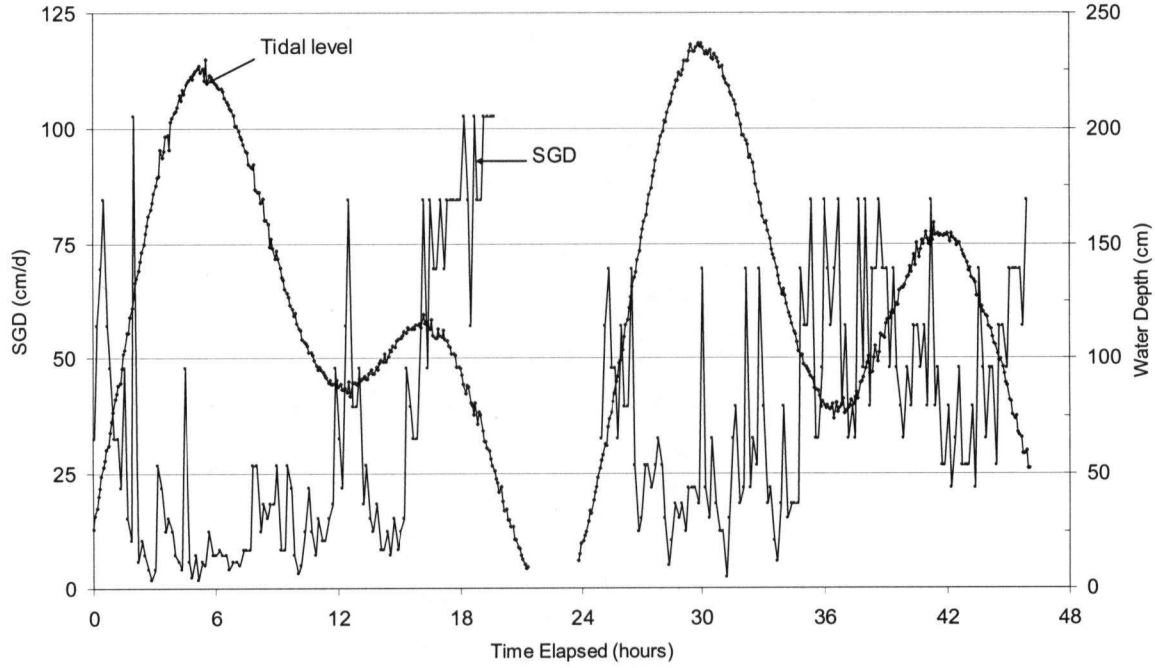

Figure 4-10: Comparison between 10 minute instantaneous measurements of SGD by a continuous heat type seepage meter and tidal levels.

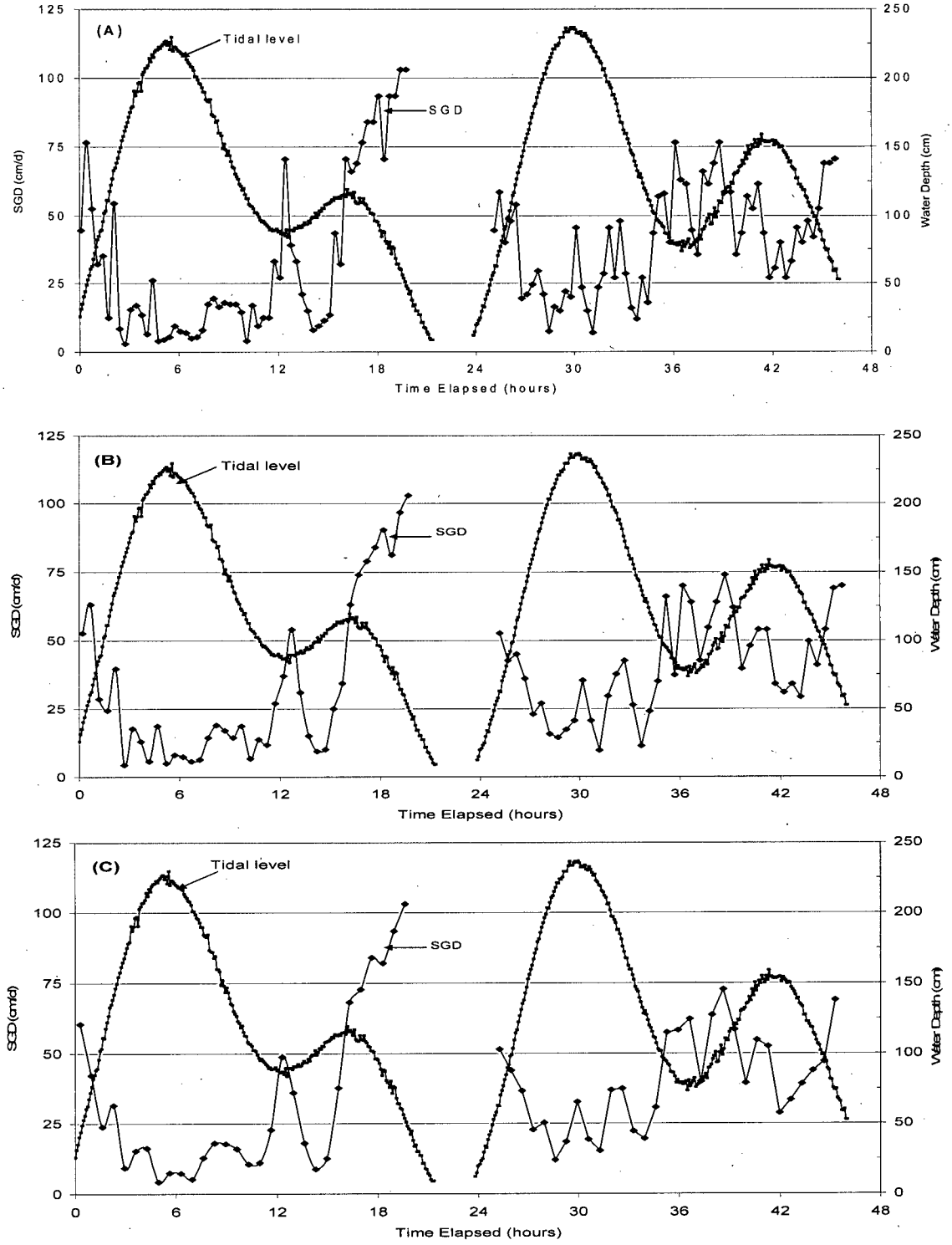

Figure 4-11: Averaged plots of 10 minute SGD measurements over different time intervals. (A) 20 minute average. (B) 30 minute average. (3) 40 minute average.

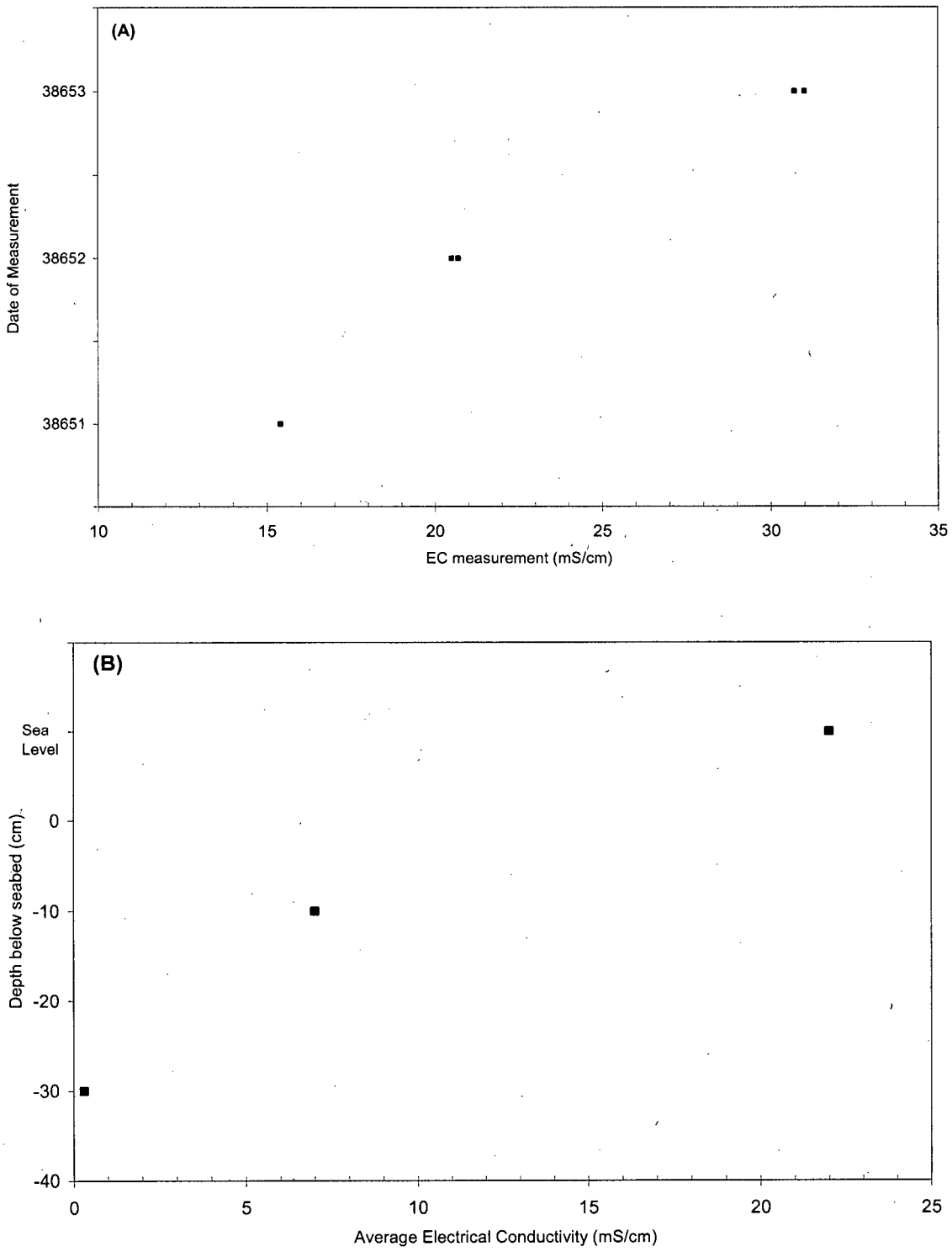

Figure 4-12: EC measurements of pore water samples collected during the low tides over the course of the experiment. (A) Seawater samples. (B) The average EC value of the water column, and 10 and 30 cm (top piezometer port) below the seabed derived from all pore water samples collected at these positions.

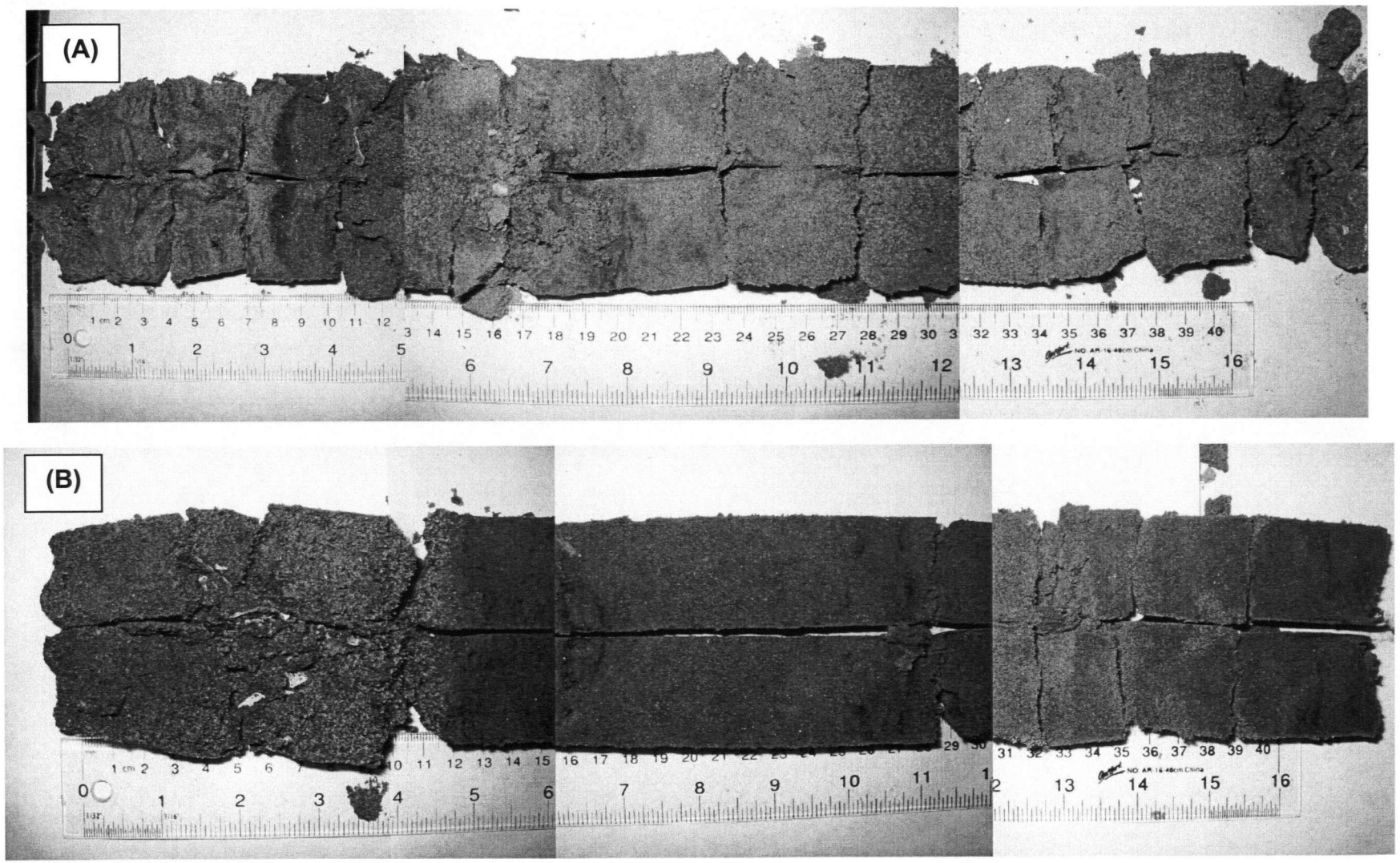

Figure 4-13: Core samples (A-Out and A-In) collected from adjacent to piezometer A. The locations of the cores relative to the piezometer in the field are shown in Figure 4-3. (A) A-Out. (B) A-In.

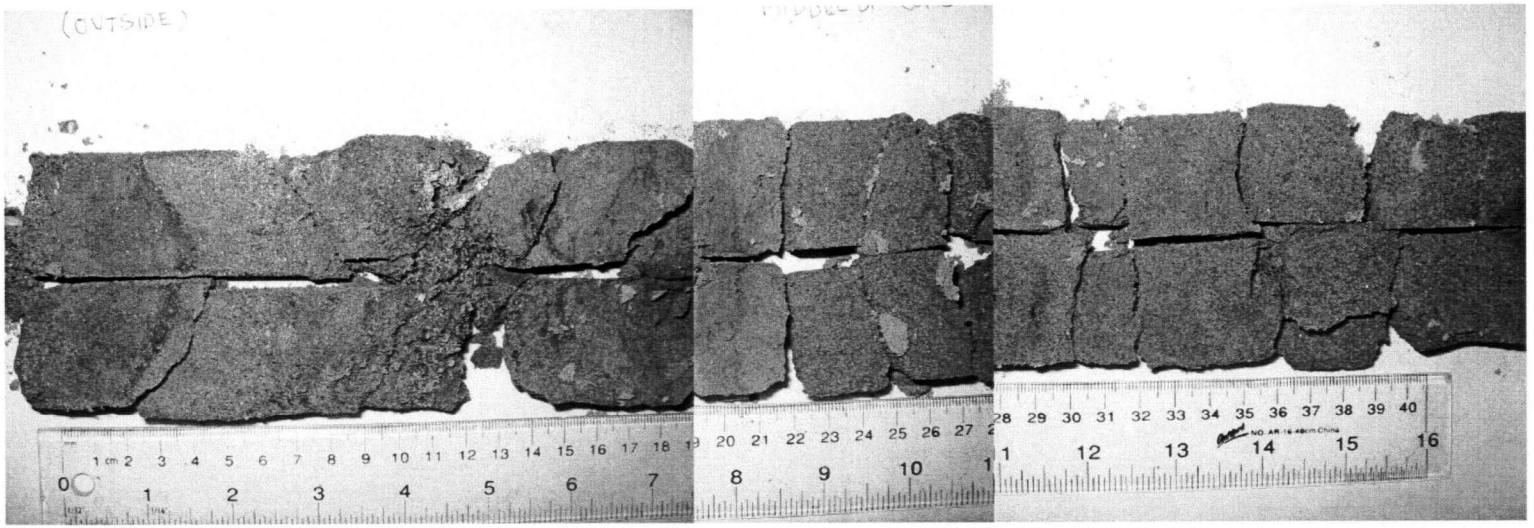

Figure 4-14: Core sample (B-In) collected from adjacent to piezometer B. The location of the core relative to the piezometer in the field is shown in Figure 4-3.

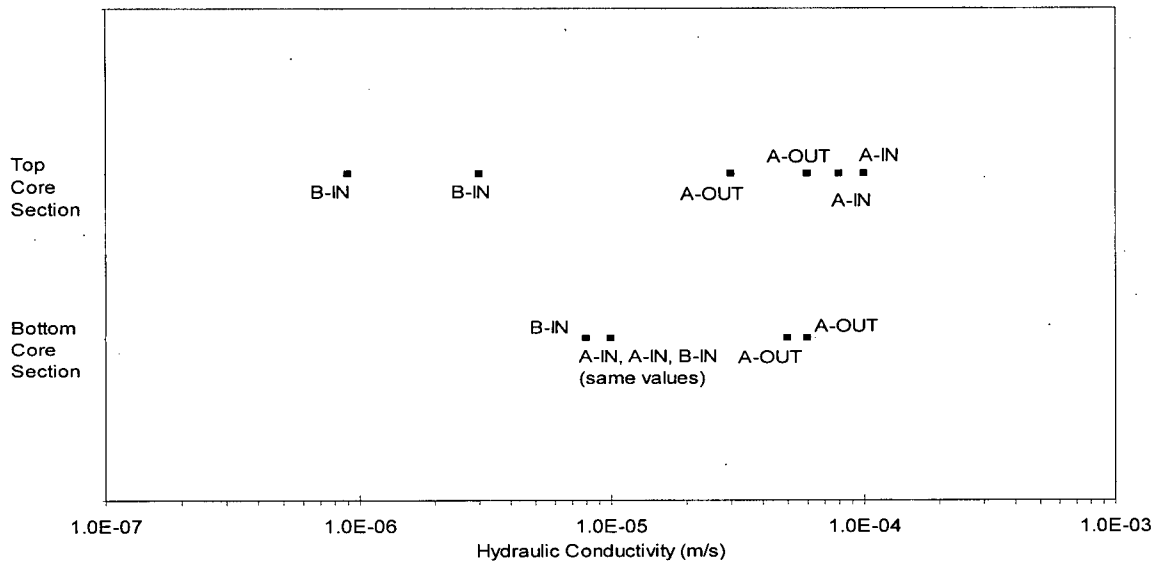

Figure 4-15: Hydraulic conductivity data derived from falling head tests for the core samples collected adjacent to the piezometers of the DPS-II. The letter labels indicate the estimates of hydraulic conductivity for a position relative to piezometer A or B, see Figure 4-3 for the location of these positions. The two estimates for each top and bottom section of core were based on using tap water and seawater as the hydraulic fluid for the falling head tests. Both estimates for the bottom core section of A-IN were 1 x 10^{-5} m/s.

5. Analyses of Field Measurements

5.1 Differential Pressure Heads and Calculated SGD Fluxes

An objective of this study is to investigate the relationship between differential fluid pressure heads and SGD flux rates, consequently it is necessary to examine the relative importance of the pressure gradient component of the SGD flux to the density-related gravity (i.e., buoyancy) component of the SGD flux. By expanding the gravity term in Darcy's Law, written in terms of fluid pressures (Equation 3.1), an equivalent freshwater head term, which represents the pressure driven component of flow, can be separated from a density related term, which represents the gravity-driven component of flow (Davies 1989).

Equivalent freshwater head at point A is expressed as:

$$H_f = \frac{P}{\rho_f g} + z \qquad \text{(Equation 5.1)}$$

where H_f is the equivalent freshwater head and ρ_f is the density of freshwater (1000 kg/m^3). The seepage flux is calculated using the following derived form of Darcy's law, expressed in terms of an equivalent freshwater head and a density-related gravity term:

$$q_z = -K_z\left(\nabla H_f + \frac{\Delta\rho}{\rho_f}\nabla z\right) \qquad \text{(Equation 5.2)}$$

where K_z is hydraulic conductivity, $\Delta\rho$ is the difference between the actual fluid density at point A and a reference fluid density. Equation 5.2 indicates seepage flux cannot be determined directly from the vertical gradient in freshwater head

and that a gravity driven component of flow must also be considered if it is of similar magnitude to the gradient in freshwater head.

Figure 5-1 shows the equivalent freshwater head gradients (dH_f/dz) that have been calculated based on the differential fluid pressure heads measured by the DPS-II at piezometers A and B, using the differential form of Equation 5.1 which is written as:

$$\frac{\delta H_f}{\delta z} = \frac{\delta}{\delta z}\left(\frac{P}{\rho_f g}\right) + \frac{\delta z}{\delta z} \qquad \text{(Equation 5.3)}$$

Direct measurements of fluid density in the field are not required for the calculation of equivalent freshwater head gradients. The first term on the right side of Equation 5.3 represents a gradient in differential fluid pressure head as shown by the following relationship:

$$\frac{\delta}{\delta z}\left(\frac{P}{\rho_f g}\right) = \frac{\delta \psi}{\delta z} \qquad \text{(Equation 5.4)}$$

Since differential fluid pressure head measurements between the measuring ports of the piezometers are obtained by the DPS-II, only the distance between the measuring ports of the piezometer is also required, to evaluate freshwater head gradients at the piezometers using Equation 5-3.

For the first high/low tidal cycle between 0 and 18 hours of the experiment, freshwater head gradients at piezometer A varied from about 0.11 at high tide to 0.33 at low tide. At piezometer B, over the same tidal cycle, freshwater head gradients ranged from 0.05 to 0.14. Over the second high/low tidal cycle between 24 and 37 hours into the experiment, the freshwater head gradients at piezometer A varied from 0.13 to 0.45 and at piezometer B from 0.05 to 0.17.

Because fluid density measurements were not obtained between the pressure measuring ports of the piezometer (i.e., at the point of the flux calculation), an upper bound for the gravity term in Equation 5.2 was constrained by assuming a fluid density equal to seawater (1025 kg/m^3) at the point of the flux calculation. It is unlikely that the fluid density in the seabed at depths between the ports of the piezometers is equal to seawater since EC measurements obtained at the top measuring ports of the piezometer at low tide indicated a significant component of freshwater. However, the possibility of seawater at these depths cannot be excluded, especially during the high tide, when the seaward movement of freshwater is at a minimum. Based on a reference density of 1000 kg/m^3, the calculated upper bound for the density-gravity term that could be expected at the field site had a magnitude of 0.025. In this case, the density- gravity component of flow is 1 order of magnitude lower than the lowest estimate for freshwater head gradient at piezometer A. However, the gravity component of flow is significant in comparison to the freshwater gradients estimated at piezometer B at high tide.

Estimates that are likely more reflective of the gravity driven component of flow at the site were calculated using actual fluid densities at the point of the flux calculation that were equivalent to the EC measurement at a depth of 10 cm below the seabed and the average of the EC measurement obtained from the pore water samples adjacent to the top port of the piezometers (30 cm below the seabed). EC was converted to fluid density using the relationships shown in Figure 5-2 and Figure 5-3 (EOSC 428/532: Field Techniques in Groundwater Hydrogeology course notes). The magnitude of the calculated density-gravity component using an actual fluid density of 1004 kg /m^3 (equivalent to EC measurement from 10 cm below seabed) was 0.004 and for an actual fluid density of 998 kg/m^3 (equivalent EC top measuring ports of piezometer) was 0.002. In these cases, the gravity driven component of flow is 2 orders of magnitude less than the lowest estimate of freshwater head gradients at the piezometers A and an order of magnitude less than the lowest freshwater head gradient at B. These findings suggest that for the conditions at the site, the pressure driven gradient component of flow is likely significantly more dominant than density gravity effects.

SGD rates were calculated based on the freshwater head gradients at piezometer A and B, for the purpose of comparison with SGD rates measured by the seepage meter. Using Equation 5.2 and assuming that gravity density effects were negligible, SGD rates at each piezometer were calculated by varying the estimate of hydraulic conductivity until a reasonable match with the SGD rates by

the seepage meter was obtained (Figure 5-4). SGD rates calculated based on the freshwater gradients at piezometer A were found to best match the SGD rates measured by the seepage meter using a hydraulic conductivity of 1.5×10^{-5} m/s. At piezometer B, a hydraulic conductivity of 4×10^{-5} m/s, best matched the SGD rates measured by the seepage meter. The hydraulic conductivity values assumed at each piezometer to calculate the best match of SGD with the field based SGD rates are within the constraints of the available hydraulic conductivity data set obtained from the core samples.

Given the variability in the available hydraulic conductivity data set (9×10^{-7} to 6×10^{-5} m/s) it is also plausible, that discharge at each of the piezometers could have been different than that recorded by the seepage meter. Michael (2003) showed that differences in SGD over spatial scales of 1 m can be similar in magnitude to differences in SGD over larger scales. The 1999 cluster experiment by Michael (2003) indicated that seepage meters located next to each other may differ greatly in discharge. For example, during the same two hour period, two seepage meters less than 2 m apart registered 5 cm/d and 37 cm/d.

Three key modifications to the experimental method that would improve the interpretation of calculated and field based SGD rates are: (1) the addition of a second seepage meter to improve the reliability of field based SGD measurements, (2) more measurements of the pore water at depths between the measuring ports of the piezometer in order to better characterize the fluid

density variation in the seabed and thus provide further insight regarding the significance of the pressure driven component of flow compared to gravity effects and, (3) a better characterization of the hydraulic conductivity at the site.

5.2 Hydrogeologic Model

Model based predictions of SGD rates and the vertical hydraulic gradients in the seabed have been developed using the finite element model FRAC3DVS (Therrien and Sudicky 1996). FRAC3DVS is used to simulate a 1D uniform density flow model that examines how SGD rates are enhanced and diminished by tidal fluctuations. A 1D model excludes the simulation of density dependent flow because convection cells that normally form due to density variations cannot be simulated by only vertical flow.

The hydrogeologic model examined is shown in schematic form by Figure 5-5. The domain of the model has dimensions of 1 m x 10 m. A transient hydraulic head boundary at the top of the domain is applied to account for the sea level fluctuations due to the semi-diurnal tides at the site. The specified head at the top boundary varies from 0.1 m to a maximum of 2.26 m with an arithmetic mean value of 1.28 m. A constant hydraulic head is specified at the base of the domain.

Two models have been constructed to provide a basis for comparison with the transient changes in vertical hydraulic head gradients in the seabed calculated based on the differential pressure head measurements by the DPS-II (section

3.5.1) and the SGD rates by the seepage meter. In Model 1 it is assumed that the model domain is homogenous. In Model 2, a domain consisting of two layers is used to characterize heterogeneity with depth.

The boundary conditions assigned to Model 1 are:

Base- No measurements are available to constrain the conditions in the sediment with depth at the field site. A constant hydraulic head value is assigned to the boundary. For the initial simulation of Model 1, a value of 1.0 m is assumed as an arbitrary value and provides a hydraulic gradient of 0.1 between the base and the top of the model domain.

Top- Along the seabed, a transient hydraulic head boundary condition is applied to simulate the semi-diurnal tides measured during the experiment at the site.

No information is available about the porosity of the sediment. A typical value of porosity for fine sand of 0.3 (Domencio and Schwartz 1997) has been specified for all simulations. Specific storage (S_s) is defined as the volume of water that an aquifer releases from or takes into storage per unit surface area of the aquifer per unit aquifer thickness per unit change in head. Specific storage is expressed as:

$$S_s = \rho_w g \left(\beta_p + \eta \beta_w\right) \qquad \text{(Equation 5.4)}$$

where ρ_w is density of water, β_p is the vertical compressibility of the porous matrix, η is the porosity of the porous matrix and β_w is the compressibility of water. Using Equation 5.4, a value of Ss for the simulations was calculated as between 1×10^{-3} to 5×10^{-5} m^{-1} based on the assumption that water is incompressible and a typical range for the vertical compressibility of loose sand to dense sand gravel (Fetter 2001). A value near the middle of the calculated range of S_s (1×10^{-4} m^{-1}) has been used for the simulations unless otherwise noted. In some cases, the sensitivity of the results to S_s has been evaluated by varying the value of S_s from 1×10^{-4} m^{-1} to 5×10^{-5} and 5×10^{-4} m^{-1}.

Hydraulic heads are simulated at vertical increments of 20 cm within the model domain. Hydraulic gradients are calculated based on simulated hydraulic heads in the domain between points at 0.3 and 0.6 m, for a datum defined at 0.6 m (i.e. a positive hydraulic gradient indicated upward flow). Simulated SGD rates are monitored by a flux output node specified along the top boundary of the domain.

Results Model 1

Figure 5-6 illustrates the hydraulic head gradients and the SGD rates for the case where it is assumed the hydraulic conductivity of the domain is equal to the geometric mean of the harmonic averages of the core sections estimated from the falling head tests (1×10^{-5} m/s). A comparison of the magnitude of the hydraulic head gradients and SGD rates with that obtained from field measurements by the DPS-II and seepage meter indicates a poor

correspondence. The simulation predicts recharge is occurring at the site at most times during the tidal cycle, which is not observed from the field measurements.

A second simulation was completed in which the bottom boundary condition was assigned a higher value of h= 2.5 m (Figure 5-7). A better agreement was obtained between the simulated hydraulic gradients and the field based hydraulic gradients values at piezometer B but not at piezometer A. In this simulation, predicted SGD rates indicated discharge at the site but were lower than field-based SGD measurements.

A third simulation was completed in which the model domain was assigned a hydraulic conductivity four times higher (4×10^{-5} m/s) than in the first two cases (Fig. 5-8). A comparison of the magnitude of the hydraulic head gradients at piezometer B and SGD rates with that obtained from field measurements by the DPS-II and seepage meter indicates a good correspondence but again not at piezometer A. Discrepancies between the simulated and field based SGD rates at approximately 20 hours after the beginning of the experiment are likely a result of seepage meter measurement artefacts caused by the falling tide, which during this time was beginning to uncover the seepage meter (section 4.2).

For the next two simulations, the S_s value was varied from 1×10^{-4} m^{-1} to 5×10^{-5} and 5×10^{-4} m^{-1} (Figure 5-9). There was no significant change in the simulated results of hydraulic gradient.

The hydraulic head at the base of the model was increased to values of 3.0 and 5.0 m in an attempt to simulate the higher hydraulic gradients at piezometer A (Figure 5-10). Although the relative magnitude of the simulated hydraulic gradients is closer to the field based measurements, it does not appear possible to explain the larger fluctuations in the transient changes in vertical hydraulic gradients at piezometer A over the tidal cycle using Model 1. Given the negligible effect of S_s on the model results, it is likely not a storage effect causing the difference between the simulated and field based results of hydraulic gradient at piezometer A using Model 1. The purpose of the second model is to provide insight to the discrepancy between the hydraulic gradients measured at piezometer A and piezometer B.

Results Model 2

To maintain consistency with Model 1, the boundary conditions are not modified. To obtain higher hydraulic gradients, a 1 m thick layer was created at the top of the domain, and assigned a lower hydraulic conductivity equal to the geometric mean of all the core sections of 2×10^{-5} m/s. There was no physical basis for the addition of a 1 m thick layer. Although the magnitude of the SGD rates is in approximate agreement with field based SGD measurements, the correspondence between simulated and field based estimates of hydraulic head gradients at piezometer A decreases after 1 day has elapsed (Fig. 5-11).

A second simulation using Model 2 was completed, in which a lower hydraulic conductivity of 1.5×10^{-5} m/s was assigned to the top layer (Figure 5-12). A comparison of the hydraulic head gradients and SGD rates with that obtained from field measurements at piezometer A by the DPS-II and seepage meter indicates a better agreement, however the magnitude of the simulated hydraulic gradient during the latter portion of the simulation (after 24 hours) are lower than field based measurements.

The hydraulic head specified at the base of the domain was increased from 2.5 to 3.0 m to account for the lower hydraulic gradients simulated in the latter portions of the simulation (Figure 5-13). The simulated hydraulic gradient over the first 20 hours of the simulation were higher than the field based measurements at piezometer A. In the period after the gap in the field measurements, the simulated results were also higher, but to a lesser extent.

For the next two simulations, the S_s value of the top layer was varied from 1×10^{-4} m^{-1} to 5×10^{-4} and 5×10^{-5} m^{-1}. There was no significant change in the simulated results of hydraulic gradient or SGD rates (results not shown).

Although a reasonable agreement was obtained between simulated hydraulic gradients using Model 2 and hydraulic gradients at Piezometer A, there was not a consistent match over the entire tidal cycle. A better characterization of the heterogeneity with depth at the field site may be useful for improving the

conceptual set up of the models and providing a better match with the field measurements at piezometer A.

The 1D flow models were also used to provide insight about the highest SGD rates observed at low tide by the field measurements at the Spanish Banks site (and also predicted by the models) compared to other coastal sites that show a time lag of a few hours between the highest SGD rates and low tide. Caulkins (2003), using a 1D model similar to the models constructed in this study, obtained results that showed the highest SGD rates occurred at the transition between high and low tide for a field site located along the northeastern Gulf of Mexico. A plot of simulated hydraulic head values with depth at different times over the tidal cycle showed that the hydraulic gradient was at a minimum at the high and low tides.

A key difference between the simulations by Caulkins (2003) and the simulations completed in this study are the values of hydraulic conductivity and specific storage specified for the domain. The domain of the model constructed by Caulkins was divided into two layers to represent a surficial aquifer and a limestone layer (Intracoastal Formation) that characterized the coastline at the field site. The upper 6 m layer of the domain was assigned a hydraulic conductivity of 1×10^{-5} m/s and S_s of 1×10^{-3} m^{-1}. The bottom 4 m layer was assigned a lower hydraulic conductivity of 1×10^{-6} m/s and S_s of 1×10^{-4} m^{-1}. The lowest hydraulic conductivity applied to the model domains in this study was 1.5

x 10^{-5} m/s. The values of hydraulic conductivity for the two layers in Model 2 used in this study were also closer in magnitude, than in the simulations by Caulkins. The S_s used by Caulkins was also varied between the layers and a higher value for S_s was applied to the top layer than for model 1 and model 2 simulations in this study.

A simulation using Model 1 was completed with a lower value of hydraulic conductivity of 1 x 10^{-6} m/s (Figure 5-14). The simulation showed little shift between the highest SGD rates and low tide. To also investigate the effect of storage on the time lag, the value of S_s was changed from 1 x 10^{-4} m^{-1} used in the previous simulations to higher and lower values of 5 x 10^{-5} and 5 x 10^{-4} m^{-1}. No significant effect was observed (results not shown).

A simulation was completed using Model 2 with a lower value of hydraulic conductivity (1 x 10^{-6} m/s) for the bottom layer. As well the S_s value of the top layer was increased to 1 x 10^{-3} m^{-1} to also match the values used by Caulkins (Figure 5-15). The results show the highest SGD rates have shifted and occur at the transition between the high and low tide.

A second simulation was completed with the upper layer thickness increased to 6 m to provide a better comparison with the simulations completed by Caulkins. The simulated SGD rates again showed a time lag between the highest SGD rates and low tide. A plot of the hydraulic head with depth in the domain at

different times over the tidal cycle showed the hydraulic gradient near the top of the domain was at a minimum at high tide (Figure 5-16).

A third simulation was completed to investigate whether it was the difference in hydraulic conductivity between the layers that caused the time lag or also the lower values of hydraulic conductivity. The upper 6 m layer was assigned a higher hydraulic conductivity of 1×10^{-4} m/s and the bottom 4 m layer was also assigned a higher value of 1×10^{-5} m/s. The results obtained showed the highest SGD rates occurred at low tide with no time lag (results not shown).

Despite some discrepancies between the simulated and field based measurements, it appears possible to satisfactorily explain the field based estimates of the transient changes in the vertical hydraulic gradient in the seabed at piezometer A and B as well as the SGD rates using a 1D uniform density flow model with boundary conditions that consider the sea level fluctuations due to semi-diurnal tides at the site. Although a reasonable agreement was obtained between simulated hydraulic gradients using Model 2 and hydraulic gradients at Piezometer A, there was not a consistent match over the entire tidal cycle. The possible discrepancy in the hydraulic gradients at piezometer A and the simulated results could be the result of heterogeneity that was not well characterized by the models. Also the error associated with the calculated hydraulic gradients (estimated as +/- 0.01) may have contributed to the difference between the simulated and field based values of hydraulic gradients. However if

measurement error was the only source for the discrepancy between the modelled and simulated results, the discrepancy should have been more consistent over the simulated period (unless the error associated with the DPS-II changed over time).

The models have also shown that the timing of the highest SGD rates relative to the low tide is sensitive to the value of hydraulic conductivity. Simulations using model 2 showed a greater time lag than model 1 simulations, suggesting heterogeneity with depth may be important in influencing the timing between the highest SGD rates and low tide.

To advance the framework for modelling SGD and hydraulic gradients at the site, data sets that would be beneficial are: (1) salinity-depth profiles in the near-shore to provide more insight about the applicability of using a uniform flow model to simulate flow at the site, (2) a better characterization of the hydraulic conductivity in the area of the deployment to constrain the heterogeneity with depth, and (3) more information about the geology at depth.

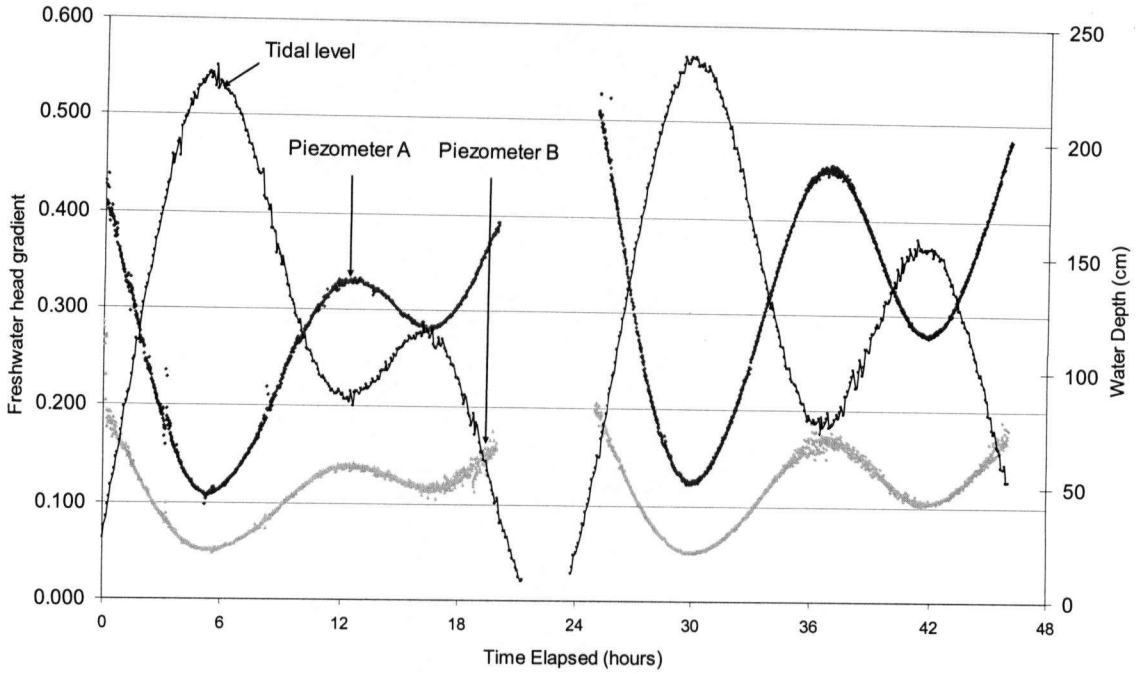

Figure 5-1: Freshwater head gradients calculated based on the differential pressure head measurements by the DPS-II at piezometer A and B.

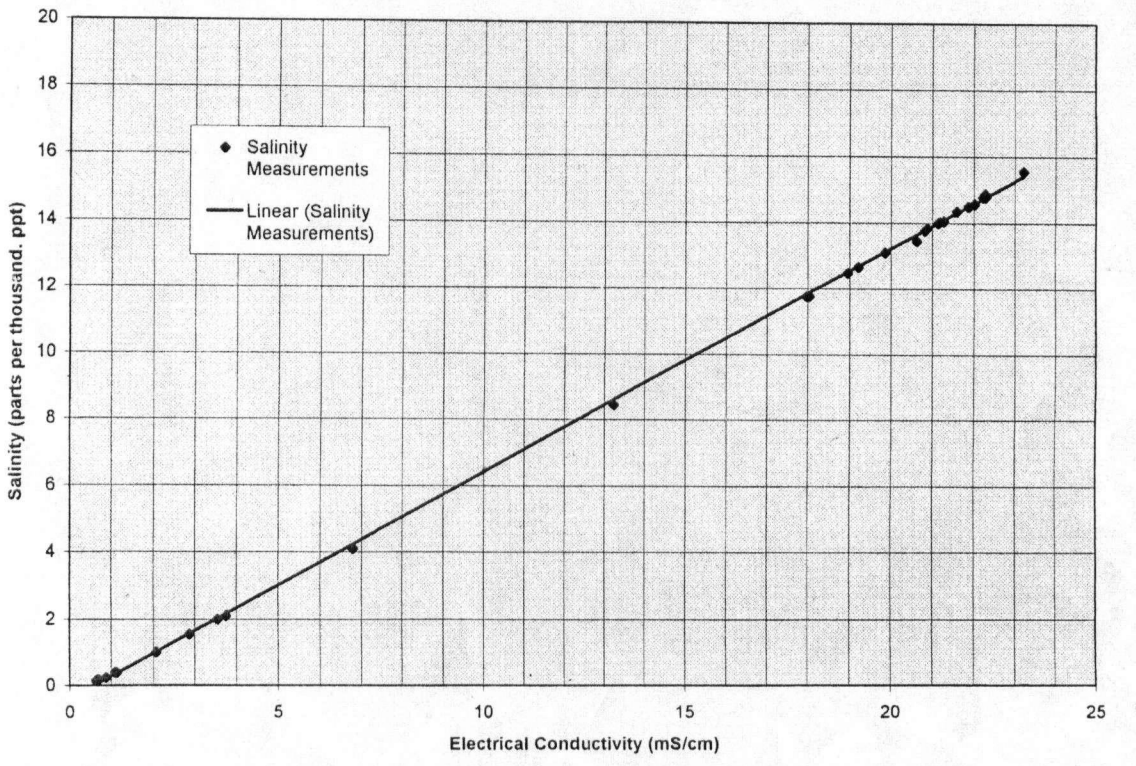

Figure 5-2: Relationship used to convert EC measurements to salinity (EOSC 482/532: Field Techniques in Groundwater Hydrogeology course notes).

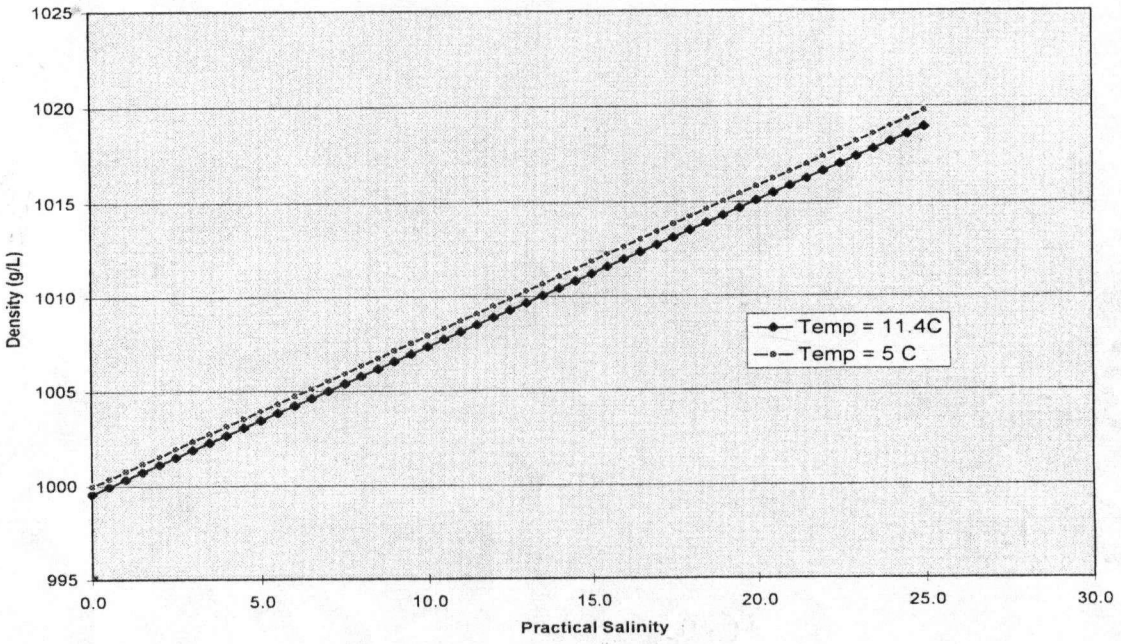

Figure 5-3: Relationship used to convert salinity to fluid density (EOSC 482/532: Field Techniques in Groundwater Hydrogeology course notes).

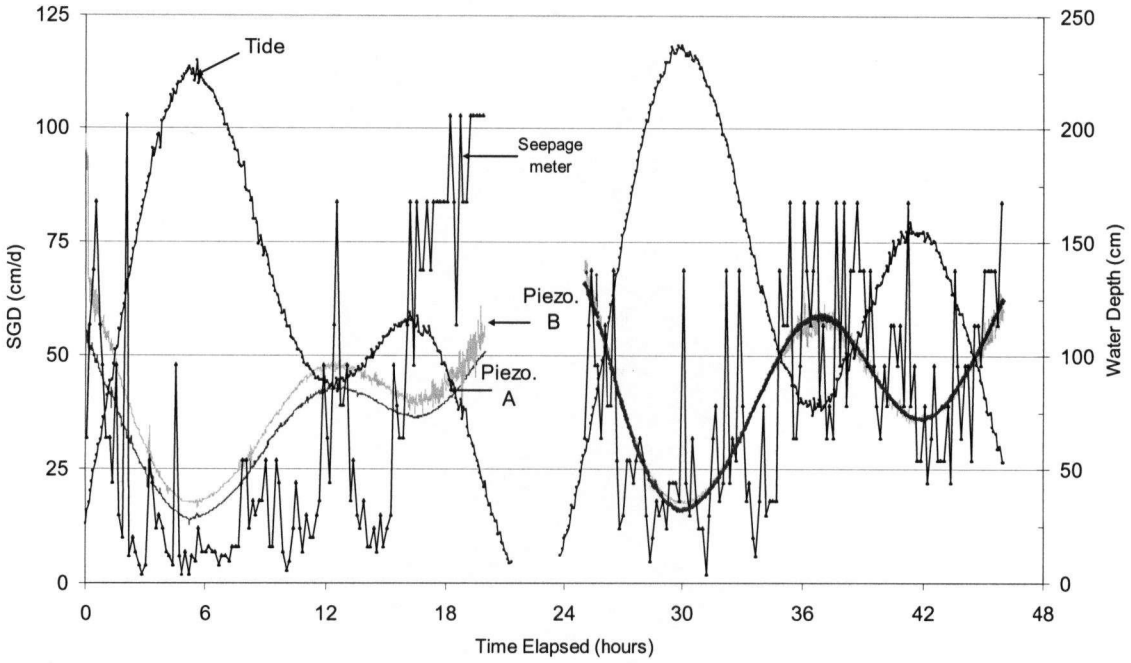

Figure 5-4: Comparison between SGD rates calculated based on the differential pressure head measurements by the DPS-II using Darcy's Law and measured SGD rates by the seepage meter. Calculated SGD rates were derived using hydraulic conductivity values of 1.5×10^{-5} m/s at piezometer A and 4×10^{-5} m/s at piezometer B, which were based on the value that provided the best match with field based SGD rates and were within the range of the available hydraulic conductivity data set.

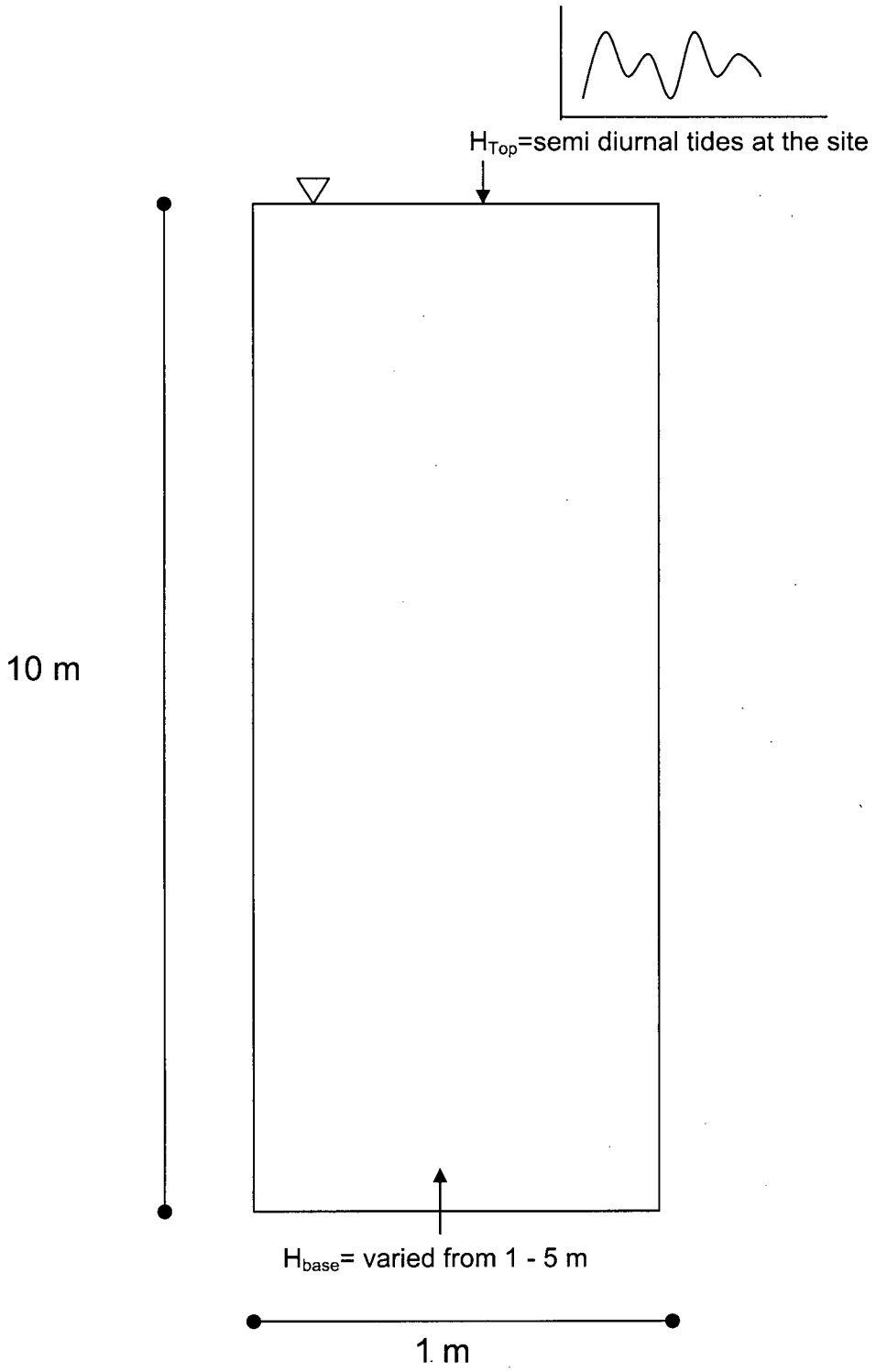

Figure 5-5: Generalized schematic of set up of hydrogeologic model examined in this study.

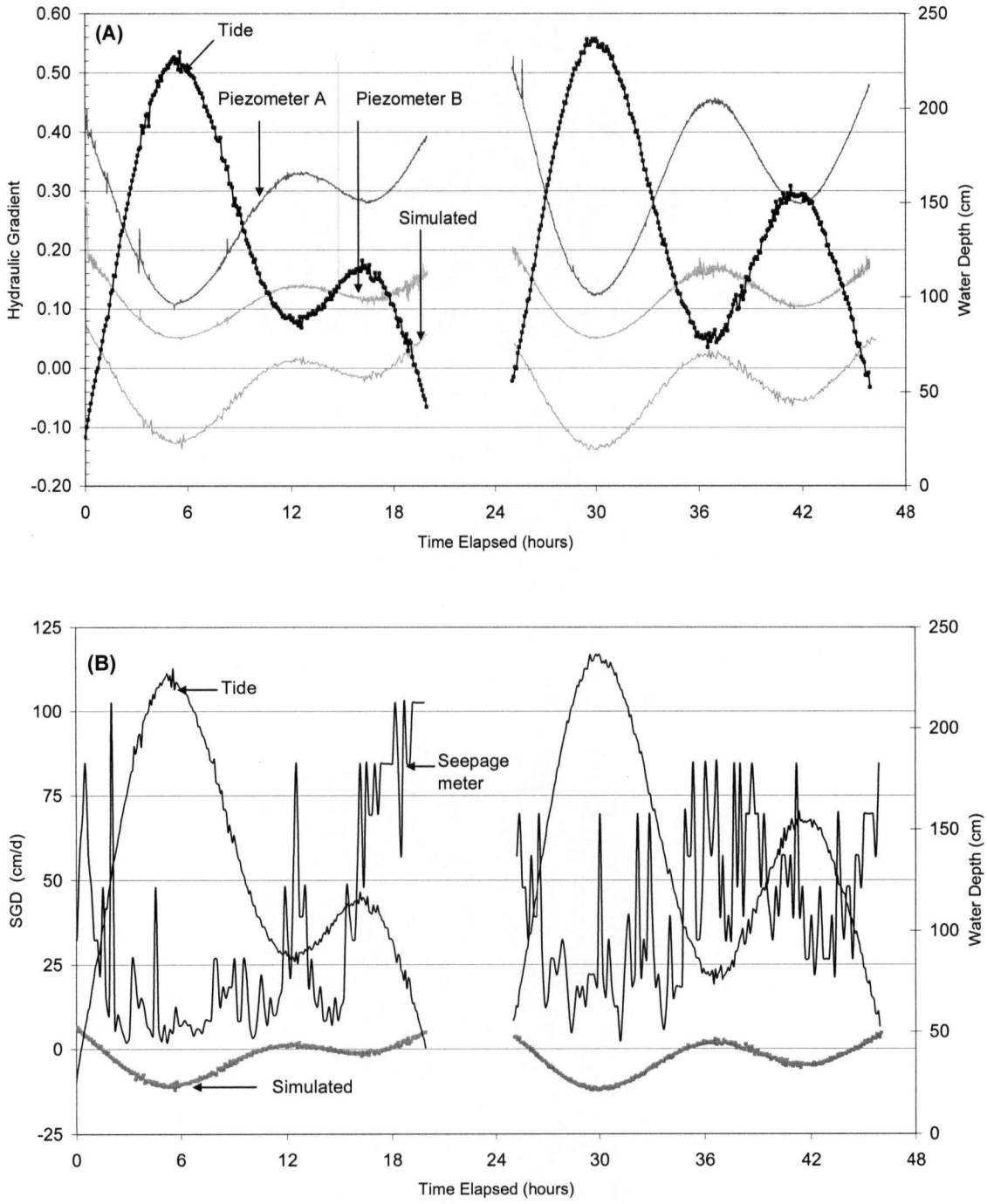

Figure 5-6: Comparison between field based measurements and Model 1 simulation: K = 1x 10^{-5} m/s, Ss = 1 x 10^{-4} m^{-1} and H_{base} = 1.0 m. (A) Hydraulic gradients between 0.3 and 0.6 m below the seabed. (B) SGD rates.

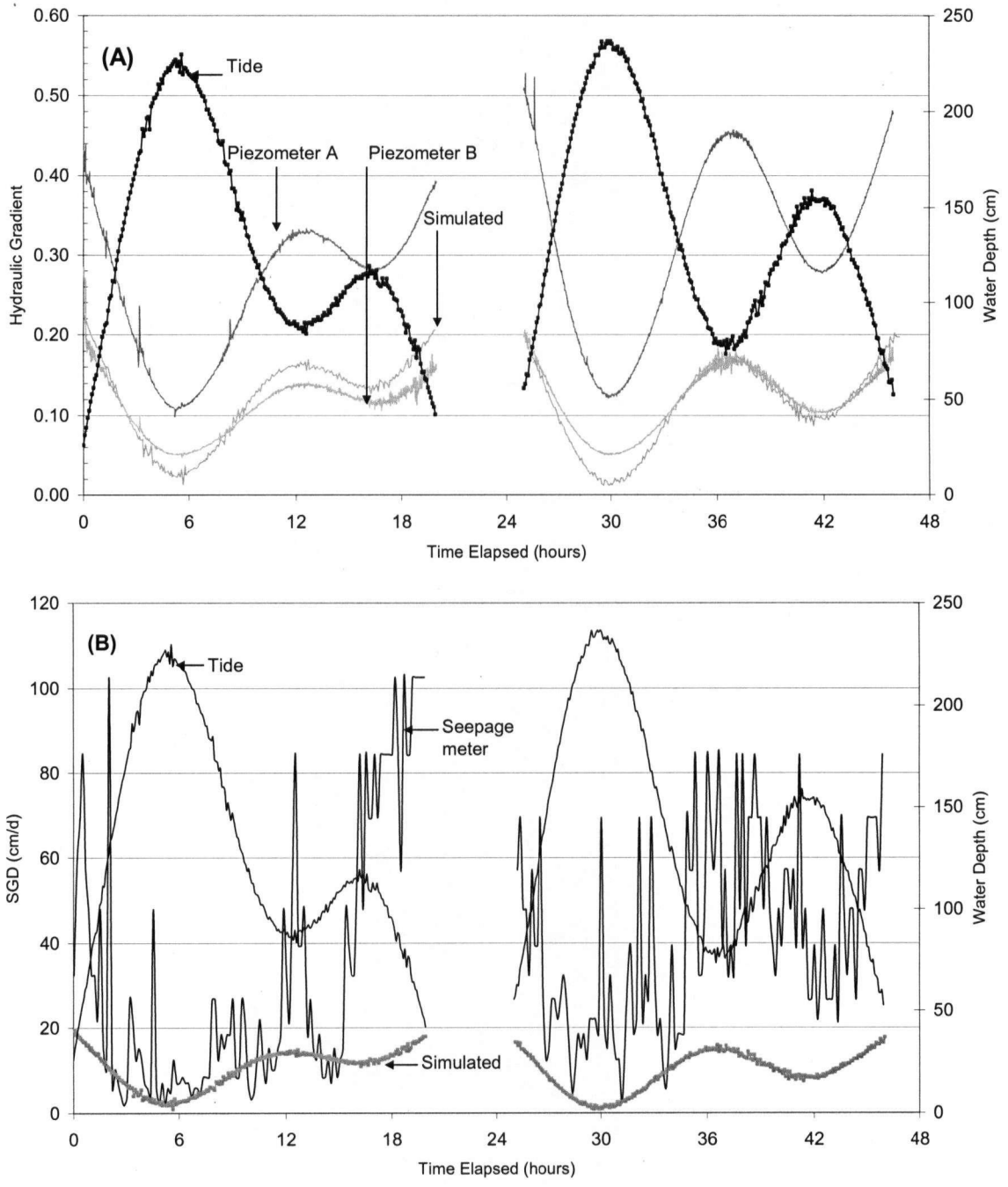

Figure 5-7: Comparison between field based measurements and Model 1 simulation: K = 1 x 10-5 m/s, Ss = 1 x 10-4 m-1 and Hbase = 2.5 m. (A) Hydraulic gradients between 0.3 and 0.6 m below the seabed. (B) SGD rates.

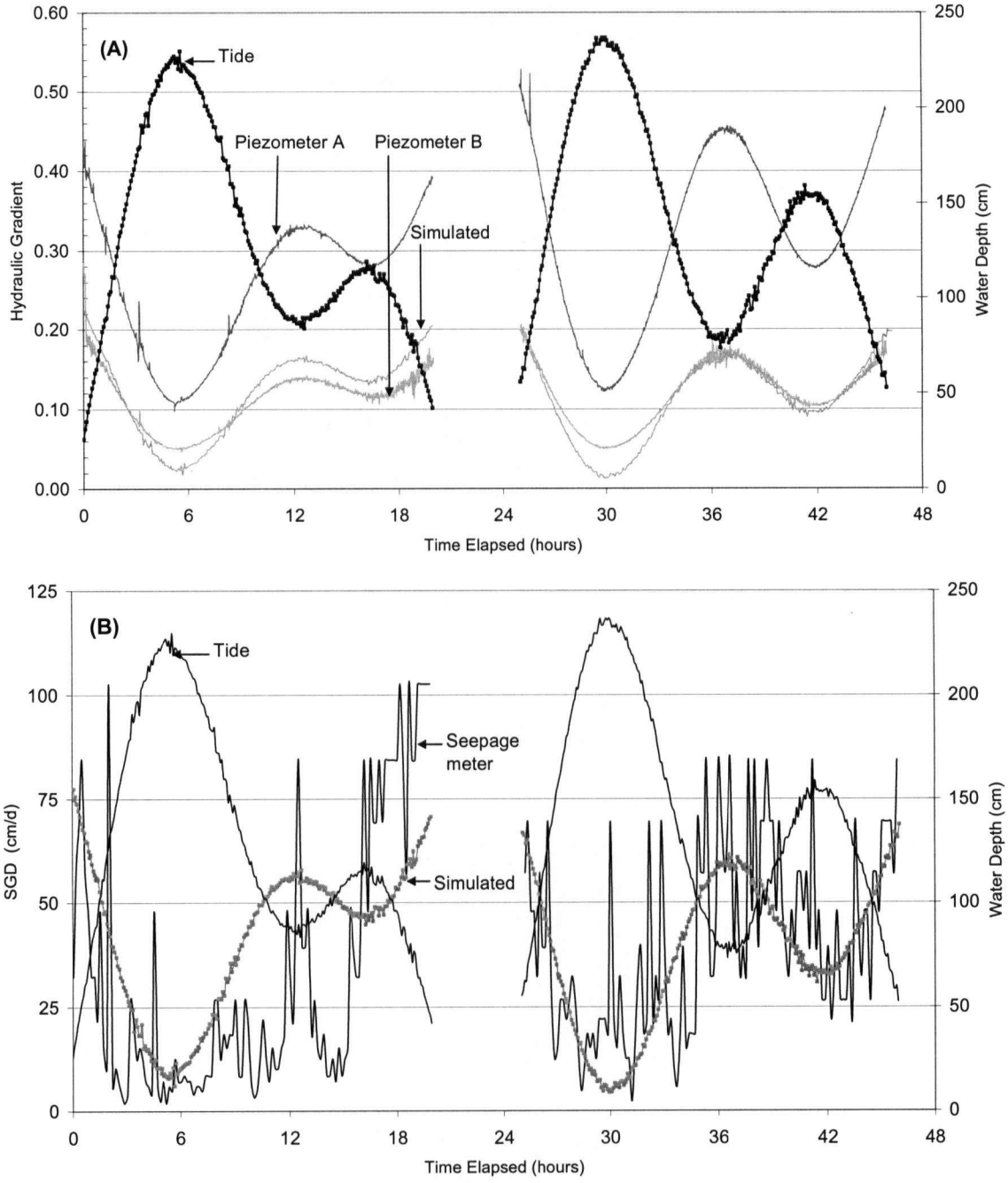

Figure 5-8: Comparison between field based measurements and Model 1 simulation: K = 4 x 10^{-5} m/s, Ss = 1 x 10^{-4} m^{-1} and H_{base} = 2.5 m. Best match of the simulated results for piezometer B data (A) Hydraulic gradients between 0.3 and 0.6 m below the seabed. (B) SGD rates.

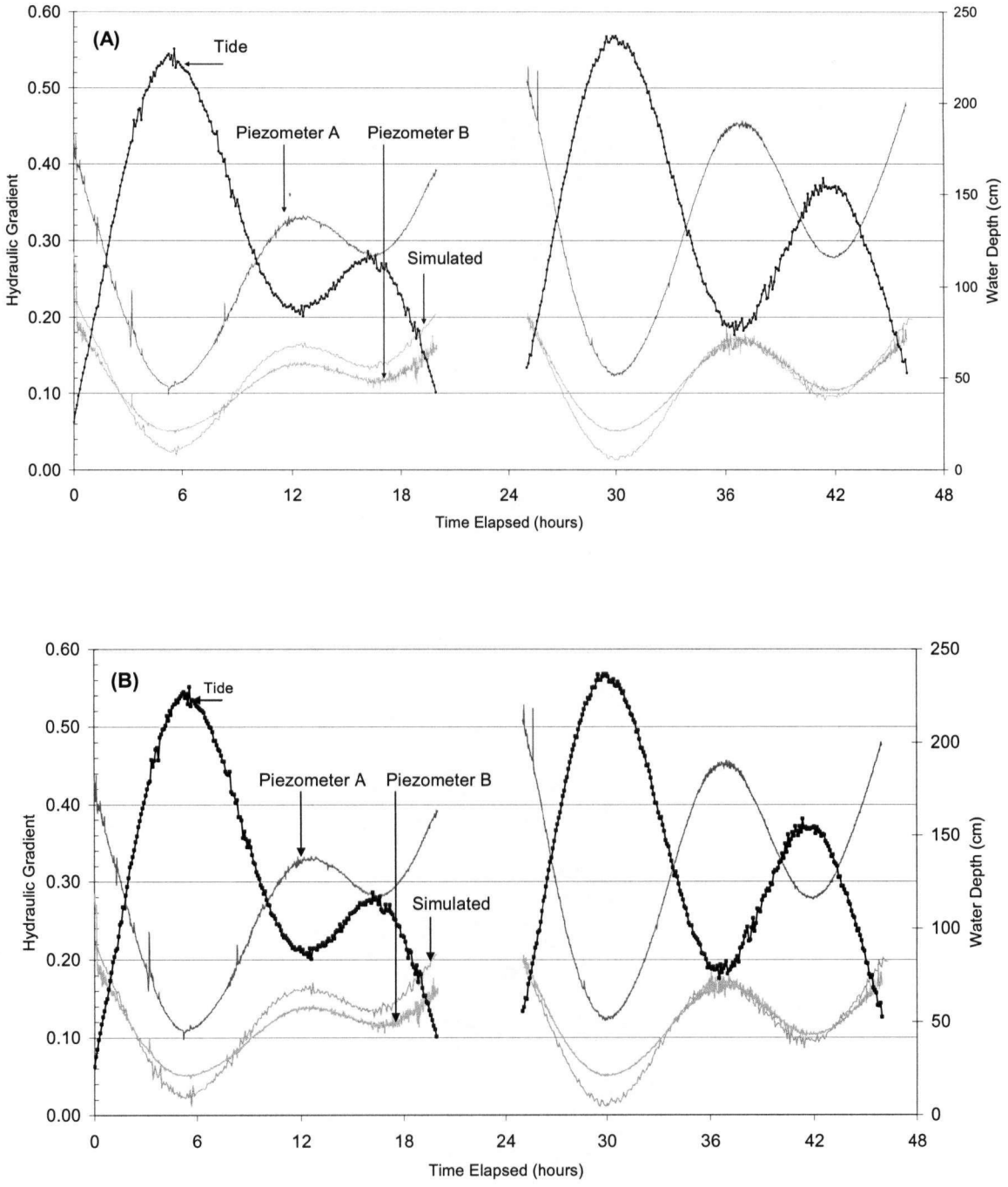

Figure 5-9: Sensitivity analysis of model 1 to values of Ss. (A) $S_s = 5 \times 10^{-5}$ m^{-1}. (B) $S_s = 5 \times 10^{-4}$ m^{-1}.

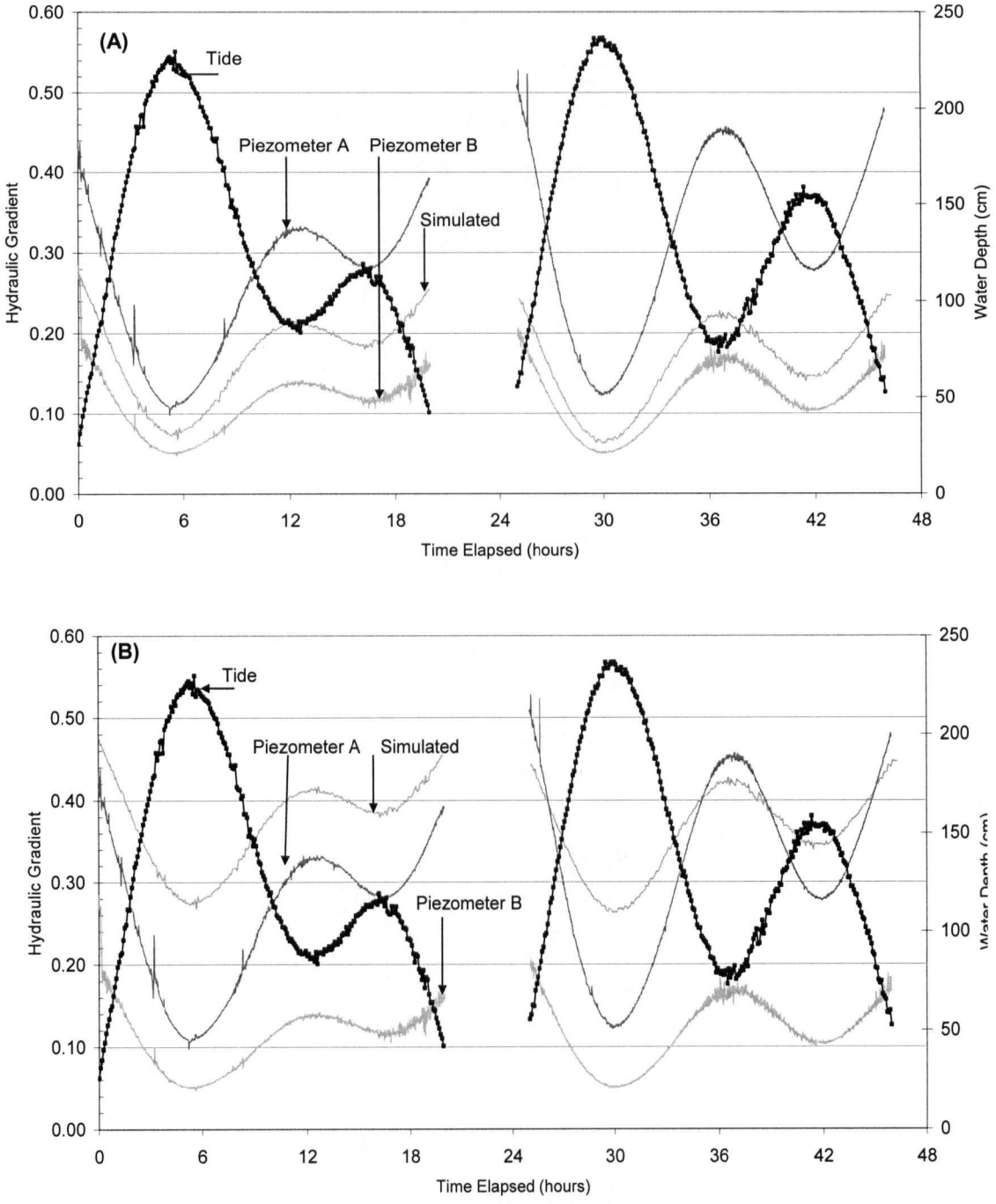

Figure 5-10: The H_{base} value for model 1 was increased to compare simulated gradients with higher hydraulic gradients at Piezometer A. (A) H_{base} = 3.0 m. (B) H_{base} = 5.0 m.

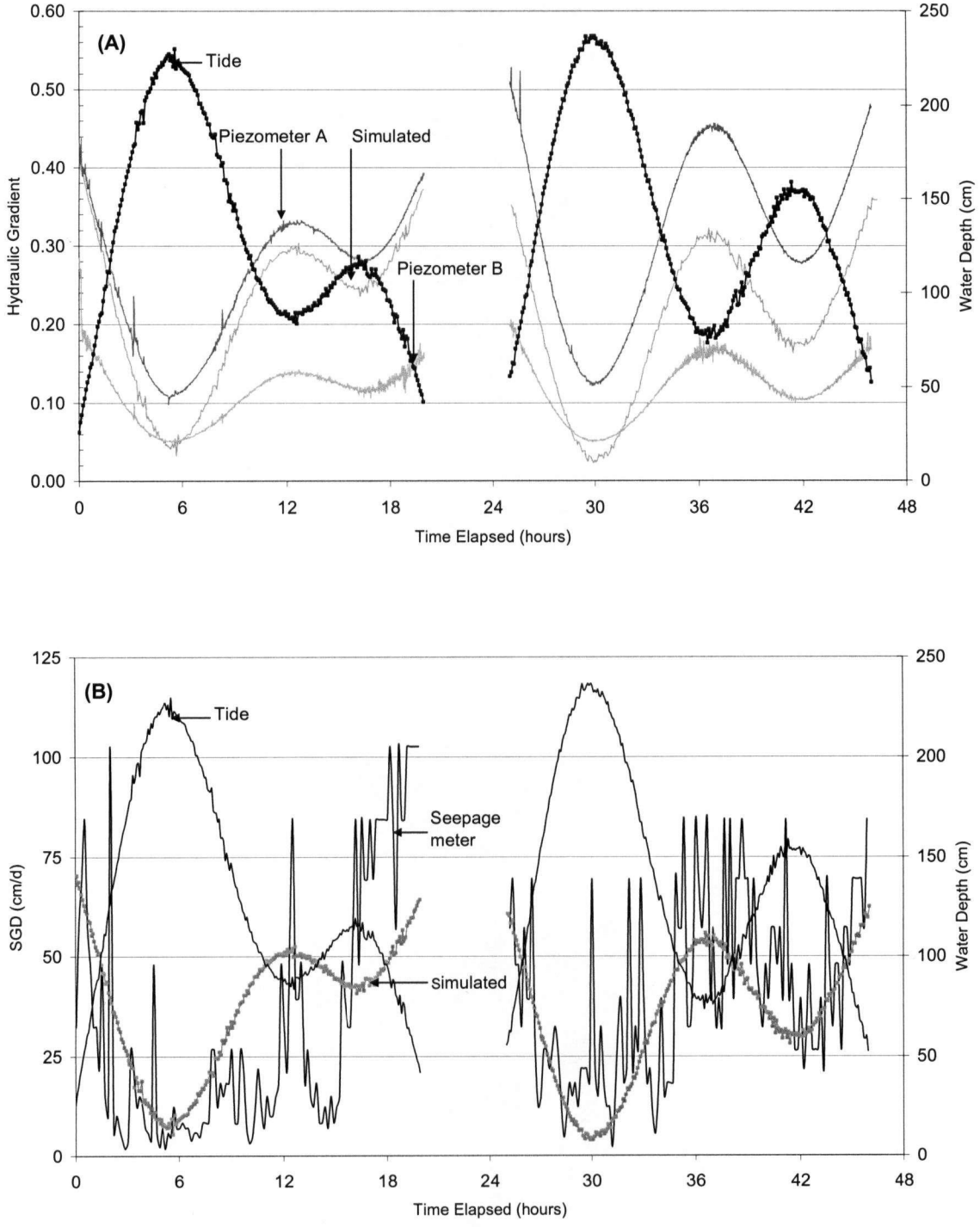

Figure 5-11: Comparison between field based measurements and Model 2 simulation: 1 m thick top layer, H_{base} = 2.5 m; $K_{TopLayer}$ = 2 x 10^{-5} m/s, $Ss_{TopLayer}$ = 1 x 10^{-4} m^{-1}; $K_{BottomLayer}$ = 4 x 10^{-5} m/s, $Ss_{BottomLayer}$ = 1 x 10^{-4} m^{-1}. (A) Hydraulic gradients between 0.3 and 0.6 m below the seabed. (B) SGD rates.

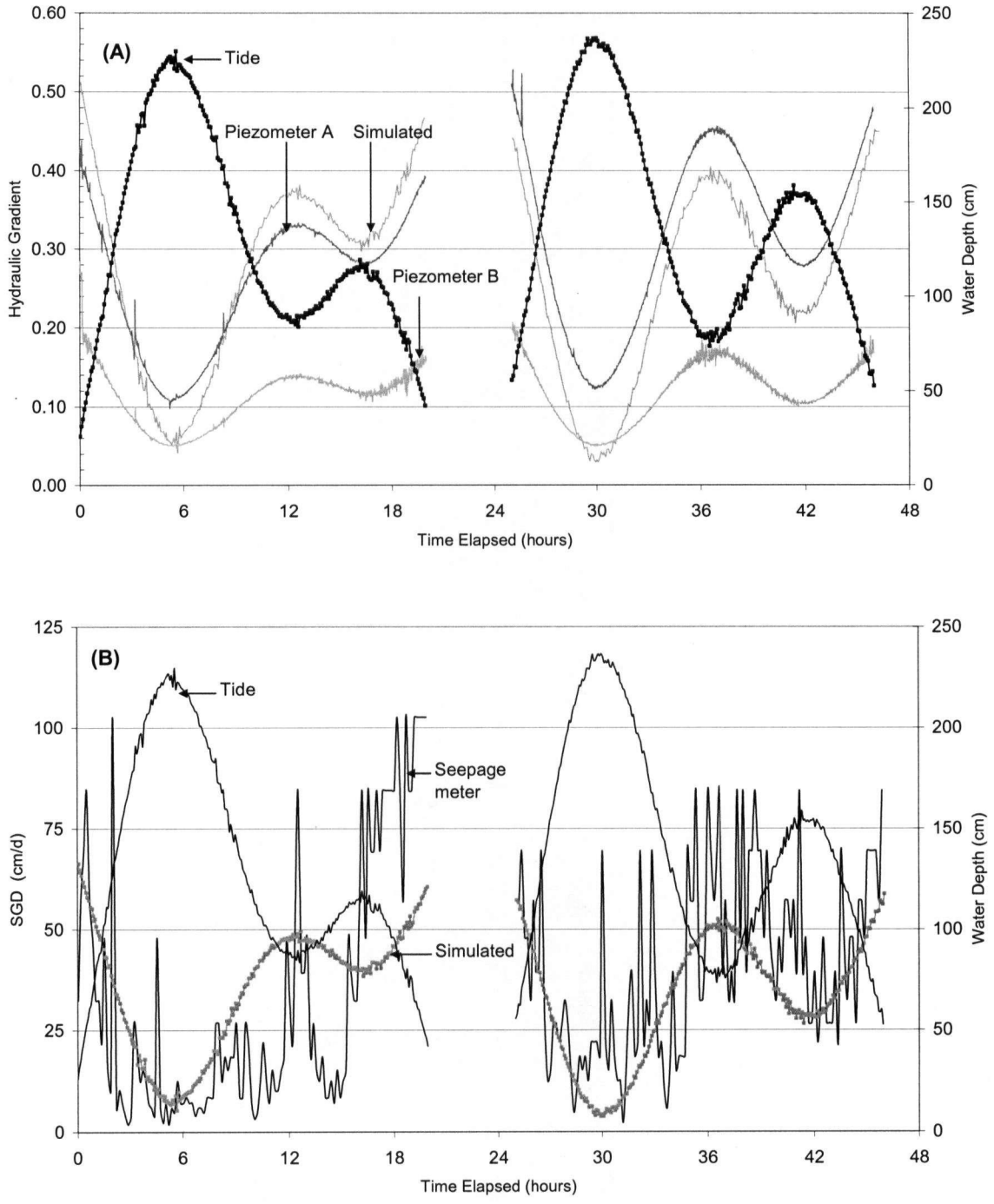

Figure 5-12: Comparison between field based measurements and Model 2 simulation: 1 m thick top layer, [1] H_{base} = 2.5 m; $K_{TopLayer}$ = 1.5 x 10^{-5} m/s, $Ss_{TopLayer}$ = 1 x 10^{-4} m^{-1}; $K_{BottomLayer}$ = 4 x 10^{-5} m/s, $Ss_{BottomLayer}$ = 1 x 10^{-4} m^{-1}. (A) Hydraulic gradients between 0.3 and 0.6 m below the seabed. (B) SGD rates.

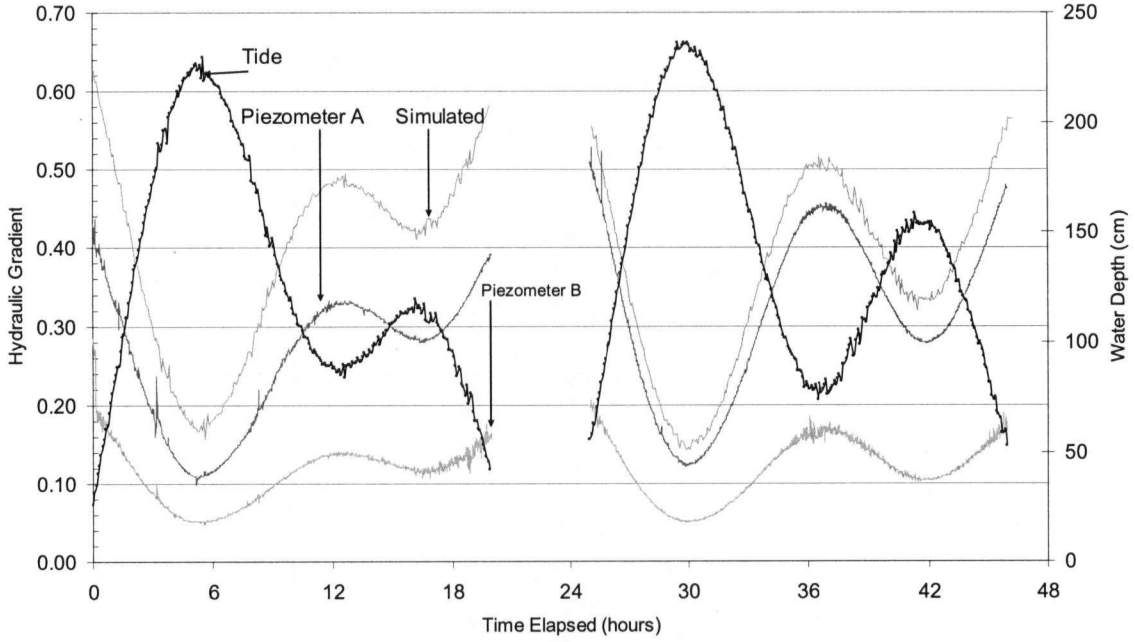

Figure 5-13: The H_{base} value for model 2 was increased to try to match the hydraulic gradients in the latter portion of the experiment (greater than 24 hours): 1 m thick top layer, [1] H_{base} = 3.0 m; $K_{TopLayer}$ = 1.5 x 10^{-5} m/s, $Ss_{TopLayer}$ = 1 x 10^{-4} m^{-1}; $K_{BottomLayer}$ = 4 x 10^{-5} m/s, $Ss_{BottomLayer}$ = 1 x 10^{-4} m^{-1}. (A) Hydraulic gradients between 0.3 and 0.6 m below the seabed. (B) SGD rates.

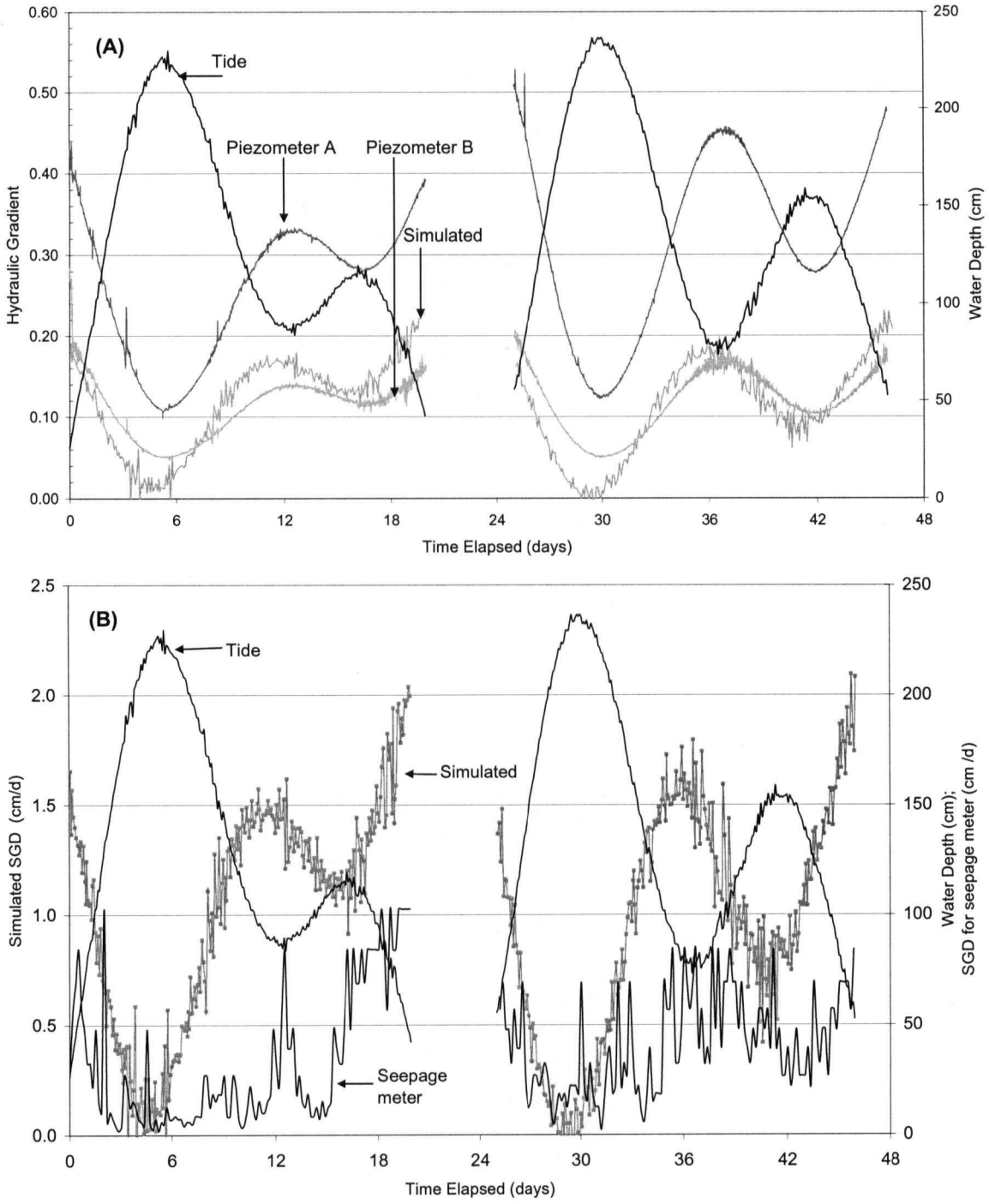

Figure 5-14: Simulation using Model 1 to investigate if a lower value of hydraulic conductivity (K = 1 x 10^{-6} m/s) would influence the timing of the highest SGD rates relative to the tidal level. Other Model 1 parameters: S_s = 1 x 10^{-4} m^{-1} and H_{base} = 2.5 m. (A) Hydraulic gradients between 0.3 and 0.6 m below the seabed. (B) SGD rates. Note the different y-axes.

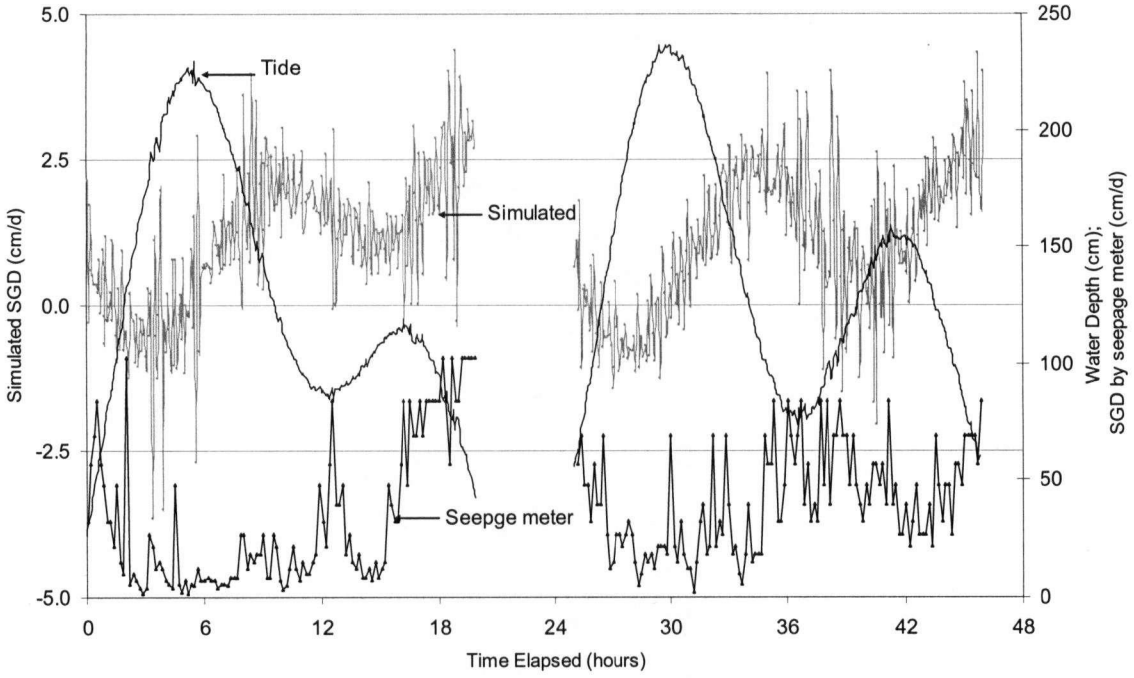

Figure 5-15: Simulation using Model 2 to investigate if values of hydraulic conductivity ($K_{BottomLayer}$ = 1 x 10^{-6} m/s) and Ss ($S_{sTopLayer}$ = 1 x 10 -3 m^{-1}) similar to those used by the model constructed by Caulkins (2003) would influence the timing of the highest SGD rates relative to the tidal level. Other Model 2 parameters: 1 m thick top layer, H_{base} = 2.5 m; $K_{TopLayer}$ = 1.5 x 10^{-5} m/s; $S_{sBottomLayer}$ = 1 x 10^{-4} m^{-1}. (A) Hydraulic gradients between 0.3 and 0.6 m below the seabed. (B) SGD rates. Note the different y-axes.

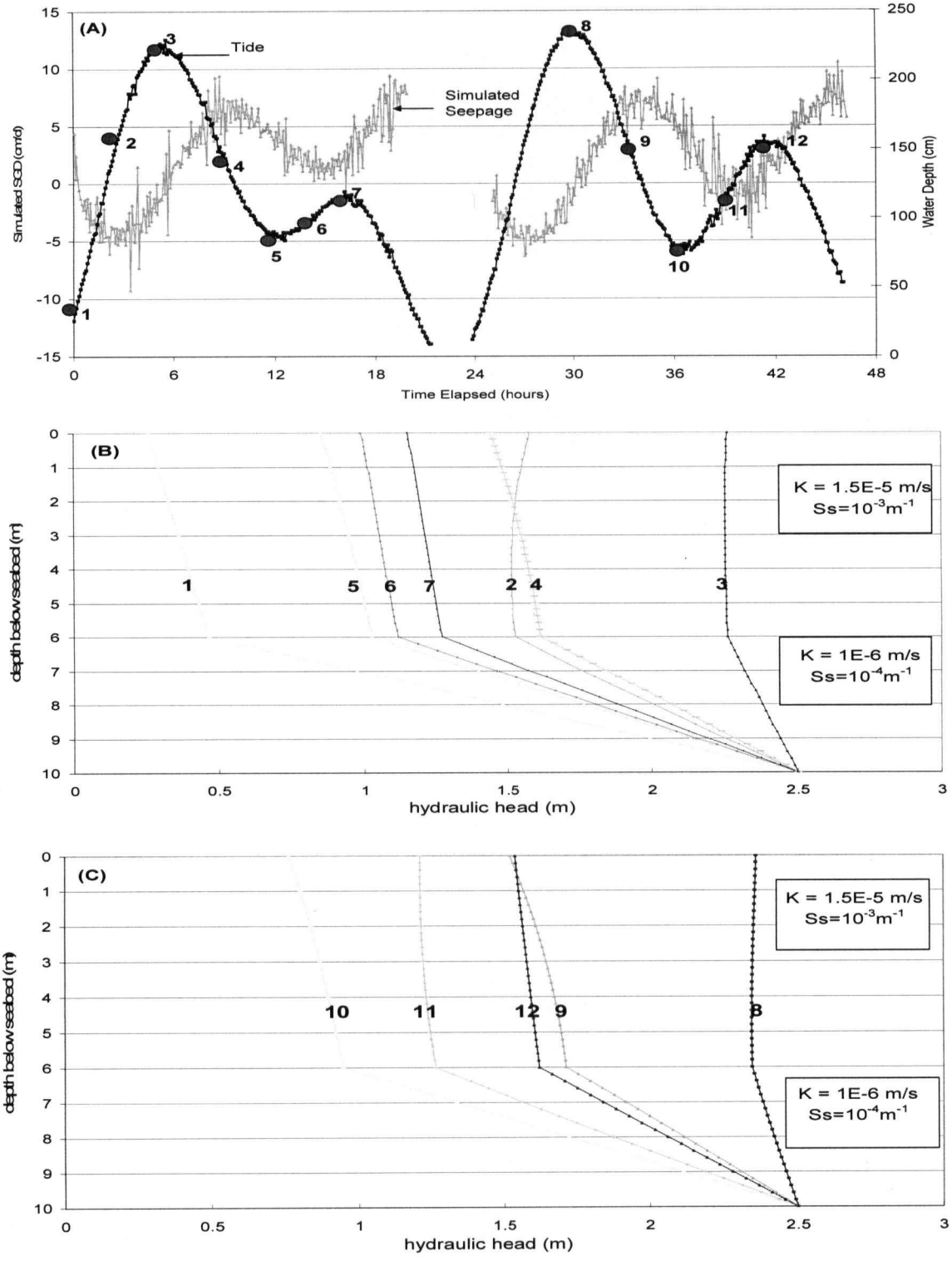

Figure 5-16: Simulation completed for comparison with modelled results by Caulkins (2003). Plots B and C show hydraulic head with depth for specified times over the tidal cycle. The number labels refer to position on the tidal cycle shown on plot A. K and Ss labels indicate the parameter values assigned for the upper 6 m layer and the bottom 4 m layer.

6. Discussion and Recommendations

6.1 Differential Pressure Heads, SGD and Tidal Levels

The field measurements of differential pressure heads (measured between 0.3 and 0.6 m below the seabed) by the DPS-II and SGD rates by the seepage meter showed a semi-diurnal pattern with the highest differential pressure heads and SGD rates occurring at low tide. A significant component of freshwater at a depth of 0.3 m below the seabed was indicated by EC measurements of pore water samples collected at low tide, which suggests that the flow of terrestrial freshwater may be a significant source of SGD at the site.

It was possible to match the SGD rates measured by the seepage meter with calculated SGD rates using Darcy's Law based on the measured differential pressure heads at each of the DPS-II piezometers and a hydraulic conductivity value within the range of the available data set derived from falling head tests completed on core samples collected from adjacent to the piezometers. A reasonable match was also obtained between predicted and field based values of SGD rates and hydraulic gradients at piezometer A and B using a 1D uniform flow model. Although a reasonable agreement was obtained between simulated hydraulic gradients and field based hydraulic gradients at Piezometer A, there was not a consistent match over the entire tidal cycle.

The results of this research suggests that the transient changes in differential pressure heads in shallow marine sediment and changes in seepage rates, are

likely predominantly in response to tidal level fluctuations, and a significant driving mechanism controlling SGD rates in the near-shore at Spanish Banks West beach.

To better constrain the interpretation of the field data sets the following modifications to the field experiment procedure and additional modeling considerations are suggested:

1. Obtaining EC measurements of the pore water over the entire tidal cycle and at vertical incremental distances of 5-10 cm to a depth of 1 m below the seabed. The additional EC measurements would be useful for supporting the results of the 1D uniform density flow model in this study. Also EC measurements of the seawater over the entire tidal cycle should be obtained to better characterize the variation in EC that was observed from the water samples collected from the water column in this study.
2. Measurements of the salinity of the discharge water may help to constrain the origin of the waters and provide more insight about the significant component of freshwater that has been measured from pore waters collected 0.3 m below the seabed. Water samples collected from the outflow of the seepage drum or the seepage drum, itself, could be used to assess the salinity of the discharge water. A conductivity probe within the drum of the seepage meter could also be used to continuously monitor the

salinity of discharge, which has been done in other studies using a continuous heat type seepage meter (Taniguchi 2006).

3. A second seepage meter would be useful for increasing the reliability of the SGD measurements. An additional seepage meter would also permit other field configurations of the DPS-II and seepage meter to be tested. As well a method to calibrate the seepage meters should be developed (the calibration curve for the seepage meter was provided when the meter was purchased) to permit periodic performance checks and accuracy of the calibration curves, similar to the calibration tests that are completed for the transducers of the DPS-II before and after field installations.
4. A higher frequency of measurements of seepage (i.e. every 1 or 5 minutes instead of 10 minutes) could be attempted to investigate the significant fluctuations in the SGD rates.
5. Collection of complete core samples from the upper 1 m of sediment. Only about a 75% partial recovery of the cores driven to a depth 0.6 m (bottom measuring port of piezometers) was achieved from the coring attempts. The core catcher was likely not able to retain the sample as the corer was being pulled up from the sediment because of the saturation of the sediment. The coring technique had only been used once previous to this attempt to recover core samples, and more experience using the tool in the field may increase the core sample recovery.
6. Estimation of the hydraulic conductivity of the core samples in the original collection tubes to minimize further disruptions to the samples. In this

study the core samples were transferred to permeameters that were compatible with a falling head test apparatus that was available in the laboratory of the department.

7. The Spanish Banks West beach provided a site in close proximity to the University, relatively high rates of SGD and accessibility to a location for loading and unloading field equipment near the field site. However, a different location may need to be considered for longer deployments (e.g. greater than 1 or 2 days), because of the significant tidal flats at the site which uncover the instruments.
8. The significance of the hydraulic gradient between land and sea in comparison to other modeling parameters such as hydraulic conductivity and specific storage could be investigated in controlling the timing of the highest SGD rates relative to the low tide. A sensitivity analysis using the models constructed in this study was completed to evaluate the effect of the values of hydraulic gradient and specific storage on the timing of the highest simulated SGD rates relative to the tidal levels. The steep cliffs at the Spanish Banks west beach likely set up higher hydraulic gradients that drive SGD in the near-shore and should also be investigated to aid with explaining the highest SGD rates observed at low tide at Spanish Banks.
9. The construction of a 2D model to investigate the effect of horizontal gradients at the site may be beneficiall in providing more insight about the usefulness of the 1D model.

6.2 Measurements by the DPS-II

The DPS-II was developed to provide measurements of the transient changes in differential pressure head in shallow marine sediment, which could be used to investigate tidal forcing as a driving mechanism of SGD in near-shore environments. The DPS-II is a new tool that can be relatively easily installed and monitored.

Key issues regarding the accuracy of an earlier version of the DPS-II used in a previous field experiment (Caulkins 2003) were addressed in this study. The significant achievements of this study with regard to the DPS-II are: (1) refining and documenting the method used for collecting data in the field, (2) minimizing the noise in the measurements of differential fluid pressure head (a tidal signal could be observed from the field data), (3) providing an estimate of the error associated with the measurements by the DPS-II, (4) identifying areas in the development of the DPS-II that need to be improved and recommending strategies to advance the DPS-II.

Recommendations to further improve and establish the performance of the DPS-II are:

1. **The calibration of the differential pressure transducers in the field configuration.** During calibration the known differential pressure heads are applied directly to the pressure sides of the transducers, as opposed

to the field tests where formation pressures in the sediment are transmitted via fluid filled tubes. Although it is recognized that a constant differential pressure head is exerted on the transducers from the fluid filled tubes, a test has not been completed to ensure that the transducer senses differential pressure changes in a similar manner in both configurations over the full range of the transducer. A calibration curve should be developed with the DPS-II in the field configuration and compared to calibration curves derived from the current calibration technique. There is not expected to be a variation between the calibrations but by completing the calibration in the field configuration, any uncertainties regarding effects from the tubing and/or the performance of the transducer are eliminated and more insight regarding the DPS-II is gained.

2. **Evaluate the effect, if any, of the pressurization of the transducers while deployed in the submersible box on the seabed.** It is assumed there is that there is no effect on the transducers and consequently calibration curve, from the pressurization (maximum water pressure 1.5 m of head) of the transducers while deployed on the seabed in the submersible box. This assumption could be investigated by deploying the transducers, while reading a constant applied zero differential pressure head, on the seabed for a tidal cycle.

3. **Assess if insertion pressures, due to the displacement of water during the insertion of the piezometers, are significant.** Insertion pressures are dependent on such factors as the rate of piezometer insertion, the dimensions of the piezometer and the hydraulic conductivity of the marine sediment. It is assumed that the measurements by the DPS-II are not affected by insertion pressures that would alter the measured differential fluid pressure heads from "true" field values. An independent measurement of the fluid pressure in the seabed (i.e. an absolute pressure transducer embedded in the seabed) during insertion of the piezometers could provide more insight regarding the effect of piezometer insertion on the fluid pressures in the shallow sediment.

4. **Completion of a laboratory test that simulates the field conditions under controlled conditions and can monitor the output of the DPS-II over a time similar to field deployments (e.g., 1-2 days).** A laboratory test of the DPS-II to simulate field conditions was attempted in this study but was not unsuccessful. The apparatus consisted of a 0.6 x 0.6 x 0.6 m box constructed of 2 cm thick wood sheets and lined with a plastic used for small backyard ponds. The piezometers of the DPS-II were positioned in the box, with two piezometers constructed of glass columns with screens at the base of the columns, attached to each of the piezometers of the DPS-II. The screens of the glass piezometers were positioned at the measuring ports of the DPS-II piezometers. The box was filled with fine

sand and saturated. A hose was used to vary the water level above the sand layer. An outlet at the base of the box permitted water to be discharged and the flow was regulated by a valve. A coarser layer composed of medium gravel was required at the base of the box to prevent the sand from clogging the outlet at the base. The piezometers of the DPS-II were prepared for testing in a similar manner as for a field deployment. Each piezometer of the DPS-II was connected to a transducer mounted in the submersible box through plastic tubing, and deaired water was pumped through the system in order to bleed the pressure ports of the transducers. The plastic tubes were filled with deaired water to permit the pressures at the ports of the piezometers to be hydraulically transmitted to the transducers. An attempt was made to set up hydraulic gradients in the sediment by varying the water level above the sand layer and/or discharging water at the base of the box. By comparing the output at each of the piezometers and also the response of the glass piezometers, insight could be gained regarding how the DPS-II may respond to tidal level fluctuations. Leakage through the liner of the box prevented prolonged testing before the sand became partially or fully unsaturated, which occurred in approximately 10-15 minutes. Another test of this nature would be useful to gain insight about the performance of the DPS-II, however a container to hold the piezometers that does not require waterproofing should be considered. A 55 gallon drum that is composed of

a thick wall (to prevent deformation from the weight of the saturated sand) may be more suitable choice.

5. **The effect of temperature on the transducers and resistors used by the DPS-II should be further investigated.** The calibration tests completed at room temperature (23^{O}C), 14-15^{O}C and 7-8^{O}C were useful to better constrain the potential shift in the calibration curves due to temperature change. However, the temperature tests did not evaluate the effect of a fluctuating temperature on measurements by the DPS-II, which could cause a greater error associated with the DPS-II measurements. Although the transducers are deployed on the seabed, it takes time for the instrument to reach a stable temperature (8 hours in this study) and if the electronics are uncovered by a low tide (as in this study) the temperature experienced by the electronics may vary. Also future tests should make an effort to differentiate between temperature effects caused by the transducers and resistors. Since the resistors are inexpensive and easy to replace, it would be advantageous to better constrain the potential temperature errors associated with the individual electronic components.

6. **The addition of a valve enabling a zero differential pressure head measurement to be applied to the system during deployment and checked against the expected zero output.** A zero check valve was not implemented in the DPS-II design because the valve was not considered a

critical feature that would improve the performance of the tool compared to the other changes in the design that were being implemented and assessed in this study. However, an ability to check the calibration of the transducers during deployment provides significant information about the performance of the DPS-II. The implementation of a zero check valve should be considered for future applications using the DPS-II. A zero check valve has been used in other differential piezometer designs (e.g. DOPPI by GEOTEK Ltd).

7. **Additional short deployments (e.g. 1-2 days) and longer deployments (e.g. 7 days) to establish the performance of the tool.** Longer deployments may generate additional questions regarding the use of the DPS-II that have not been considered in this study. In general, for each deployment of the DPS-II that is carried out under different testing conditions (e.g. environment, time) the effect of the specific conditions for that test on the performance of the DPS-II should be considered. For example, longer deployments of the DPS-II may require more insight to the likelihood of gas bubbles forming in the fluid filled tubes that are used to transmit the formation pressures at the measuring ports of the piezometers to the transducers. Temperature effects on the fluid in the tubes could cause degassing to occur over time, which is likely not a key issue in shorter tests. No gas bubbles have been observed in the fluid filled tubes of the DPS-II after test lasting less than 1 day or after the deployment in this study (almost 48 hours). No tests have been completed

to specifically investigate the potential for gas bubbles forming in the fluid filled tubes of the DPS-II.

7. Conclusions and Summary

This research focused on improving the accuracy and refining the installation method of a new tool (DPS-II) developed for measuring differential pressure heads in shallow marine sediment, and was achieved in part by resolving the difficulties in obtaining accurate differential pressure head measurements by an earlier version of the tool (DPS-I). Another key objective of this research was to use the measurements of differential pressure heads by the DPS-II to investigate the relationship between transient changes in differential pressure heads in shallow marine sediment, SGD rates and tidal level fluctuations at a field site located at Spanish Banks West beach. Spanish Banks West beach was chosen for the location of this study because the site met many of the logistical demands for field testing.

In this study, the highest differential pressure heads measured between 0.3 and 0.6 m below the seabed by the DPS-II and the highest SGD rates by a continuous heat type seepage meter occurred at low tide. The average measurements of the EC at depths of 10 and 30 cm below the seabed (8 mS/cm and 0.3 mS/cm respectively) were different by an order of magnitude, which suggested the fluid density within the shallow marine sediment at the site may not be uniform. To better understand the relationship between the transient changes in differential fluid pressure heads, SGD rates and tidal level fluctuations, the significance of density effects on flow had to also be considered. A comparison between the magnitude of calculated equivalent freshwater head

gradients and the density driven component of flow at the site indicated the relative importance of density on flow was likely negligible. SGD rates calculated using Darcy's Law based on the transient changes in differential pressure head measured at each of the DPS-II piezometers and a value of hydraulic conductivity within the constraints of the available hydraulic conductivity data set, provided a good match with SGD rates by the seepage meter. Two uniform density 1D flow models were used to predict the SGD rates and hydraulic gradients at 0.3 and 0.6 m below the seabed. Simulations using Model 1, that assumed a homogeneous domain, showed a reasonable agreement between the predicted and field based SGD rates and hydraulic gradients at piezometer B. It did not appear possible to obtain a good match between the simulated and field based hydraulic gradients at piezometer A using Model 1. A better agreement was obtained between the hydraulic gradients at piezometer A and simulated results using Model 2, which assigned a lower hydraulic conductivity layer to the upper 1 m of the domain. Despite the better agreement with hydraulic gradients at piezometer A using Model 2, the results were not consistently a good match over the entire tidal cycle. A better characterization of fluid density with depth and time (e.g., over the tidal cycle) as well as heterogeneity at depth at the site may provide insight to better explain the hydraulic gradients at piezometer A. Recommendations to improve the field procedure and further constrain the interpretation of the field results have been suggested in section 6.1.

Measurements of differential pressure heads in the seabed were successfully recorded by the DPS-II over a period of about 48 hours. The result of this work suggest that using a careful measurement approach, the DPS-II can measure the transient changes in shallow marine sediment to an accuracy of about +/- 3 mm. Several recommendations have been proposed in section 6.2 to further advance the DPS-II.

References

Andersen, G. R., Bennett, R., Barber, M., Todorovski, L. and Maynard, G. (1996). "A Multi-sensor Piezometer for Shallow Marine Sediments in Coastal Environments." Geotechnical Testing Journal 19(4): 373-383.

Ataie-Ashtiani, B., Lockington, D.A. and Volker, R.E. (1999). "Tidal effects on sea water intrusion in unconfined aquifers." Journal of Hydrology 216: 17-31.

Barry, D. A., and Li, L. (2000). "Wave induced beach groundwater flow." Advances in Water Resources 23: 325-337.

Barry, D. A., Dong, P., Li, L., Jeng, D.S. and Seymour, B.R. (2005). "Two dimensional approximation for tide induced water table fluctuations in a sloping sandy beach." Advances in Water Resources 28: 1040-1047.

Barwell, V. K., and Lee, D.R. (1981). "Determination of horizontal-to-vertical hydraulic conductivity ratios from seepage measurements on lake beds." Water Resource Research 17: 565-570.

Basu, A. R., Jacobsen, S. B., Poreda, R. J., Dowling, C., and Aggarwal, P. (2001). "Large Groundwater Strontium Flux to the Oceans from the Bengal Basin and the Maine Stontium Isotope Record." Science 293(1470-1473).

Belanger, T. V., and Montgomery, M.T. (1992). "Seepage Meter Errors." Limnology and Oceanography 37(8): 1787-1795.

Bennett, R. H., and Faris, J.R. (1979). "Ambient and dynamic pore pressures in fine-grained submarine sediments: Mississippi Delta." Appl. Ocean. Res. 1(3): 115–123.

Bennett, R. H., Davis, E.E., Horel, G.C., Li, H., MacDonald, R.D., and Villinger, H. (1991). "Pore Pressures and Permeabilities Measured in Marine Sediments with a Tethered Probe." Journal of Geophysical Research 96(B4): 5975-5984.

Bennett, R. H., Hulbert, M.H., Meyer, M.M., Lavoie, D.M., Briggs, K.B., Lavoie, D. L., Baerwald, R.J. and Chiou, W.A. (1996). "Fundamental response of pore-water pressure to microfabric and permeability characteristics : Eckernforde Bay." Geo-Marine Letters 16(3): 182-188.

Boehm, A. B., Shellenbarger, G. G. and Paytan A. (2004). "Groundwater Discharge: Potential Association with Fecal Indicator Bacteria." Environ. Sci.Technol. 38(13): 3558-3566.

Bokuniewicz, H. (1980). "Groundwater seepage into Great South Bay, New York." Estuarine Coastal Mar. Sci. 15: 13-15.

Bokuniewicz, H. (1992). "Analytical descriptions of subaqueous groundwater seepage." Estuaries 15(4): 458-464.

Bokuniewicz, H., Buddemeier, R., Maxwell, B., and Smith C. (2003). "The typological approach to submarine groundwater discharge (SGD)." Biogeochemistry 66: 145-158.

Bokuniewicz, H., Pollock, M., Blum, J. and Wilson, R. (2004). "Submarine ground water discharge and salt penetration across the sea floor." Ground Water- Oceans special Issue 42(7): 983-989.

Boyle, D. R. (1994). "Design of seepage meter for measuring groundwater fluxes in the nonlittoral zones of lakes-Evaluation in a boreal forest lake." Limnology and Oceanography 39(3): 670-681.

Burnett, B., Taniguichi, M. and Oberdorfer J. (2001). "Measurement and significance of the direct discharge of groundwater into the coastal zone." Journal of Sea Research 46(2): 109-116.

Burnett, B., Chanton, J., Christoff, J., Kontar, E., Moore, W., O'Rourke, D., Paulsen, R., Smith, C., Smith, L. and Taniguichi, M. (2002). "Assessing methodologies for measuring groundwater discharge to the ocean." EOS 83(11): 117-128.

Burnett, B., Bokuniewicz, H.J., Huettel, M., Moore, W. and Taniguchi, M. (2003). "Groundwater and pore water inputs to the coastal zone." Biogeochemistry 66: 3-33.

Burnett, B., Aggarwal, P.K., Bokuniewicz, H., Cable, J.E., Charette, M.A., Kontar, E., Krupa, S., Kulkarni, K.M., Loevelss, A., Moore, W.S., Oberdorfer, J.A., Oliveiria, J., Ozyurt, N., Povinec, P., Privitera, A.M.G., Rajar, R., Ramessur, R.T., Scholten, J., Stieglitz T., Taniguchi M. and Turner J.V. (2006). "Quantifying submarine groundwater discharge in the coastal zone via multiple methods." Science of the Total Environment in press.

Burnett, W. C., and Dulaiova, H. (2003). "Estimating the dynamics of groundwater input into the coastal zone via continuous radon-222 measurements." Jour. Environmental Radioactivity 69: 21-35.

Cable, J. E., Burnett, W.C., Chanton, J.P. and Weatherly G.L. (1996). "Estimating groundwater discharge into the northeastern Gulf of Mexico using radon-222." Earth and Planetary Science Letters 144(591-604).

Cable, J. E., Burnett, W.C., Chanton, J.P., Corbett, D.R. and Cable, P.H. (1997a). "Field evaluation of seepage meters in the coastal marine environment." Estuarine, Coastal and Shelf Science 45: 367-375.

Cable, J. E., Burnett, B. and Chanton, J.P. (1997b). "Magnitude and variations of groundwater seepage along a Florida marine shoreline." Biogeochemistry 38: 189-205.

Capone, D. G., and Slater, J.M. (1990). "Interannual patterns of water table height and groundwater derived nitrate in nearshore
sediments." Biogeochemistry 10: 277–288.

Caulkins, J. (2003). Master Thesis: Characterization and investigation of submarine groundwater discharge from a coastal aquifer into the nearshore environment. Earth and Ocean Sciences. Vancouver, The University of British Columbia.

Chanton, J. P., Burnett, B., Dulaiova, H., Corbett, D.R. and Taniguchi, M. (2003). "Seepage rate variability in Florida Bay driven by Atlantic tidal height." Biogeochemistry 66: 187-202.

Charette, M., and Sholkovitz, E. (2002). "Oxidative precipitation of groundwater -derived ferrous iron in the subterranean estuary of a coastal bay." Geophysical Research Letters 29(10): 1444.

Cherkauer, D. S., and Nader, D.C. (1989). "Distribution of groundwater seepage to large surface-water bodies: The effect of hydraulic heterogeneities." Journal of Hydrology 109: 151-165.

Church (1996). "An underground route for the water cycle." Nature 380: 579-580.

Coleman, H. W., Steele, W. G. (1989). Experimentation and uncertainty analysis for engineers, John Wiley & Sons.

Corbett, D. R., Chanton, J., Burnett, B., Dillon, K., and Rutkowski, C. (1999). "Patterns of groundwater discharge into Florida Bay." Limnology and Oceanography 44(4): 1045-1055.

Davies, P. B. (1989). Variable-density ground-water flow and paleohydrology in the waste isolation pilot plant (WIPP) region, Southeastern New Mexico. Albuquerque, NM, U.S. Geological Survey: 24-29.

Davis, E. E., Horel, G.C., MacDonald, R.D., Villinger, H., Bennett, R.H., Li, H. (1991). "Pore pressures and permeabilities measured in marine sediments with a tethered probe." Journal of Geophysical Research 1991(96): 5975-5984.

Destouni, G., and Prieto, C. (2003). "On the possibility for generic modeling of submarine groundwater discharge." Biogeochemistry 66: 171-186.

Domenico, P. A., and Schwartz, F. (1998). Physical and chemical hydrogeology. New York, Wiley.

Downing, J. A., and Peterka, J. J. (1978). "Relationship of rainfall and lake groundwater seepage." Limnology and Oceanography 23(4): 821-825.

Dunnicliff, J., and Green, G. (1988). Geotechnical instrumentation for monitoring field performance. New York, Wiley.

Fang, W. W., Langseth, M. G., and Schultheiss, P.J. (1993). "Analysis and application of in-situ pore pressure measurements in marine sediments." Journal of Geophysical Research 98(B5): 7921-7938.

Fellows, C. R., and Brezonik, P.L. (1980). "Seepage flow into Florida lakes." Water Resource Bulletin 16: 635-641.

Fetter, C. W. (2001). Applied hydrogeology. Upper Saddle River, N.J, Prentice Hall.

Freeze, R. A., and Cherry, J. (1979). Groundwater. Englewood Cliffs, N.J, Prentice-Hall.

Fukuo, Y., and Kaihotsu, I. (1988). "A theoretical analysis of seepage flow of the confined groundwater into the lake bottom with a gentle slope." Water Resources Research 24(11): 1949-1953.

Hanna, T. H. (1985). Field instrumentation in geotechnical engineering, Clausthal-Zellerfeld, Federal Republic of Germany.

Harvey, F. E., Rudolph, D. L., and Frape, S. (1997). "Measurement of hydraulic properties in deep lake sedimets using a tethered pore pressure probe: applications in the Hamilton Harbour, western Lake Ontario." Water Resources Research 33(8): 1917-1928.

Huettel, M., and Gust, G. (1992). "Solute release mechanisms from confined sediment cores in stirred benthic chambers and flume flows." Mar. Ecology Progress Series 82: 187-197.

Huettel, M., Ziebis, W., and Forster, S. (1996). "Flow-induced uptake of particulate matter in permeable sediment." Limnology and Oceanography 41(2): 309-322.

Johannes, R. E. (1980). "The ecological significance of the submarine discharge of groundwater." Marine Ecology Progress Series 3: 365-373.

Kaleris, V., Lagas, G., Marczinek, S., and Piotrowski, J.A. (2002). "Modelling submarine groundwater discharge: an example from the western Baltic Sea." Journal of Hydrology 265: 76-99.

Kim, G., and Hwang, D. (2002). "Tidal pumping of groundwater into the coastal ocean revealed from submarine 222Rn and CH4 monitoring." Geophysical Research Letters 29(14).

Kitheka (1997). "Groundwater outflow and its linkage to coastal circulation in a mangrove-fringed creek in Kenya." Estuarine, Coastal and Shelf Science 47: 63-75.

Kohout, F. A. (1964). The flow of fresh water and salt water in Biscayene Aquifer of the Miami area, Florida; in sea water in coastal aquifers, U.S. Geological Survey Water-Supply Paper 1613-C: 12-31.

Krupa, S. L., Belanger, T.V., Heck, H.H., Brok, J.T., and Jones, B.J. (1998). "Krupaseep-the next generation seepage meter." J. Coastal Res 25: 210-213.

La Roche, J., Nuzzi, R., Waters, R., Wyman, K., Falkowski, P.G., and Wallace, D.W.R. (1997). "Brown tide blooms in Long Island's coastal waters linked to interannual variability in groundwater flow." Glob Change Biol 3: 397-410.

Lee, D. R. (1977). "A device for measuring seepage flux in lakes and estuaries." Limnology and Oceanography 22(1): 140-147.

Lee, D. R. (1977). "A device for measuring seepage flux in lakes and estuaries." Limnology and Oceanography 22: 140-147.

Lee, D. R., and Harvey, F. E. (1996). "Installing piezometers in deepwater sediment." Water Resources Research 32(4): 1113-1118.

Li, H., and Jiao, J. (2002). "Tide-induced seawater-groundwater ciruclation in a multi-layerd coastal leaky aquifer system." Journal of Hydrology 274: 211-224.

Li, L., Barry, D.A., Stagnitti, F., and Parlange, J.Y. (1999). "Submarine groundwater discharge and associated chemical input to a coastal sea." Water Resources Research 35(11): 3253-3259.

Libelo, E. L., and MacIntyre, W.G. (1994). "Effects of surface-water movement on seepage-meter measurements of flow through the sediment-water interface." Hydrological Journal 2: 49-54.

Massel, S. R. (2001). "Circulation of groundwater due to wave set -up on a permeable beach." OCEANOLOGIA 43(3): 279-290.

Massel, S. R., Przyborska, A., and Przyborski, M. (2004). "Attenuation of wave-induced groundwater pressure in shallow water. Part 1." Oceanologia 46(3): 383-404.

Michael, H. A., Lubetsky, J., and Harvey, C. (2003). "Characterizing submarine groundwater discharge: A seepage meter study in Waquuoit Bay, Massachusetts." Geophysical Research Letters 30(6).

Michael, H. A., Mulligan, A.E., and Harvey, C.F. (2005). "Seasonal oscillations in water exchange between aquifers and the coastal ocean." Nature 436: 1145-1148.

Moore, W. (1996). Large groundwater inputs to coastal waters revealed by 226Ra enrichments. Nature. Nature Letters. 380: 3.

Moore, W. (1999). "The subterranean estuary: A reaction zone of ground water and sea water." Marine Chemistry 65: 111-125.

Moore, W., Krest, J., Taylor, G., Roggenstein, E., Joye, S., and Lee, R. (2002). "Thermal evidence of water exchange through a coastal aquifer: Implications for nutrient fluxes." Geophysical Research Letters 29(14): 1-4.

Moore, W., and Wilson, A. (2005). "Advective flow through the upper continental shelf driven by storms, buoyancy, and submarine groundwater discharge." Earth and Planetary Science Letters 235: 564-576.

Moore, W. S. (1997). "High fluxes of radium and barium from the mouth of the Ganges-Brahmaputra River during low river discharge suggests a large groundwater source." Earth and Planetary Science Letters 150(141-150).

Mu, Y., Cheng, A.D., Badiey M., and Bennett, R. (1999). "Water wave driven seepage in sediment and parameter inversion based on pore pressure data." International Journal for Numerical and Analytical Methods in Geomechanics 23: 1655-1674.

Murdoch, L., Kelly, C., and Susan, E. (2003). "Factors affecting the performance of conventional seepage meters." Water Resources Research 39(6): 1163.

Nielsen, P. (1990). "Tidal dynamics of the water table in beaches." Water Resources Research 26(9): 2127-2134.

Norton, H. N. (1989). Handbook of transducers. Englewood Cliffs, NJ, Prentice Hall.

Oberdorfer, J. (2003). "Hydrogeologic modeling of submarine groundwater discharge: comparison to other quantitative methods." Biogeochemistry 66: 159-169.

Paulsen, R., Smith, F. C., O'Rourke, D., and Wong, T. (2001). "Development and evaluation of an ultrasonic ground water seepage meter." Ground Water 39: 904-911.

Paulsen, R., O'Rourke, D., Smith, F. C., and Wong, T. (2004). "Tidal load and salt water influences on submarine ground water discharge." Ground Water- Oceans Issue 42(7): 990-999.

Piteau Associates Engineering Ltd. (2002). UBC properties trust hydrogeological and geotechnical assessment of Northwest Area UBC campus, Vancouver, Piteau Associates Geotechnical and Hydrogeological Consultants: 13-14.

Rasmussen, L. L., Chanton, J.P., Meacham, S.P., Furbish, D.J. and Burnett, W.C. (2002). "Groundwater flow, tidal mixing, and haline convection in coastal sediments: field and modeling studies." Continental Shelf Res. in press.

Raubenheimer, B., and Guza, R.T. (1999). "Tidal water table fluctuations in a sandy ocean beach." Water Resources Research 35(8): 2313-2320.

Rosenberry, D. O. (2005). "Integrating seepage heterogeneity with the use of ganged seepage meters." Limnology and Oceanography 3: 131-142.

Schultheiss, P. J. (1989). "Pore pressures in marine sediments: An overview of measurement techniques and some geological and engineering applications." Marine Geophysical Researches 12: 153-168.

SCOR/LOICZ Working Group 112 (2000). Assessment and Management Implications of Submarine Commission (Integrated Coastal area Management (ICAM) Program), Scientific Committee on Oeanic Research (SCOR) and Land-Ocean Interactions in the Coastal Zone (LOICZ): 1-27.

Setra Systems Setra systems model 230 installation guide.

Shaw, R. D., and Prepas, E.E. (1989). "Anomalous, short -term influx of water into seepage meters." Limnology and Oceanography 34(7): 1343-1351.

Shaw, R. D., Shaw, J.F.H., Fricker E., and Prepas E.E. (1990a). "An integrated approach to quantifying groundwater transport of phosphorus to Narrow Lake, Alberta." Limnology and Oceanography 35(4): 870-886.

Shaw, R. D., and Prepas, E.E. (1990b). "Groundwater-lake interactions:I. Accuracy of seepage meter estimations of lake seepage." J. Hydrol 119: 105-120.

Shinn, E. A., Reich, C.D., and Hickey, T.D. (2002). "Seepage meters and Bernoulli's revenge." Estuaries 25: 126-132.

Sholkovitz, E., Herbold, C., and Charette M. (2003). "An automated dye-dilution based seepage meter for time-series measurement of submarine groundwater discharge." Limnology and Oceanography: 16-28.

Shum, K. T., and Sundby, B. (1996). "Organic matter processing in continental shelf sediments-the subtidal pump revisited." Marine Chemistry 53: 81-87.

Simmons, C. T., Fenstemaker, T. R., and Sharp, J.M. (2001). "Variable-density groundwater flow and solute transport in heterogeneous porous media: approaches, resolutions and future challenges." Journal of Contaminant Hydrology 52: 245-275.

Slomp, C. P., and Van Cappellen, P. (2004). "Nutrient inputs to the coastal ocean through submarine groundwater discharge: controls and potential impacts." Journal of Hydrology 295: 64-86.

Smith, A. J., and Nield, S.P. (2003). "Groundwater discharge from the superficial aquifer into Cockburn Sound Western Australia: estimation by inshore water balance." Biogeochemistry 66: 125-144.

Smith, L., and Zawadzki, W. (2003). "A hydrogeologic model of submarine groundwater discharge: Florida intercomparison experiment." Biogeochemistry 66: 95-110.

Taniguchi, M., and Fukuo,T. (1993). "Continuous measurements of ground-water seepage using an automated seepage meter." Groundwater 31(4): 675-679.

Taniguchi, M. (1993). "Evaluation of vertical groundwater fluxes and thermal properties of aquifers based on transient temperature- depth profiles." Water Resources Research 29(7): 2021-2026.

Taniguchi, M. (1995). "Change in groundwater seepage rate into Lake Biwa, Japan." Jpn. J. Limnol. 56: 261-267.

Taniguchi, M., and Fukuo, Y. (1996). "An effect of seiche on groundwater seepage rate into Lake Biwa, Japan." Water Resources Research 32(2): 333-338.

Taniguchi, M. (1999). "Disturbances of temperature-depth profiles due to surface climate change and subsurface water flow:1. An effect of linear increase in surface temperature caused by global warming and urbanization in Tokoyo metropolitan area, Japan." Water Resources Research 35(5): 1507-1517.

Taniguchi, M., and Iwakawa, H. (2001). "Measurements of submarine groundwater discharge rates by a continuous heat type automated seepage meter in Osaka Bay, Japan." Journal of Groundwater Hydrology 43(4): 271-277.

Taniguchi, M. (2002). "Tidal effects on submarine groundwater discharge into the ocean." Geophysical Research Letters 29(12).

Taniguchi, M., Burnett, B., Cable, J.E., and Turner, J.V. (2002). "Investigation of submarine groundwater discharge." Hydrological Processes 16: 2115-2129.

Taniguchi, M., Burnett, W. C., Smith, C. F., Paulsen, R. J., O'Rourke, D., Krupa, S. L. and Christoff, J. L. (2003). "Spatial and temporal distributions of submarine groundwater discharge rates obtained from various types of seepage meters at a site in the Northwestern Gulf of Mexico." Biogeochemistry 66: 35-53.

Taniguchi, M., Burnett, B., Cable, J.E., and Turner, J.V. (2003). Assessment methodologies for submarine groundwater discharge, Elsevier.

Taniguchi, M., and Iwakawa, H. (2004). "Submarine groundwater discharge in Osaka Bay, Japan." The Japanese Society of Limnology.

Taniguchi, M., Ishitobi, T., and Saeki, K. (2005). "Evaluation of time-space distributions of submarine ground water discharge." Groundwater 43(3): 336-342.

Taniguchi, M., Ishitobi, T., and Shimada, J. (2006). "Dynamics of submarine groundwater discharge and freshwater-seawater interface." Journal of Geophysical Research 111(10/29/2005): CO10008 (1-9).

Taylor, J. (1997). An introduction to error analysis: The study of uncertainties in physical measurements. Sausalito, Calif, University Science Books.

Therrien, R., and Sudicky, E.A (1996). "Three-dimensional analysis of variably-saturated flow and solute transport in discretely-fractured porous media." Jour. Contam. Hydrology 23: 1-44.

Turner, I. L., and Masselink, G. (1998). "Swash infiltration-exfiltration and sediment transport." Journal of Geophysical Research 103: 30,813-30,824.

UBC Hydrogeology program (2004). EOSC 428/532 Field Techniques in Groundwater Hydrogeology course notes.

Uchiyama, Y., Nadaoka, K., Rolke, P., Sadachi, K., and Hiroshi, Y. (2000). "Submarine groundwater discharge into the sea and associated nutrient transport in a sandy beach." Water Resources Research 36(6): 1467-1479.

United States Navy (2003). Coastal contaminant migration monitoring: The trident probe and ultraseep system. San Diego, California, Systems Center SPAWAR: 1-23.

Urakoshi, T., Tokunaga,T., and Mogi, K. (2003). Determination of pressure field and hydraulic diffusivity of sub sea formations by continuous measurments of pore pressures. AGU fall meeting.

Urakoshi,T.,Tokunaga,T.,Mogi,K., 2005, Estimation of pore pressure field and hydraulic properties of sub-sea formation at submarine groundwater discharge area. Journal of Groundwater Hydrology, 47, no. 2, pp.181-197. (in Japanese, with English abstract)

Urgeles, R., Canals, M., Roberts, J., and SNV "Las Palmas" Shipboard Party" (2000). "Fluid flow from pore pressure measurements off La Palma Canary Islands." Journal of Volcanolgy and Geothermal Research 101: 253-271.

Valiela, I., Costa, J., Foreman, K., Teal, J.M., Howes, B., and Aubrey, D. (1990). "Transport of groundwater-borne nutrients from water-sheds and their effects on coastal waters." Biogeochemistry 10: 177-197.

Van Dam, J. C. (1999). "Groundwater fluxes in the global hydrological cycle: past, present, future." J. of Hydrology 144: 405-427.

Wilson, A. M. (2005). "Fresh and saline groundwater discharge to the ocean: A regional perspective." Water Resources Research 41: 2016-2027.

Woessner, W. W., and Sullivan, K.E. (1984). "Results of Seepage Meter and Mini-Piezometer Study, Lake Mead, Nevada." Groundwater 22(5): 561-567.

Yim, C. S., and Mohsen, M.F.N. (1992). "Simulation of Tidal Effects on Contaminant Transport in Porous Media." Groundwater 30(1): 78-86.

Young, J. E. (1996). Tracing groundwater flow into the Northwestern Gulf of Mexico using naturally occuring Radon-222. Florida State University.

Zekster, I. S., Dzhamalov, V.A, and Meskheteli, A.V. (1983). "Role of submarine groundwater discharge in the water balance of Australia." IAHS-AISH Publication, No 142 "Groundwater in Resources Planning": 209-219.

Zekster, I. S. (1996). Groundwater discharge in the coastal zone, LOICZ/Russian Academy of Sciences: Texel, Netherland/Moscow: 122-123.

Appendix A: Method for Calibration of Differential Pressure Transducers

Method for Calibration of Differential Pressure Transducers

Background

The relationship between the input and output of a measuring system is established during the calibration of a system. The calibration curve enables a measurement system's direct output to be interpreted during an actual measurement. By the application of a range of known values to the input and observation of the system output, a calibration curve for the measurement system can be developed. Calibration methods may vary widely. The main issue in a calibration is that the value of the input applied to the transducer and the errors associated with that value are known. The expected error of the applied inputs must be smaller than those allowed for the transducer. Most transducers are subject to a static calibration, which is performed under room conditions and includes letting the input stabilize at various values before an output reading is recorded. These values are generally selected at equal increments, with the input first increasing and then decreasing.

Calibrations were completed before and after field deployments and following any modifications to the electronics of the DPS-II such as re-wiring or replacement of a transducer. As a result of the measurement system including two differential pressure transducers with independent inputs and outputs, separate calibrations particular to each transducer were required.

Calibration Method

Bleeding the Pressure Ports of the Transducer

Prior to transducers being calibrated the pressure ports of the transducer were bled to eliminate any air in the lines or pressure cavities of the transducer. The following steps

were taken to bleed the pressure ports of the transducer and begin the calibration of the transducers:

1. The transducers were positioned in the submersible box that is used to house the transducers during DPS-II deployments.
2. The pressure ports of the transducer are connected to water columns that are attached to a stand, via swagelok connections on the submersible box.
3. To begin calibration of the first transducer (either transducer A or B), the two valves regulating flow toward the transducer are opened. The two valves regulating flow to the other transducer remain closed. Deaired tap water, which has been dyed with colouring, is pumped using a peristaltic pump from a 4L glass container, through an inlet on the manifold and past the sides of the pressure transducer. The deaired water flows out from the transducer and discharges from the top of the water columns (Figure AA-1). Deaired water is used for the calibration to minimize sources of air bubbles. Air bubbles in any part of the measurement system such as the water columns or pressure cavities of the transducer may cause discontinuities which can affect fluid pressure measurements and thus the accuracy of the calibration. The deaired water is dyed blue using food colouring to easily identify any air bubbles present in the water columns.
4. As the transducer pressure ports are being pressurized with the deaired water, the pressure ports of the transducer are bled. The bleeding of the pressure ports allow air bubbles to escape from the pressure cavities of the transducer. The procedure for bleeding the pressure ports is described in the Setra model 230 transducer installation guide. The procedure involves backing off the bleed screws until only bubble free liquid flows out (Figure AA-2). After the pressure

ports have been bled, the valves regulating flow toward the transducer are closed and the pumping of deaired water stopped.

Applying Known Differential Pressures Heads and Transducer Observing Transducer Output

A differential pressure measurement is obtained from a pressure measured relative to a reference pressure. In the case of the differential pressure transducers used by the DPS-II (Setra Systems model 230, range +/- 0.5 PSID), differential pressures are measured at the high pressure side relative to the low pressure side. Known pressures are applied to the high and low pressure sides the transducer to yield a known difference in pressure. The pressure heads are applied by varying the water levels in the water columns connected to each of the transducer pressure sides. The change in water levels are read from rulers affixed next to the water columns. A syringe coupled to a plastic tube was used to remove or add water from the water columns. The operating range of the Setra Systems model 230 differential pressure transducer is +/- 35 cm of water. This operating range was taken as the upper and lower limits of the differential pressure measurement system for the calibrations.

1. Initially 40 cm of water is applied to both sides of the transducer to yield an applied differential pressure head of 0. The output of the transducer at this applied pressure is recorded. The output of the system in response to the known differential pressure input is displayed using the Campbell Scientific datalogger support software, PC208W Version 3.2 (Figure AA-3).
2. The applied pressure to the low pressure side is decreased by 5 cm increments until a differential pressure head of + 35 cm is obtained. At each 5 cm interval of change in pressure head the output of the transducer is recorded.

3. The water column connected to the low pressure side is refilled to a water level of 40 cm to again produce a 0 differential pressure. The output of the zero applied differential pressure head is recorded and compared to the initial value obtained for a zero applied differential pressure.
4. The water column connected to the high pressure port is decreased by 5 cm increments until a differential pressure head of - 35 cm is reached. At each 5 cm interval of change in pressure head the output of the transducer is recorded.
5. The known input and corresponding system output recorded at each 5 cm increment is used to yield a calibration curve of system output (mV) vs. known applied differential pressure head (cm).
6. The calibration procedure is repeated again for the transducer to obtain a second calibration curve for the purpose of comparison with the first calibration.

References

Norton Harry N. (1989). Handbook of transducers. Englewood Cliffs, NJ, Prentice Hall.

Setra Systems Model 230 Installation Guide.

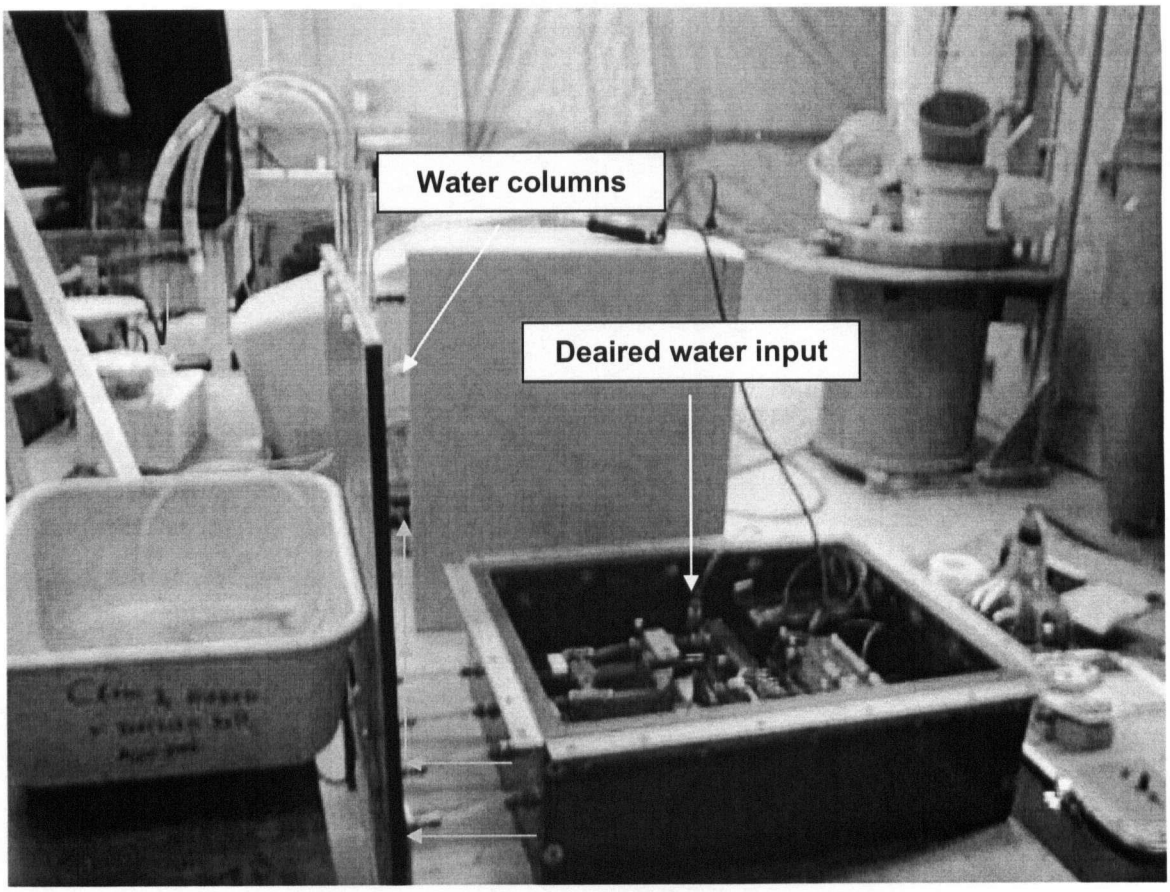

Figure AA-1: Flow path of deaired water (blue arrows) during preparation for bleeding the pressure ports of the transducer.

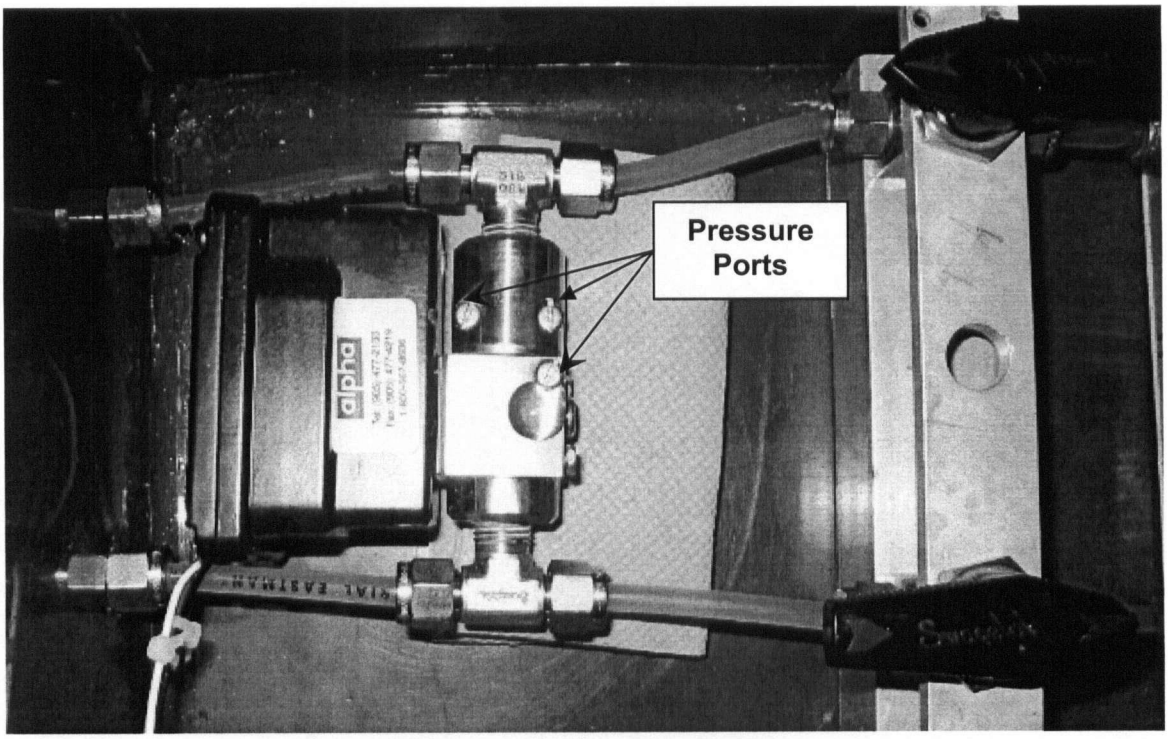

Figure AA-2: Bleeding of a pressure port of the Setra 230 differential pressure transducer.

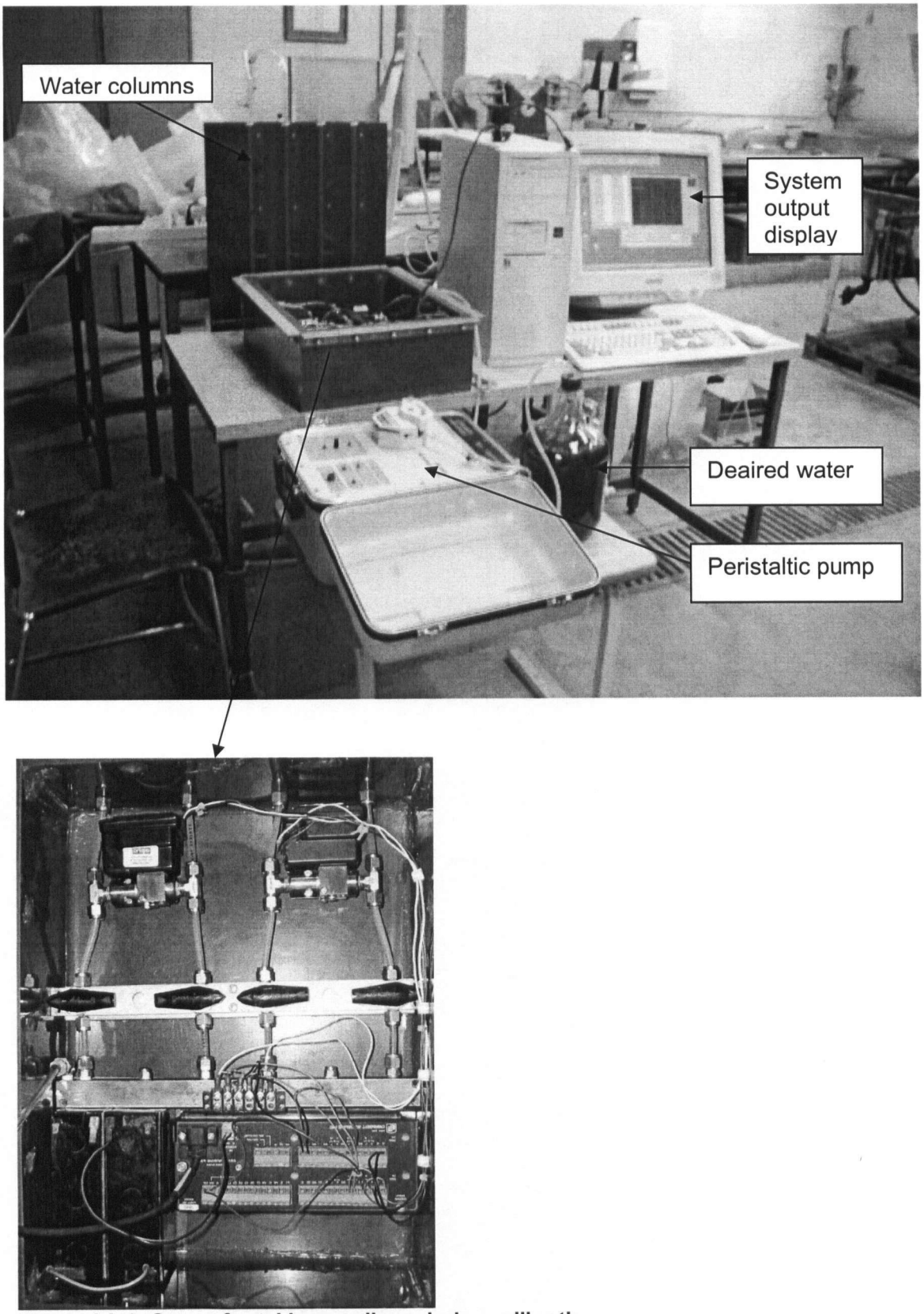

Figure AA-3: Set up for taking readings during calibration

Appendix B: Wiring Configuration of the Electronic Components of DPS-II

Wiring Configuration of the Electronic Components of DPS-II

Set Up of the Differential Pressure Measurement System

Figure AB-1 shows the organization of the electronic components making up the data acquisition part of the DPS-II.

The data acquisition components consisted of:

1. Two Setra System model 230 differential pressure transducers, which measured the differential pressure between two points in the seabed and than converted this measurement into a usable electrical output.
2. A Campbell Scientific CR10X datalogger, which controlled the frequency of the differential pressure measurements as well as the storage and display of the measurements.
3. Two 10K Ohm resistors, which created a voltage divider to provide an acceptable range over which the CR10X datalogger could receive the output from the transducers.
4. A power supply to provide the required voltages to the transducers and CR10X.

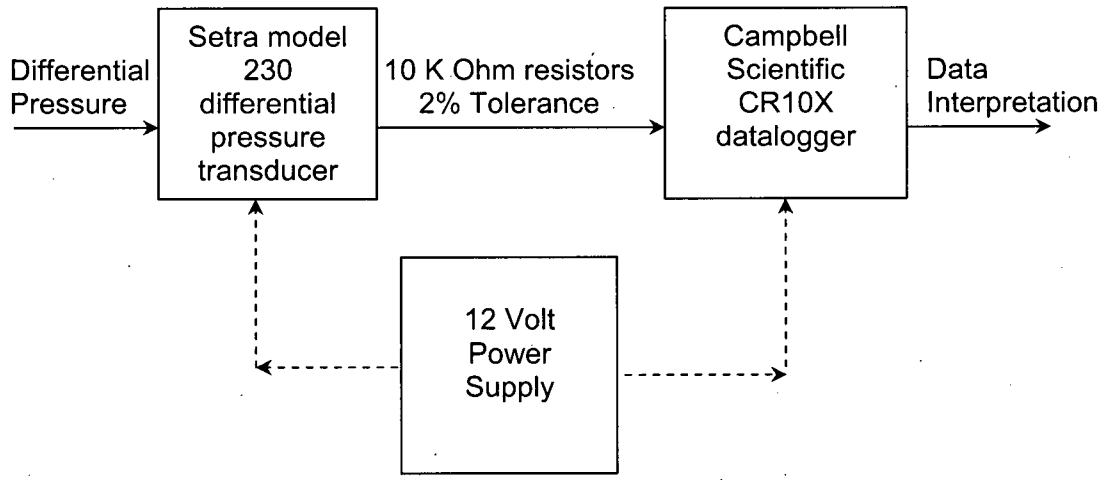

Figure AB-1: Flow chart illustrating the interaction between the data acquisition components of the DPS-II.

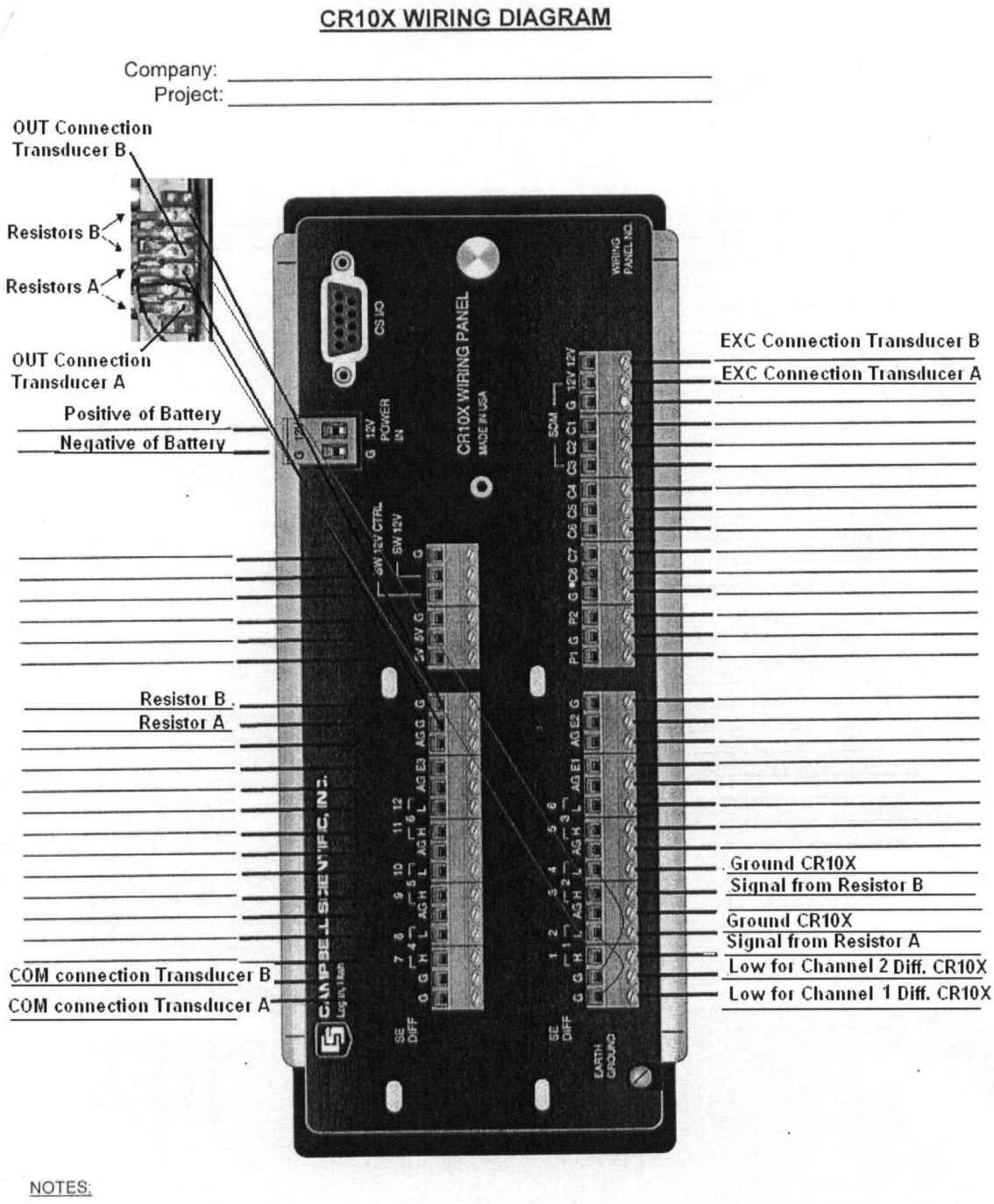

Figure AB-2: Wiring of the Electronic Components through the CR10X.

Appendix C: Calibration Curve for Continuous Heat Type Seepage Meter

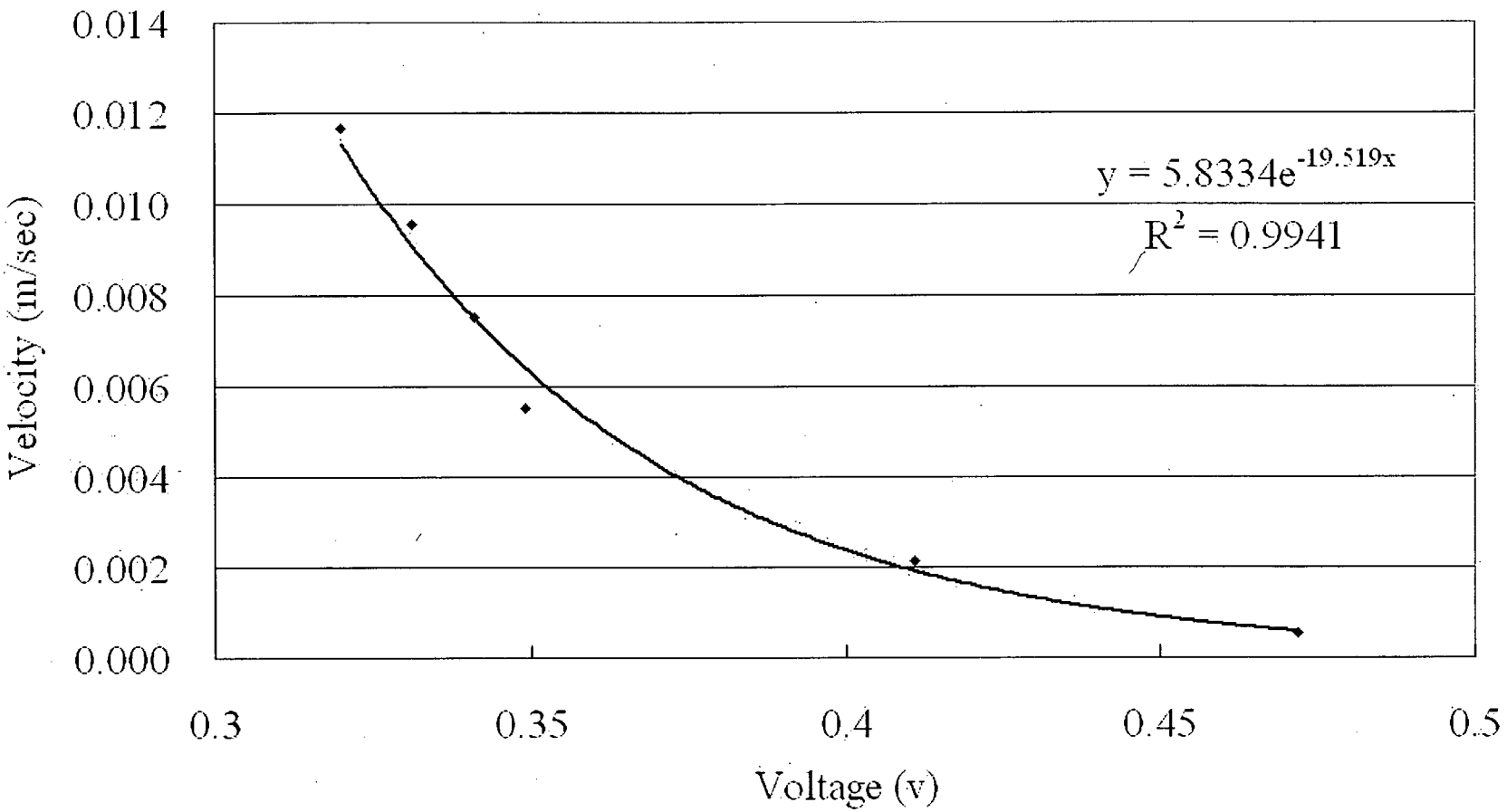
0.014
0.012
0.010
0.008
0.006
0.004
0.002
0.000
Velocity (m/sec)
y = 5.8334e-19.519x
R2 = 0.9941
0.3
0.35
0.4
0.45
0.5
Voltage (v)